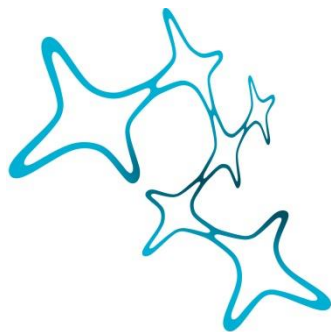


Investigating Mechanisms of Axon-Oligodendrocyte Precursor Cell Communication *in vivo*

Roberta Marisca



Graduate School of
Systemic Neurosciences
LMU Munich



Dissertation der
Graduate School of Systemic Neurosciences der
Ludwig–Maximilians–Universität München

19th March 2021

Supervisor:

Dr. Tim Czopka

Institute of Neuronal Cell Biology

Technische Universität München

First Reviewer: Dr. Tim Czopka

Second Reviewer: Prof. Dr. Jovica Ninkovic

Third Reviewer: Prof. Dr. Dirk Dietrich

Date of Submission: 19th March, 2021

Date of Defense: 10th November, 2021

ACKNOWLEDGMENT

So many people contributed in different ways to make my PhD work possible and I would like to express my deepest gratitude to all of them.

First, I am deeply grateful to my supervisor Dr. Tim Czopka for giving me the opportunity to work on this project and for providing an environment where I always felt motivated to reach my goals. Thank you for your constant guidance and constructive feedbacks. Besides my supervisor, I would like to thank the other members of my Thesis Advisory Committee Prof. Dr. Jovica Ninkovic and Dr. Hernán Lopez-Schier for taking their time to hear about my work and for their insightful comments. I would also like to thank the GSN, for giving me a great opportunity to expand my scientific knowledge and improve my soft skills. A special thank goes to Stefanie and Lena for their great support during this journey.

I would like to express my sincere gratitude to all the members of the Czopka, Misgeld and Godinho labs, not only for their valuable scientific inputs, but also for creating a very pleasant working environment. Thanks to Nic and Selin for the nice scientific and casual chats. A particular thank goes to all the members of my lab, former and new ones; it was great to work with all of you and to spend time together, also outside the lab. Thanks to Laura and Tobias, with whom I shared a fantastic publication. My profound gratitude goes to Eleni, Franzi and Stavros, thanks for supporting me and being always ready to talk. I found great new friends.

I want to say a warm thanks to my best friends in Italy, in particular to Giulia and Paola; I am so lucky to have you both in my life. I am very grateful to Federica and Carlotta, for sharing the good and the challenging moments of our PhDs holding each other up. Lastly, but not less important, I want to thank my wonderful family and my husband. Thanks to my sister and Cristian for being always there for me and ready to long phone calls. I'm so blessed to have you in my life. Grazie mamma e papà for always having my back and giving me the strength to pursue my dreams. I would be completely lost without you. Thanks Sebastian, for cheering on me, dealing with my moody swings, for your patience and care. Having you in my life is such a precious gift.

ABSTRACT

Myelination of axons can adaptively change in response to nervous system activity, with implications for structure and function of neural circuits. New myelin is made by the differentiation of specified oligodendrocyte precursor cells (OPCs). OPCs constitute an abundant population throughout the central nervous system (CNS) lifelong, but only some of these cells differentiate to myelinating oligodendrocytes at any given time. It is known that OPCs express neurotransmitter receptors through which they can sense neuronal activity, which affects OPC proliferation as well as their differentiation to myelinating oligodendrocytes. However, it remained unclear whether all OPCs communicate with axons in the same way, or whether differences exist between OPCs to integrate and respond to nervous system activity. Therefore, the aim of my PhD work was to investigate mechanisms of axon-OPC interactions to understand whether all OPCs similarly integrate neural activity and if they all contribute to myelination.

I used existing transgenic lines and I generated new transgenic reagents to specifically label OPCs and axons with fluorescent reporters and genetically encoded calcium indicators in zebrafish. This approach allowed me to visualise these two cell types in the CNS and to study their calcium signatures to investigate their interaction. Two subpopulations of OPCs with distinct cellular behaviours and fates have been identified in the spinal cord. One OPC subgroup was primed to differentiate, while the other one not. Therefore, I wondered whether OPCs also differentially communicate with axons. I have generated lines that allowed me for the first time to perform *in vivo* calcium imaging of OPCs at high resolution from subcellular domains to whole tissue population levels using the genetically encoded calcium sensor GCaMP6. My analysis of OPC calcium signatures at the single cell and population level using light-sheet imaging revealed different types of GCaMP signals. Most OPCs exhibited GCaMP transients in process microdomains. However, in some OPCs, calcium transients spread throughout the entire cell. Dual colour imaging using GCaMP in OPCs and the red shifted calcium indicator RGECO in neurons showed that whole cell calcium transients in OPCs frequently occurred in response to neuronal calcium rises. I used pharmacological approaches

to manipulate neural activity and found that the frequency of OPC GCaMP signals was increased and decreased when neuronal activity was enhanced and blocked, respectively. I investigated OPC calcium signatures at the population level using volumetric timelapse imaging in animals where all OPCs express GCaMP. These experiments revealed that whole cell GCaMP signals could appear in different patterns, in which only single cells, groups of cells, or the entire OPC population within a field of view light up. In order to investigate these signals over even larger distances, I developed assays for whole animal analysis of the OPC calcium signatures using encoded Calcium Modulated Photoactivatable Ratiometric Integrator (CaMPARI). Using this additional approach, I could detect characteristic boundaries between neighbouring OPCs which displayed similar intracellular calcium level. Together, my single cell and population analysis of OPC calcium signatures showed that the probability and amplitude of somatic calcium transients was significantly higher in non-myelinating OPCs when compared to OPCs that are primed to differentiate. In order to further explore possible functions of these OPCs calcium signatures, I manipulated neural activity using 4-Aminopyridine (4-AP), which specifically increased proliferation of OPCs that do not directly differentiate. Furthermore, by expressing a calcium exporting pump in OPCs, I could demonstrate that OPC divisions triggered by 4-AP required intracellular calcium signaling.

In summary, my studies show that OPCs exhibit different types of calcium transients and that OPCs with different properties and fates differentially communicate with axons. This provides new insights into mechanisms of axon-OPC communication and the mechanisms by which oligodendrogenesis is regulated by distinct OPC subpopulations in response to neural activity.

Table of contents

| | |
|--|----|
| ACKNOWLEDGMENT | iv |
| ABSTRACT | v |
| LIST OF ABBREVIATIONS..... | ix |
| 1 INTRODUCTION | 1 |
| 1.1 Functions of oligodendrocytes | 1 |
| 1.2 History and markers for oligodendrocyte lineage cells | 5 |
| 1.3 Oligodendrocyte lineage dynamics throughout life | 8 |
| 1.4 Functional properties of oligodendrocyte precursor cells..... | 10 |
| 1.4.1 Regional differences - grey and white matter | 10 |
| 1.4.2 Electrophysiological and gene expression differences | 12 |
| 1.5 Regulation of oligodendrocyte dynamics by neuronal activity | 16 |
| 1.5.1 Experience-dependent OPC behaviour..... | 16 |
| 1.5.2 Activity-dependent OPC behaviour | 18 |
| 1.5.3 Role of axon-OPC synaptic contacts in regulating OPC behaviour | 19 |
| 1.6 The role of calcium in oligodendrocyte lineage cells | 23 |
| 1.6.1 Calcium in axon-OPC interactions | 23 |
| 1.6.2 Visualising calcium signalling dynamics in oligodendrocyte lineage cells | 26 |
| 1.7 Summary | 28 |
| 1.8 Aims and experimental strategy..... | 29 |
| 2 MATERIAL AND METHODS..... | 30 |
| 2.1 Cloning | 30 |
| 2.2 Transgenic lines | 35 |
| 2.3 mRNA transposase synthesis and DNA microinjection for sparse labelling | 36 |
| 2.4 Immunostaining and imaging of fixed samples..... | 37 |
| 2.5 Live cell imaging | 39 |
| 2.6 Assessment of zebrafish swimming behaviour..... | 42 |
| 2.7 Mivacurium chloride treatment..... | 42 |
| 2.8 Capsaicin treatment..... | 43 |
| 2.9 4-aminopyridine treatment | 43 |
| 2.10 Tetrodotoxin treatment..... | 43 |
| 2.11 Splitomicin treatment | 43 |
| 2.12 UV-light treatment..... | 44 |
| 2.13 Image processing | 44 |
| 2.14 Data analysis | 44 |
| 2.15 Statistics | 47 |

| | | |
|-------|--|-----|
| 2.16 | Buffers and Solutions..... | 47 |
| 3 | RESULTS..... | 50 |
| 3.1 | OPC characterisation in the zebrafish spinal cord..... | 50 |
| 3.1.1 | OPC localisation in the zebrafish spinal cord..... | 50 |
| 3.1.2 | OPC properties within the zebrafish spinal cord and their contribution to myelination..... | 57 |
| 3.1.3 | Axon-OPC synaptic contacts in zebrafish..... | 61 |
| 3.2 | OPC calcium dynamics..... | 70 |
| 3.2.1 | GCaMP transients of individual OPCs..... | 70 |
| 3.2.2 | Somatic GCaMP transients at the cell population level..... | 77 |
| 3.2.3 | Integrating calcium dynamics in OPCs using CaMPARI..... | 85 |
| 3.3 | Neuron – OPC interactions..... | 90 |
| 3.3.1 | Neural activity manipulation..... | 90 |
| 3.3.2 | Calcium events in OPCs induced by neural stimulation..... | 96 |
| 3.3.3 | Neural activity manipulation effects on OPC cell fate..... | 99 |
| 4 | DISCUSSION..... | 107 |
| 4.1 | Key questions and findings..... | 107 |
| 4.2 | OPC properties and fates..... | 109 |
| 4.3 | Hierarchy between OPC subgroups..... | 114 |
| 4.4 | Integration of external stimuli by OPCs..... | 117 |
| 4.5 | OPC calcium dynamics..... | 120 |
| 4.6 | Neuronal manipulation effects on OPC..... | 126 |
| 4.7 | Future perspective..... | 130 |
| 5 | REFERENCES..... | 132 |
| 6 | PUBLICATIONS..... | 143 |
| 7 | EIDESTATTLICHE VERSICHERUNG..... | 144 |
| 8 | DECLARATION OF AUTHOR CONTRIBUTION..... | 145 |

LIST OF ABBREVIATIONS

| | |
|-------------------------|--|
| 4-AP..... | 4-amminopyridine |
| AMPA/KA..... | α -amino-3-hydroxy-5-methyl isoxazole propionic acid/ kainate |
| Ca ²⁺ | calcium |
| CaMPARI..... | Calcium Modulated Photoactivatable Ratiometric Integrator |
| CNO..... | clozapine-N-oxide |
| CNPase..... | 2', 3'-cyclic-nucleotide 3'-phosphodiesterase |
| CNS..... | central nervous system |
| Csn..... | capsaicin |
| Cspg4..... | Chondroitin sulfate proteoglycan 4 |
| Cx..... | connexin |
| dpf..... | day post fertilisation |
| DREADD..... | Designer Receptor Exclusively Activated by a Designer Drug |
| EAE..... | experimental autoimmune encephalomyelitis |
| EdU..... | 5-ethynyl-2'-deoxyuridine |
| ER..... | endoplasmic reticulum |
| FCS..... | fetal calf serum |
| FingR..... | Fibronectin intrabody generated with mRNA display |
| GABA _A | gamma-aminobutyric acid |
| GECI..... | genetically encoded calcium indicator |
| GM..... | grey matter |
| GPR17..... | G-protein receptor 17 |
| HDAC..... | histone deacetylase |
| K ⁺ | potassium |
| K _v | voltage gated potassium |
| MAG..... | myelin associated glycoprotein |
| MAP2..... | microtubules-associated protein 2 |
| MBP..... | myelin basic protein |
| MCT1..... | monocarboxylate transporter 1 |
| MS..... | multiple sclerosis |
| MYRF..... | myelin regulatory factor |
| Na ⁺ | sodium |

| | |
|-----------|--|
| Nav | voltage gated sodium |
| NCX | Na ⁺ /Ca ²⁺ exchanger |
| NG2 | Neuron-glia antigen 2 |
| Nkx2.2 | NK2 Homeobox 2 |
| NMDAR | N-methyl-D-aspartate receptors |
| O-2A | oligodendrocyte-type-2 astrocyte progenitor cells |
| Olig1 | oligodendrocyte transcription factor 1 |
| Olig2 | oligodendrocyte transcription factor 2 |
| OPC | oligodendrocyte precursors cell |
| P | postnatal age |
| PDGF | platelet-derived growth factor |
| PFC | prefrontal cortex |
| PLP | myelin proteolipid protein |
| PNS | peripheral nervous system |
| PSD95 | postsynaptic density protein 95 |
| ROIs | regions of interest |
| scRNA-seq | single cell RNA-sequencing |
| Sox10 | Sry-like HMG box10 |
| TRPV1 | transient receptor potential cation channel subfamily V member 1 |
| TTX | tetrodotoxin |
| VGCCs | voltage-gated Ca ²⁺ channels |
| VGCs | voltage-gated ion channels |
| WM | white matter |

1 INTRODUCTION

The nervous system plays a role in almost every aspect of our life, allowing our body to sense messages from distal anatomical regions and to transform them into reactions. The nervous system can be subdivided in the central nervous system (CNS), which consists of brain and spinal cord, and the peripheral nervous system (PNS), which comprises the nerves that connect the CNS to the peripheral organs. Neurons and glia cells are the two main cell types of the nervous system. Neurons are specialised for electrical signalling over long distances, while glial cells provide support, electrical insulation to neurons, and remove debris. The term “neuroglia” was at first coined by Rudolf Virchow and refers to the connective non-neuronal structures that join the neurons together. This was the only function recognised to glial cells. Indeed, glia derives from the ancient Greek word “γλία” which means “glue” (Virchow, 1856). In the last decade of the 19th century, glial cells stopped being considered one homogeneous population. In the early 1900s Ramón y Cajal described the presence in the neuroglia population of astrocytes and a third element. In 1919 Pío del Río-Hortega found that the third element consisted of two different cell types, which he named microglia and oligodendrocytes (Sierra et al., 2016). Since their discovery, nothing major happened, until recently when it was discovered that astrocytes, microglia and oligodendrocytes are also diverse within their populations, having as well different physiological roles. Therefore, glia cells are beginning to be considered as crucial regulators of neuronal structure and function (Khakh and Deneen, 2019; Foerster et al., 2019; Masuda et al., 2020).

1.1 Functions of oligodendrocytes

Most axons in our CNS are surrounded by an insulating structure called myelin, composed primarily of lipids and proteins. The area of the CNS that contains myelinated axons is named white matter because myelin is enriched in lipids and appears white. Differently, the grey matter

area mostly consists of neuronal cell bodies. Myelin is made by oligodendrocytes, a glia cell type. One first major function of oligodendrocytes is to produce myelin to wrap the axons and enable fast nerve conduction. Myelin does not wrap continuously the whole axon but creates intermittent gaps, between consecutive myelin sheaths, called nodes of Ranvier. Nodes are rich in voltage gated sodium and potassium channels which open when an action potential propagates through an axon. As a consequence, myelin allows the axon to conserve energy as the depolarisation is happening only at the nodes, and not along the entire axon. In addition to myelination, oligodendrocytes provide axonal metabolic support by transferring energy metabolites from their cell bodies to axons (Fünfschilling et al., 2012; Lee et al., 2012). Indeed, oligodendrocytes express monocarboxylate transporter 1 (MCT1), a transporter of monocarboxylic acids like lactate and pyruvate. The loss of this transporter in oligodendrocytes caused axon degeneration, suggesting to play a crucial role in axon survival (Lee et al., 2012). The formation of new myelin is a dynamic process and increases in myelination occur almost lifelong in response to neural activity, or to restore myelin to repair demyelinated axons. Myelin changes, in terms of sheath elongation and myelin thickness, can modulate the conduction velocity, to optimise the synchronisation of action potentials arrival from connected circuits (Fields, 2015). New myelin is formed by the differentiation of specified oligodendrocyte precursor cells (OPCs) during postnatal development (Zhu et al., 2008) and throughout life (Dimou et al., 2008; Young et al., 2013). OPCs constitute a big portion of the total CNS cell population, in white matter (8–9%) and in grey matter (2–3%). OPCs tile the entire brain, are the major dividing cell population of the CNS and maintain constant their density (Fig. 1.1) (Dawson et al., 2003; Dimou et al., 2008).

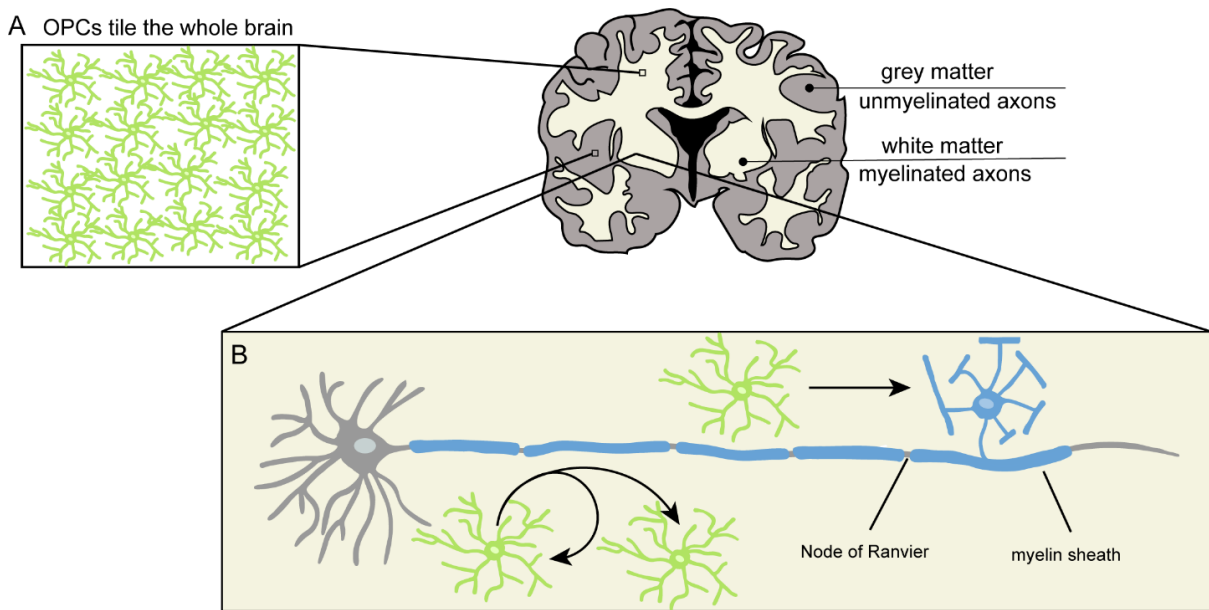


Fig. 1.1 Oligodendrocytes in the CNS

Schematic representing OPCs in the CNS. **A)** OPCs tile the entire brain and they constitute a large part of the CNS population, being present both in white matter and grey matter. **B)** OPCs (in green) are very proliferative and they can differentiate to give rise to myelinating oligodendrocytes (in blue) which are the cell that myelinate axons. Myelinated axons are located in the white matter region of the CNS. Neurons (in grey) are the cells that get myelinated, myelin (in blue) wrap around the axon and increases speed conduction through the gaps created between consecutive myelin sheaths called nodes of Ranvier.

OPCs respond to neural activity to increase myelination and differentiate into myelinating oligodendrocytes, but most of them don't differentiate. Also in demyelinating diseases such as multiple sclerosis (MS), or other neurological conditions such as spinal cord injury, myelin gets disrupted and OPCs respond by differentiating into myelinating oligodendrocytes to restore myelination (Duncan et al., 2009). However, it has been shown that OPCs often fail to differentiate into oligodendrocytes, causing a persisting demyelinated condition (Wolswijk et al. 1998). This arises the question whether some OPCs receive the signal that triggers their differentiation and others don't, or whether not all OPCs have the same properties and are able to sense brain activity. Many studies are now focusing on OPC features and on their lineage progression, to understand which factors regulate their cell fate.

Oligodendrocytes are important not only to mediate fast signal conduction in the nervous system, but also because they provide essential metabolic support for the axons. Oligodendrocytes derive from the differentiation of OPCs. However, OPCs constitute a large population of the CNS and not all of them differentiate in response to neural activity, or in demyelinating condition, suggesting that not all OPCs are identical. The next sections will provide an overview of oligodendrocyte precursor cell biology, their features in their lineage progression towards myelinating oligodendrocytes, their heterogeneity and how their lineage progression can be controlled by intrinsic and extrinsic factors.

1.2 History and markers for oligodendrocyte lineage cells

Since the beginning of the 20th century, astrocytes, oligodendrocytes and microglia were considered the major population of glial cells in the CNS. At that time, the existence of OPCs was still unknown due to the lack of markers able to label these cells in histological analysis. In 1976, using electron microscopic autoradiograms, cells referred to as “oligodendroblasts” were described in the optic nerve. These cells differ from mature oligodendrocytes by their more diffuse and lightly stained chromatin (Skoff et al., 1976). The transition from OPCs to myelinating oligodendrocytes follows characteristic changes identified according to their increase in complex morphology, the expression pattern of specific markers and their ability to proliferate, migrate and differentiate. Three major states along oligodendrocyte lineage progression can be defined: OPCs, premyelinating oligodendrocytes and myelinating oligodendrocytes. Different states can be traced using different markers (Fig. 1.2). These markers comprise of cell surface antigens and transcription factors. OPCs were at first recognised using the A2B5 antibody, which is a cell surface ganglioside epitope, utilised to label the oligodendrocyte-type-2 astrocyte progenitor cells (O-2A). These cells in serum-free medium were shown to differentiate into oligodendrocytes, but in fetal calf serum (FCS) medium were reported to give rise to type II astrocytes, for this reason they were called O-2A. Another prominent surface antigen to label OPCs is NG2 (Neuron-glia antigen 2), a chondroitin sulfate proteoglycan, which was originally found to be expressed by neural cells (Stallcup, 1981). NG2-positive cells in culture were indeed O-2A cells and were also differentiating into oligodendrocytes under serum-free conditions. The NG2 expression was then lost during differentiation into mature oligodendrocytes (Raff et al., 1983). After migration from the germinal zone, NG2-positive cells were distributed in the CNS by the end of the first postnatal week (Nishiyama et al., 1996a, b). These cells are still present in the adult CNS, are mitotic and can also differentiate into oligodendrocytes (Levison et al., 1999). For all these features, NG2-expressing cells are also called oligodendrocyte precursor cells (OPCs). NG2 is currently used as a marker to label oligodendrocyte lineage at early developmental stages, but with the

caveat that NG2-expressing cells can also be pericytes (Ozerdem et al., 2001). Another commonly used antigen surface to label OPC is PDGFR- α , the receptor for platelet-derived growth factor α . NG2-expressing cells expressed also PDGFR- α *in vivo* in the rat CNS (Pringle et al., 1992). The survival and proliferation of NG2 cells is dependent on the platelet-derived growth factor (PDGF) *in vitro* (Richardson et al., 1988). In addition to surface antigens, there are also transcription factors used to label oligodendrocyte lineage cells. In particular, two of them, Olig2 (Oligodendrocyte transcription factor 2) and Sox10 (Sry-like HMG box10), are expressed throughout the oligodendrocyte lineage (Lu et al., 2000; Zhou et al., 2000; Kuhlbrodt et al. 1998). Olig2 expression is also expressed in immature neuronal progenitors (Takebayashi et al., 2000). The transcription factor Olig1 (Oligodendrocyte transcription factor 1) was also found to be localised to the OPC nucleus, and in the cytoplasm of myelinating oligodendrocytes in the white matter of the adult mouse (Arnett et al., 2004). Another transcription factor, upregulated in OPCs, is Nkx2.2 (NK2 Homeobox 2) which is downregulated once OPCs differentiate (Fu et al., 2002).

As OPCs start to differentiate, they are called pre-myelinating oligodendrocytes and start to downregulate some OPC markers and express new markers. Amongst them are the surface antigens 2', 3'-cyclic-nucleotide 3'-phosphodiesterase (CNPase) and myelin proteolipid protein (PLP). (Kuhn et al., 2019). Interestingly, PLP is also an early marker for OPCs and it is important for OPCs process integrity and migration (Harlow et al., 2014). Myelinating oligodendrocytes expressed the surface antigens myelin basic protein (MBP) which appears together with myelin associated glycoprotein (MAG) as well as the transcription factor myelin regulatory factor (MYRF) (Linnington et al., 1984; Barbarese et al., 1988; Emery et al., 2009).

To summarise, after the discovery of OPCs, several markers have been identified to label oligodendrocyte lineage cells, allowing the discrimination among different developmental stages along the lineage progression. However, it is necessary to combine different markers to discern among the different stages, as some of the markers overlap. Moreover, marker expression might vary between different animal models.

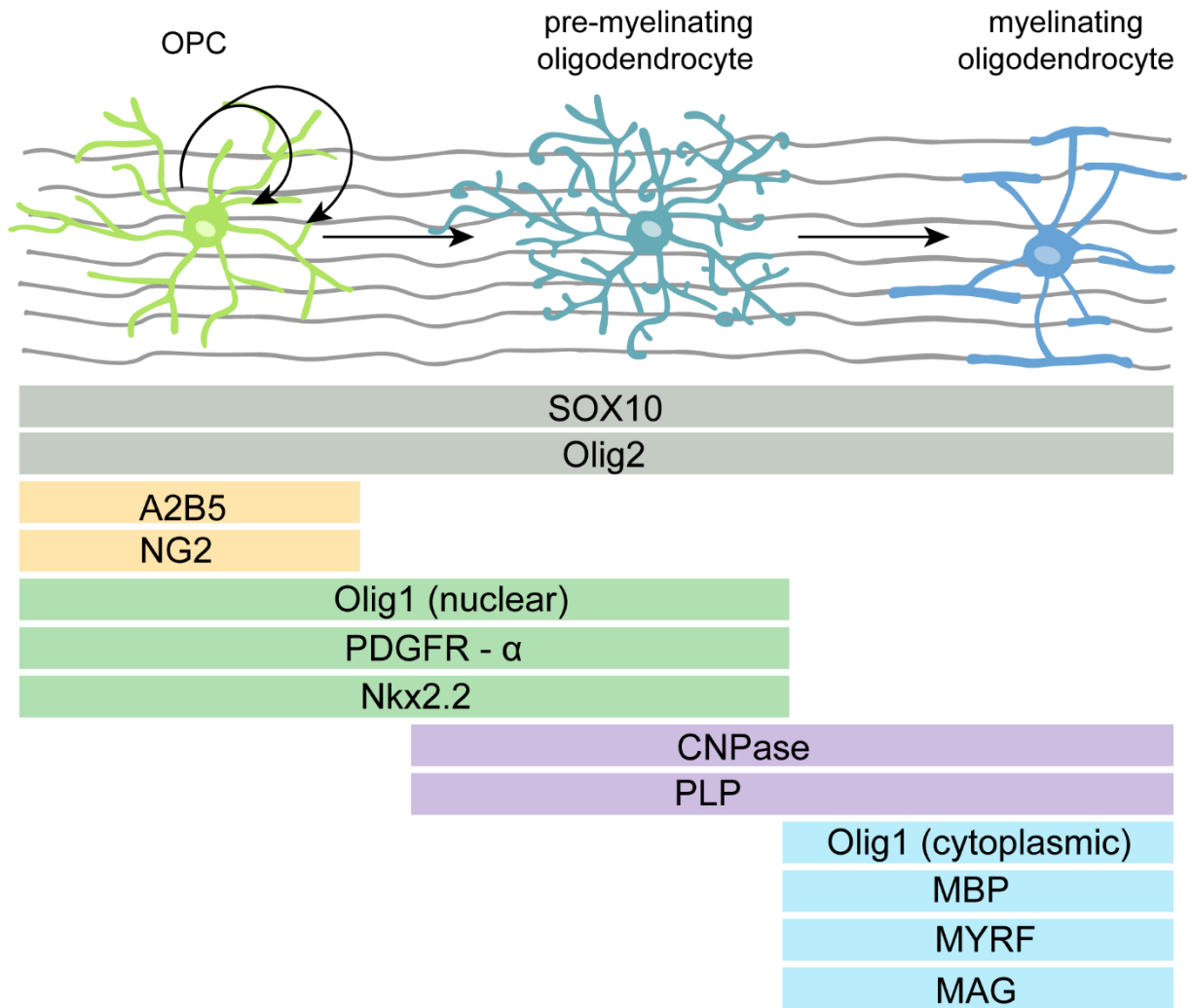


Fig. 1.2 Oligodendrocyte lineage markers

Markers to label oligodendrocyte lineage cells during their cell progression towards mature oligodendrocytes. Cells in the OPC state are proliferative cells. When OPCs start to differentiate they acquire a more complex morphology, they start to touch axons and are called pre-myelinating oligodendrocytes. In the last state of the lineage progression, myelinating oligodendrocytes wrap the axons with myelin sheaths. SOX10 and Olig2 are expressed throughout the whole oligodendrocyte lineage. NG2 and the A2B5 label OPCs. Nkx2.2, PDGFR— α and Olig1(nuclear) are used to label oligodendrocyte at early developmental stages. CNPase and PLP are early markers of myelinating oligodendrocytes. Finally, Olig1(cytoplasmic), MBP, MYRF and MAG are expressed in myelinating oligodendrocytes. Adapted from Kuhn et al., 2019.

1.3 Oligodendrocyte lineage dynamics throughout life

The identification of several OPC markers, done by histological analysis, paved the way to *in vivo* studies. This allowed for a more detailed characterisation of oligodendrocyte lineage cell progression and gave the chance to study OPCs in their physiological environment.

After arising from the ventricular germinal zones of the brain and the spinal cord, OPCs migrate throughout the tissue to populate the CNS (Richardson et al., 2006). During and after migration, OPC behaviour has been characterised both in the developing zebrafish spinal cord and adult mouse cortex *in vivo*. Time lapse imaging revealed that OPCs constantly remodel their processes to continuously explore the environment around them and retract them when they get in contact with other OPCs (Kirby et al. 2006; Hughes et al., 2013). OPCs have shown proliferative features comparable to stem cells, being the most proliferative cells of the brain parenchyme (Dimou et al., 2008). OPCs continue to maintain their density and to differentiate into myelinating oligodendrocytes also throughout adulthood, confirming a strong fate interrelation between these two populations (Dimou et al., 2008; Young et al., 2013). OPCs in the adult somatosensory cortex maintain their numbers under physiological conditions by symmetrical divisions to generate two daughter OPCs, or by asymmetric divisions where they give rise to one daughter oligodendrocyte and one OPC (Hughes et al., 2013; Zhu et al., 2011). In the developing mouse brain, the majority of recently divided OPCs differentiate into oligodendrocytes during a specific temporal window of 3–8 days (Hill et al., 2014). In the cortex of young rats, around 20 % of pre-myelinating oligodendrocytes die and in adult mouse cortex around 78% degenerate within two days after differentiation (Trapp et al., 1997; Hughes et al., 2018). Once OPCs start the differentiation process, they extend their processes to establish contacts with target axons. Afterwards, oligodendrocyte processes start to form a myelin sheath around the axon by adding new wrap underneath previous ones and elongating along the axon (Snaidero et al., 2014).

Studies in developing zebrafish and in rodent cell cultures have reported that each oligodendrocyte has a narrow time window to establish myelin sheaths once generated

(Czopka et al., 2013; Watkinson et al., 2008). While differentiating into myelinating oligodendrocytes, OPCs produce several short myelin sheaths, which then start elongating and/or retracting around target axons. In zebrafish, each individual oligodendrocyte makes new myelin sheaths during a short time frame of about 5 hours. After this time window, no additional myelin segments are formed (Czopka et al., 2013).

Under disease conditions such as demyelination models, it was found that in the adult rat spinal cord, 5-bromo-2'-deoxyuridine (BrdU) is incorporated by proliferating OPCs around the lesion, as these cells migrate into the lesion and differentiate into oligodendrocytes (Watanabe et al., 2002). This output was further corroborated by a condition in which two-photon laser ablation of several OPCs triggered an immediate proliferative OPC response in order to replace the lost cells and restore their density (Hughes et al., 2013).

To summarise, OPCs, after migration and proliferation, become uniformly distributed throughout the grey and white matter of the CNS. They have a strong proliferative potential and they differentiate into myelinating oligodendrocytes during development, adulthood and in demyelinating conditions. Therefore, OPCs of different intrinsic age, newly born, quiescent in OPC state or differentiating toward myelinating oligodendrocytes are present at the same time in different brain regions. It thus appears that OPC population might be constituted by OPCs with different properties which I will describe in details in the next section.

1.4 Functional properties of oligodendrocyte precursor cells

OPCs constitute a large cell population and not all of them differentiate into myelinating oligodendrocytes. Moreover, OPCs are generated in multiple waves from the ventricular germinal zones and populate different regions of the CNS (Kessaris et al., 2006). This suggests that already from their origin there might be differences amongst OPC populations. Moreover, depending on the surrounding environment, OPCs located in different regions of the CNS might have different properties. This has important implications in myelination because different OPC phenotypes may contribute differently to differentiation and proliferation. It is therefore necessary to investigate the OPC properties and to focus on their ability to integrate signals from neurons, as myelination can be activity-dependent. Investigations into OPC heterogeneity have reported conflicting results. Even if some studies have claimed that OPCs in the hippocampus and corpus callosum show homogeneous electrophysiological properties, more recent studies have recognised OPCs as a heterogeneous cell population (Clarke et al., 2012; De Biase et al., 2010; Spitzer et al., 2019).

1.4.1 Regional differences - grey and white matter

Differences in the ability of OPCs whether to proliferate or to differentiate have been found between OPCs localised to white matter (WM) and grey matter (GM) regions. A fate mapping study, using the tamoxifen-induced Cre-recombination system driven by *olig2* to label OPCs in the cerebral cortex has revealed differences in terms of proliferation and differentiation between WM and GM OPCs. In the WM, most OPCs differentiated to give rise to myelinating oligodendrocytes, whereas GM OPCs were mostly proliferating but remained undifferentiated (Dimou et al., 2008). To clarify whether the different differentiation properties were linked to intrinsic cell diversity or whether they rather resulted from environmental factors, homotopic and heterotopic transplantations in the mouse cerebral cortex were performed.

WM-derived OPCs differentiate more frequently than GM-derived cells, even when transplanted in the GM environment (Viganó et al., 2013). This indicates that there are intrinsic differences between these cells, though, at the same time, environmental cues could have influenced their nature before the transplantation. Despite being highly differentiating cells, WM OPCs were also shown to be more proliferative than the GM ones and that their rate of division decreased with age (Young et al., 2013). Moreover, it was reported that WM OPCs exhibit a greater proliferative response to PDGF, previously shown to regulate OPC proliferation, and which induced a stronger response in the younger WM OPCs (Hill et al., 2013). G-protein receptor 17 (GPR17) has also been observed to be differently expressed in OPCs and to influence their contribution to myelination. Indeed, GPR17 inhibited OPC differentiation and it is considered as an intrinsic timer of myelination (Chen et al., 2009). A fate map tracing of GPR17 expressing OPCs, revealed that GPR17 was expressed only in a portion of OPCs, predominantly more common in GM than WM OPCs. Cells expressing GPR17 remained in an undifferentiated state for a long period, compared to OPCs that were not expressing this receptor.

However, after stab wound injury or cortical ischemia, OPCs expressing GPR17 start to differentiate at higher rate compared to physiological conditions, meaning that OPCs change their behaviour when more myelin is required (Viganó et al., 2016).

Differences between OPCs have also been found in the spinal cord. During development, most OPCs in the spinal cord originate from the ventricular zone, while only a minority arises from the dorsal zone. Interestingly, even if during perinatal period ventrally derived cells were found in the whole spinal cord, including the dorsal axonal tracts, in adulthood these dorsal tracts became predominantly populated by dorsally derived oligodendrocytes. This suggests that the dorsally-derived oligodendrocytes preferentially myelinate dorsal tract axons (Tripathi et al., 2011). Moreover, dorsally-derived OPCs exhibited enhanced recruitment and differentiation, in response to demyelination. It was also shown that dorsally-derived OPCs are less able to differentiate with ageing, while ventrally-derived OPCs continue to show the same differentiation rate during the life span (Crawford et al., 2016).

Differences amongst OPCs in terms of cell fate have been identified between white and grey matter OPCs, even if both have proliferative capacity, the first ones have a higher differentiation potential. These data recognise local environment as an extrinsic factor in determining OPC cell fate.

1.4.2 Electrophysiological and gene expression differences

OPCs express a wide range of neurotransmitter receptors, which makes them responsive to neuronal activity. Differences in electrophysiological properties have been found within the oligodendrocyte lineage. Despite the expression of sodium (Na^+) and potassium (K^+) channels, OPCs are not able to trigger action potentials and the expression of these channels is downregulated as OPCs differentiate into myelinating oligodendrocytes (De Biase et al., 2010; Kukley et al., 2010). However, in another study, two distinct types of OPCs were identified in the rat white matter CNS. One type receives synaptic inputs and express voltage-gated sodium (Na_v) and voltage-gated potassium (K_v) channels that can generate action potentials, the other type lacks both these features (Káradóttir et al., 2008). This OPC ability in showing action potential has not been identified in other model systems yet, suggesting that this might be a rat specific feature. Independent of whether subsets of OPCs can fire action potential or not, electrophysiological differences have also been found between white and grey matter OPCs. A whole-cell patch-clamp study in cortical slices demonstrated that white matter and grey matter OPCs exhibit different K^+ and Na^+ channel expression profiles (Chittajallu et al., 2004). In a recent work, physiological properties of OPCs have been characterised in detail across different brain regions and ages, using single cell electrophysiological recordings. OPCs acquired K_v channels at first, followed by Na_v channels and N-methyl-D-aspartate receptors (NMDAR) which reached their peak of expression at the time when OPCs start to differentiate into myelinating oligodendrocytes, and declined when OPCs lose their myelination potential. α -amino-3-hydroxy-5-methyl isoxazole propionic acid/ kainate (AMPA /KA) receptors were identified in almost all OPCs after birth and their densities increased with age. (Spitzer et al.,

2019). In the same study, bulk RNA sequencing analysis were performed and OPCs with different electrophysiological properties express as well different molecular signatures depending on the age. Embryonic OPCs have more migrating signatures, at postnatal age 12 (P12) OPCs expressed genes involved in proliferation and differentiation, which then decreased at P80. Genes for cell cycle regulation were similarly downregulated in OPCs from older animals. The authors also focused on the expression of genes related to Na_v channel and glutamatergic NMDAR and found that their expressions were increasing in OPCs from embryonic until post-natal age and remained constant further on (Spitzer et al., 2019). However, these were bulk studies at different developmental stages which did not take into account that there are cells at different stages of their lineage progression within the tissue. Therefore, it remains still unresolved whether these cells constitute different types of OPCs or whether they rather represent OPCs at different cell stages.

In the last few years, several studies have taken advantage of single cell RNA-sequencing (scRNA-seq) to investigate gene expression with single cell resolution, and better characterise the function of individual cells, but also to identify differences among the OPC cell population. In the first scRNA-seq oligodendrocyte lineage cells study, the transcriptome of about 5000 cells was analysed. Oligodendrocyte lineage cells were isolated from 10 distinct regions of the anterior-posterior and dorsal-ventral axis of the mouse juvenile and adult CNS. Thirteen distinct cell populations were found and further analysis identified a path connecting all the different populations from OPCs to myelinating oligodendrocytes. In the juvenile CNS, across different regions, distinct cell populations were similarly expressed, whereas in the adult brain a group of mature oligodendrocyte was enriched in specific regions. OPCs were recognised as one cell type and were co-expressing PDGFR- α and Cspg4 (Chondroitin sulfate proteoglycan 4, known also as NG2). 10 % of OPCs also expressed cycling genes consistent with their proliferative behaviour.

Instead, myelinating oligodendrocytes could be categorised into six mature distinct states, suggesting heterogeneity amongst them (Marques et al., 2016). A subsequent study from the same group, focused on the transcriptome of OPCs from the mouse forebrain and spinal cord

at embryonic, juvenile and adult stages using bulk and single-cell RNA-seq. They found that embryonic OPCs appear as a heterogeneous population. However, scRNA-seq revealed similar transcriptional profiles of OPCs in the post-natal spinal cord and brain, concluding that OPCs arising from different parts of the embryonic germinal zones are in the end similar to each other during development (Marques et al., 2018). This means that the heterogeneity found amongst different brain regions is not cell intrinsic and it does not depend on OPC origins but rather induced by local environment at later timepoint.

To conclude, OPCs have been identified as a functionally heterogeneous population, in particular, when looking at their gene expression and electrophysiological properties, which differ between brain regions and animal age. These differences might also explain distinct abilities for OPCs to differentiate.

However, it remains unclear whether different OPC properties mirror different states along lineage progression, or whether represent different subtypes of OPCs. A link between different gene expression profiles together with their electrophysiological responses and the cell fate potential of different OPCs is still missing. The Spitzer *et al.* study was based on bulk RNA sequencing to compare OPC population at different ages, however, to identify differences between cell types, a single cell resolution study is necessary. This would allow us to better delineate a complete profile of the characteristics of different OPC subpopulations, to understand whether they are following their lineage progression or if they represent different subtypes. Therefore, it will be useful to understand how OPCs sense neuronal activity and contribute to myelination (Fig. 1.3).

In the next section, I will illustrate mechanisms that trigger OPC differentiation and proliferation, and their role in regulating myelination.

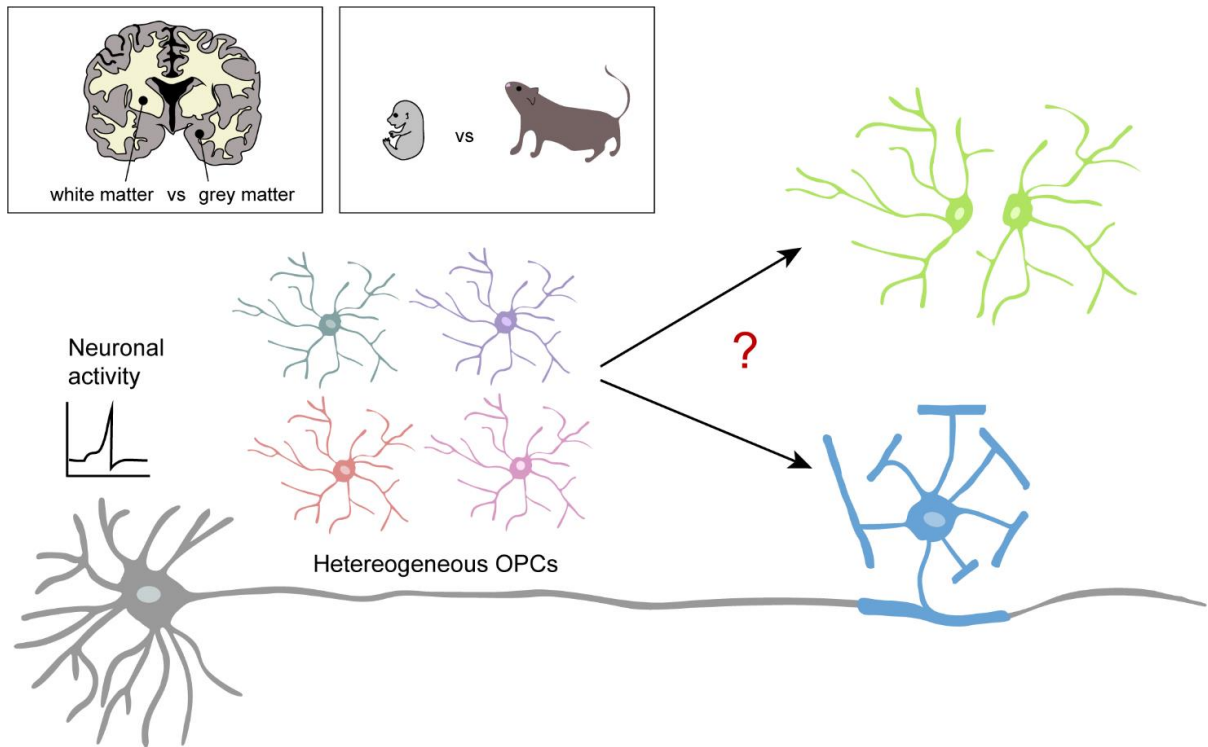


Fig. 1.3 OPC heterogeneity: open questions

Schematic explaining the open questions about OPC heterogeneity and functions. OPCs are not homogenous, they have differences amongst regions, ages and also different physiological properties and gene expression. The correlation amongst these differences and OPC fates and functions are still not clear. It would be useful to associate different OPC populations with their ability to integrate neuronal activity and to contribute to myelination.

1.5 Regulation of oligodendrocyte dynamics by neuronal activity

OPCs are able to proliferate and differentiate not only during development, but also during adulthood and in demyelinated conditions. OPCs have been shown to play an active role in what is called adaptive myelination, which are the changes in myelination that occur in response to neural activity and which have the potential to modify circuit function. Changes in myelination have been documented to depend on social experience, motor learning, and experimental manipulation of neuronal activity (Mount and Monje, 2017). The proliferation of OPCs, their differentiation to myelinating oligodendrocytes and/or the selection of target axons by differentiating OPCs are the major cellular events underlying adaptive myelination.

1.5.1 Experience-dependent OPC behaviour

Recent studies suggest that adaptive myelination can be modulated by learning a new task, as well as by social and sensory experiences. On a macro level, white matter changes have been identified in human adult brain following training of a complex visual-motor skill or after learning to play the piano (Scholz et al., 2009; Steele et al., 2013). Increases in myelin was also identified in adults after learning a new language (Schlegel et al., 2012). Rats trained to learn a single-pellet reaching task showed higher white matter in the sensory motor cortex, as well as an increase in myelin staining, which correlated with the learning rate (Sampaio-Baptista et al., 2013). Oligodendrocyte contribution to enhanced myelination after motor skill learning was studied in mice that had to learn a new complex motor skill. Increased OPC proliferation and differentiation into myelinating oligodendrocytes was found in mice that learned to run on a wheel with irregularly spaced rungs. Blocking the myelin regulatory transcription factor in OPCs, prevented new oligodendrocyte formation and new motor skill learning, thus suggesting that new oligodendrocyte and myelin generation is fundamental for learning a new motor complex skill (McKenzie et al., 2014).

In a subsequent study, from the same group, it was shown that new oligodendrocytes are required both in early and late stages of motor skill learning (Xiao et al., 2016). In a more recent study, the importance of motor learning to modulate myelination was further investigated in developmental and remyelinating conditions. Immediately after motor learning, no increase in OPC proliferation was detected, instead oligodendrogenesis was enhanced in a time-dependent manner and OPCs were directly differentiating to give rise to new myelinating oligodendrocytes. In addition, motor learning improved remyelination in a demyelination model, involving both new and mature oligodendrocytes (Bacmeister et al., 2020).

Despite learning, another external cue that can influence myelination and oligodendrocyte lineage cells is related to social experience. Social isolation of juvenile mice after weaning resulted in alterations in white matter development. In particular, oligodendrocytes showed reduced ramification, shorter process length and each cell formed less internodes. Myelin thickness was also reduced in isolated mice despite no differences being found in axon diameters (Makinodan et al., 2012). Impaired myelination and decrease in myelin gene transcripts were also found in the prefrontal cortex (PFC) of prolonged socially deprived adult mice and importantly, re-integration of social contacts was sufficient to restore myelination (Liu et al., 2012).

Sensory experience also modulates myelin plasticity. Unilateral whisker clipping in mice increased OPC proliferation in the deprived barrel cortex (Mangin et al., 2012). In a following study, it was shown that whisker deprivation increased apoptosis of newly generated OPCs and the number of mature oligodendrocytes was decreased. These data suggest that the increase in OPC proliferation was happening to compensate for the loss of oligodendrocytes. The subsequent apoptosis might be explained as an OPC response to maintain their constant cell population number (Hill et al. 2014). Investigation of myelin plasticity in adult mice revealed that sensory enrichment increased oligodendrocyte integration and new myelin formation, without changes in pre-existing myelin sheath length in the somatosensory cortex (Hughes et al. 2018).

1.5.2 Activity-dependent OPC behaviour

Axons play an important role in regulating their own myelination. Despite the fact that myelination depends on axonal diameter, where larger axons are myelinated before small ones, not all axons of the same diameter are necessarily myelinated (Hildebrand et al., 1993; Tomassy et al., 2014). Cultured OPCs differentiate into oligodendrocytes also in presence of synthetic fibers similar to neurons in shape and size. This suggests that differentiation can happen also in absence of axo-glial signalling, with only the physical presence of an axon-like structure. Moreover, fiber diameter appeared to be critical for OPC differentiation, as fibers with at least 0.4 μM were preferred to smaller ones (Lee et al. 2012). However, since oligodendrocytes in the CNS myelinate axons, it would make sense that axons control their numbers and instruct OPCs to differentiate. This idea has been investigated since the early 90s when Barres and Raff showed that a transection of the developing rat optic nerve results in significantly reduced OPC proliferation, suggesting the role of axonal electrical activity in inducing OPC division (Barres and Raff, 1993). Following studies highlighted the effects of activity on axon-choice when OPC differentiated to myelinating oligodendrocytes. Neurotoxins that block or increase neuron action potential, prevent or enhance respectively myelinogenesis *in vitro* (Demerens et al., 1996). Other experiments carried out using root ganglion cell cultures confirmed an activity-dependent regulation of myelination, in which glutamate released from synaptic vesicles along axons induced myelin formation around electrically activated axons (Wake et al., 2011). The first study to prove the potential role of neuronal activity *in vivo* was done using optogenetic stimulation of the premotor cortex in awake mice. Stimulation of neuronal activity, once again, induced OPC proliferation, differentiation and myelination; notably, myelin sheaths were thicker after optogenetic stimulation. In addition to these effects, oligodendrogenesis and myelination induced by neuronal activity correlated with motor behavioural improvement (Gibson et al., 2014). Neuronal activity plays a key role in determining which axons get myelinated and the myelin sheaths number and length. Indeed, an *in vivo* zebrafish study shows that blocking activity of specific axons, reduces the number of axons that get myelinated. Oligodendrocytes that wrapped silenced neurons formed shorter

sheaths that were also retracting more frequently (Hines et al., 2015). In another *in vivo* zebrafish study, it was shown that inhibition of synaptic vesicle release from neurons decreased the number of myelinated axons, in particular each oligodendrocyte produced 30% less myelin sheaths (Mensch et al., 2015). These effects were also described in mammalian CNS using a pharmacogenetic approach to stimulate neuronal activity, which resulted in an increase of OPC proliferation and differentiation in juvenile and adult mice, enhancing myelination of stimulated axons (Mitew et al., 2018). The role of neuronal activity was also studied in demyelinated conditions. Repeated optogenetic stimulation of demyelinated axons in mice corpus callosum induces OPC differentiation into myelinating oligodendrocytes, and remyelination, restoring axonal conduction (Ortiz et al., 2019).

1.5.3 Role of axon-OPC synaptic contacts in regulating OPC behaviour

Neuronal activity plays an important role to modulate myelination by influencing the behaviour of oligodendrocyte lineage cells. The mechanisms that regulate the interaction between neurons and oligodendrocyte lineage cells are still not fully described. Since 2000 it is known that OPCs make functional synapses with neurons. Bergles *et al.* used patch-clamp recordings of OPCs in hippocampal slices and showed that stimulation of excitatory axons induced OPC depolarisation. The release of glutamate vesicles from axons elicited currents in OPCs mediated by AMPA receptors. Glutamatergic activity was linked to calcium (Ca^{2+}) rises in OPCs which were blocked using a selective antagonist of Ca^{2+} -permeable AMPA/kainate receptors. Axon-OPC synapses were further confirmed by electron microscopy in the hippocampus which identified typical synaptic features like pre- and post-synaptic vesicle densities (Bergles et al., 2000). OPCs also receive GABAergic synapses from inhibitory interneurons in hippocampus. Interneuronal firing leads to transient activation of GABA_A (gamma-aminobutyric acid) receptors on OPCs (Lin and Bergles, 2004). Moreover, oligodendrocyte lineage cells exhibit functional NMDA receptors in the cerebellum and corpus callosum (Káradóttir et al., 2005). Disruption of NMDAR specifically in OPCs and

oligodendrocytes *in vitro* and *in vivo* does not alter OPC proliferation, differentiation and myelination neither in experimental autoimmune encephalomyelitis (EAE), a model of human MS (Biase et al. 2011; Guo et al. 2012) The role of NMDA-mediated currents in OPCs and differentiation into oligodendrocytes is still unclear, since NMDAR ablations showed increased Ca^{2+} mediated by AMPAR, suggesting that NMDARs and AMPARs can functionally compensate across their roles (De Biase et al. 2011).

Axon-OPC synapses have been found also in white matter brain regions. Two studies described that vesicular release of glutamate, from unmyelinated axons, is detected by glutamate receptors in OPCs in the corpus callosum (Kukley et al., 2007; Ziskin 2007). Interestingly, OPCs, unlike other cells in the CNS, relocated after division and kept in their processes synaptic junctions which were inherited by the daughter cells. This result suggests that OPCs were born with synapses and could immediately establish connections with neurons (Kukley et al., 2008). OPCs form a transient and highly organised network with interneurons in the developing neocortex, showing a peak in connectivity that coincides with oligodendrogenesis (Orduz et al., 2015). Recently, a study of the effects of hypoxia on OPCs revealed that hypoxia causes loss of GABA_A receptor-mediated synapses, increased OPC proliferation and delayed oligodendrocyte myelination. This result indicates that GABAergic signalling can modulate OPC behaviour in mice *in vivo* (Zonouzi et al., 2015). The role of axon-OPC synapses has been investigated *in vivo* also in a toxin-induced demyelination model. Demyelinated axons form synaptic contacts to OPCs, glutamatergic activity instructs OPCs to differentiate into new myelinating oligodendrocytes that recover their lost function (Gautier et al., 2015). OPC-axon synaptic contacts modulate both proliferation and differentiation, and this can be regulated by different patterns of neuronal activity. High neuronal firing in the corpus callosum increases OPC proliferation, low frequencies increase the numbers of pre-myelinating oligodendrocytes and all stimulations promoted differentiation of OPCs in oligodendrocytes, suggesting that neurons through their firing can tune OPC behaviour (Nagy et al., 2017). The functional role of AMPARs in oligodendrocyte lineage cells was identified manipulating these receptors specifically at the level of axon-OPC synapses *in vivo*. Point

mutation of the GluA2 subunit, which increase the calcium-permeability of AMPA receptors, enhanced OPC proliferation and reduced their differentiation into oligodendrocytes (Chen et al., 2018). Loss of AMPA receptor signalling specifically in oligodendrocyte lineage cells via double and triple knockouts of the *gria2-4* genes encoding AMPAR subunits, did not alter OPC proliferation but also decreased the survival of mature oligodendrocytes (Kougioumtzidou et al., 2017).

All together, these studies illustrate that axon-OPC establish synaptic contacts. However, the function of these contacts is still not clear, as neuronal activity through glutamatergic and GABAergic signalling via axon-OPC synapses modulate both OPC proliferation and differentiation.

In this section, changes in myelination were highlighted focusing on the conditions that can influence OPC differentiation. In particular, myelination is regulated by neuronal activity modulated in different ways associated with animal experience, such as learning and social interaction (Fig. 1.4). Neuronal activity induces changes in oligodendrocyte lineage cell progression, affecting both proliferation and differentiation of OPCs and alters as well myelin sheath structure. OPCs sense neuronal activity through the expression of neurotransmitter receptors and they receive synaptic inputs from neurons. The mechanisms by which neuronal activity affects OPC cell fate and myelination have to be further investigated, taking into account OPC heterogeneity and considering that OPC subtypes may respond differently to neuronal activity. In this way, it will be possible to reach a better understanding of the relationship between changes in oligodendrocyte lineage cells, and functional alterations to fine-tune axon conduction within the neural network.

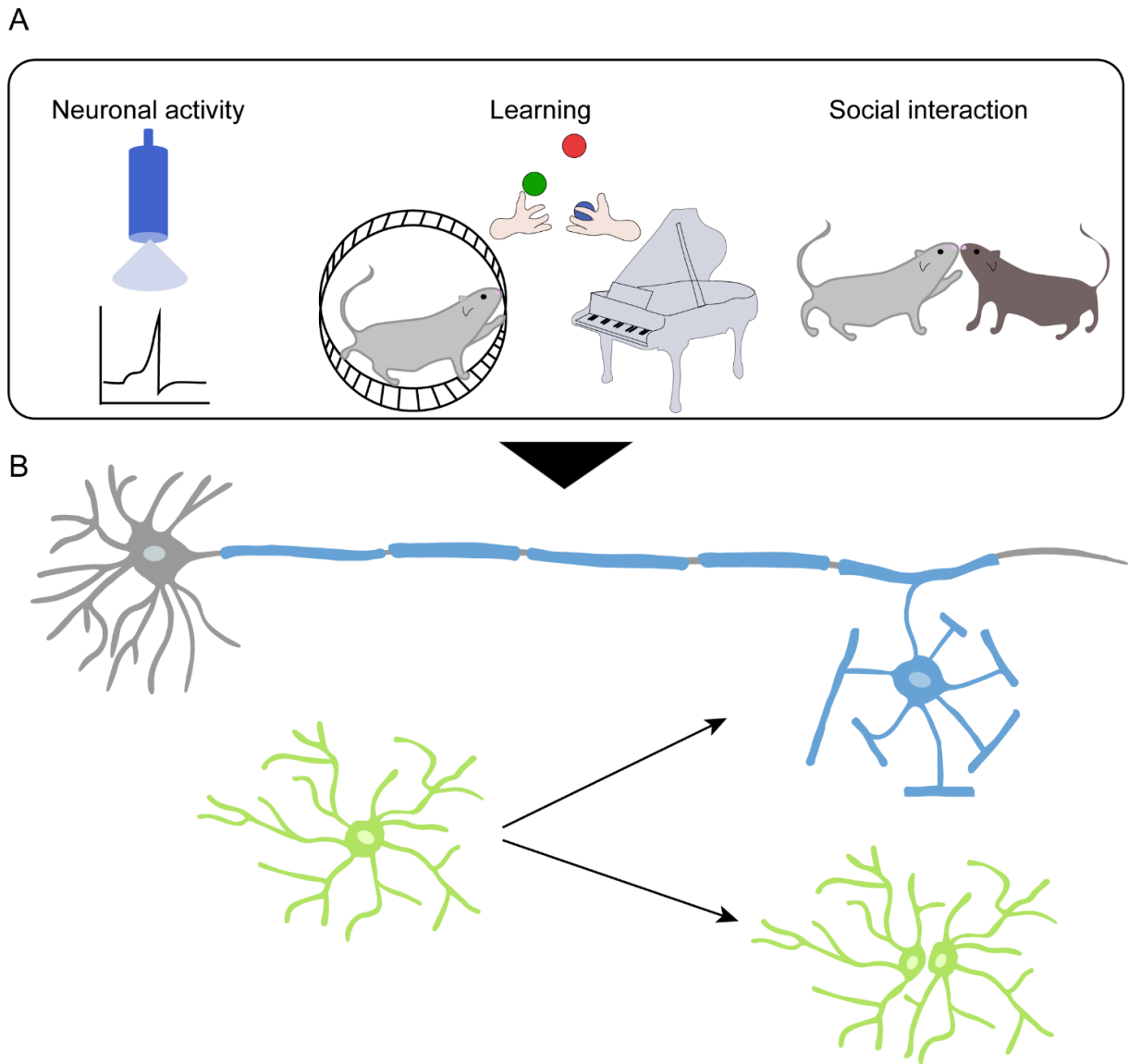


Fig. 1.4 Factors that modulate OPC behaviour

A) Schematic showing the factors that influence myelination. Neuronal activity, different types of learning (motor learning, juggling and practicing the piano) and social interaction modulate positively myelin changes. **B)** Effects of the cues showed in A on oligodendrocyte lineage cells and myelination. Neuronal activity and experience induce both OPC proliferation and differentiation into myelinating oligodendrocytes. Adapted from Mount and Monje, 2017.

1.6 The role of calcium in oligodendrocyte lineage cells

In the previous sections, I discussed the synaptic features of OPCs and their physiological properties. Despite the fact that OPCs express several voltage-gated ion channels (VGCs), the function of these channels and in general the role of OPC synaptic contacts is not clear yet. In neurons, synaptic signals can trigger action potentials and calcium signalling. Calcium is an important second messenger related to various cellular processes including cell migration, proliferation and neurotransmission. Intracellular calcium rises induced by synaptic signalling are also present in oligodendrocyte lineage cells, but the functions and mechanisms that involve calcium signalling need to be further investigated in oligodendrocytes.

1.6.1 Calcium in axon-OPC interactions

Synaptic stimulations to elicit calcium in OPCs were not able to produce action potentials, suggesting that synaptic inputs are too weak in OPCs. In OPCs, calcium rises are dynamic and can derive from intracellular or extracellular sources (Haberlandt et al., 2011). Ca^{2+} -permeable AMPA-receptors are the main source of Ca^{2+} in OPCs and this was confirmed by the elevated expression level of *gria2* gene that encodes the AMPA receptor subunit responsible for calcium permeability (Marques et al., 2016). However, OPCs also express voltage-gated Ca^{2+} channels (VGCCs) through which Ca^{2+} can enter from the extracellular space (Fulton et al., 2010). Additionally, Ca^{2+} can be released from intracellular stores upon different stimulations. OPCs express voltage-gated Na^+ channels but fail to produce action potentials typical of neurons, this might be due to the weakness of the synaptic input, which might be not sufficient to cause the required depolarisation in the cell to activate the VGCCs (Velez-Fort et al., 2010; Sun et al., 2016). However, Káradóttir *et al.*, described a type of OPCs in the CNS white matter capable to generate action potential (Káradóttir et al. 2008).

Stimulation-induced Ca^{2+} elevations in slice hippocampal OPCs can be achieved through several pathways: VGCCs, Ca^{2+} -permeable AMPA-receptors, group I metabotropic glutamate-

receptors and calcium release from the endoplasmic reticulum (ER). Moreover, electrical stimulation of presynaptic neurons caused post-synaptic Ca^{2+} elevations in the highly motile OPC arborisations, and not in the soma region (Haberlandt et al., 2011). Ca^{2+} rises evoked by the activation of Na^+ channels and $\text{Na}^+/\text{Ca}^{2+}$ exchangers (NCX) in OPCs have been also found to be involved in cell migration and to be triggered through GABAergic receptors (Tong et al., 2009). VGCCs can also impact OPC migration as shown by an *in vitro* study in which OPC migration was blocked by pharmacological inhibition of Cav1.2, a L-type VGCC (Paez et al. 2009). In a recent and well described work, Sun *et al.* used hippocampal slices to investigate the role of calcium in OPCs to integrate neuronal activity. In this study, glutamatergic synaptic input generated a linear response in OPCs which gradually increased dendritic calcium elevations depending on the stimulus strength, meaning that OPC calcium levels reflect the level of synaptic activity. Both somatic and localised to OPC processes calcium signals had a much slower decay time compared to neurons. This was the first evidence describing calcium as an important signal to link synaptic input through neurotransmitter release with a stimulus-dependent neuronal activity (Sun et al., 2016). Two-photon *in vivo* imaging of genetically encoded Ca^{2+} indicators expressed in OPCs revealed that olfactory sensory stimulation triggers a strong Ca^{2+} response in OPC processes that are input specific (Rungta et al., 2018).

To summarise, calcium is involved in several pathways in oligodendrocyte lineage cells related to axon-OPC interactions. I have given a general overview about how intracellular calcium can be mediated in OPCs by individual receptors and channels (Fig. 1.5). Calcium localisation, amplitude and signal transduction pathways might regulate different cellular functions amongst the oligodendrocyte lineage. Not much is known about how calcium rises modulate OPC behaviour and myelination. In the next section I will illustrate the influence of calcium changes in oligodendrocyte lineage cell behaviour and function.

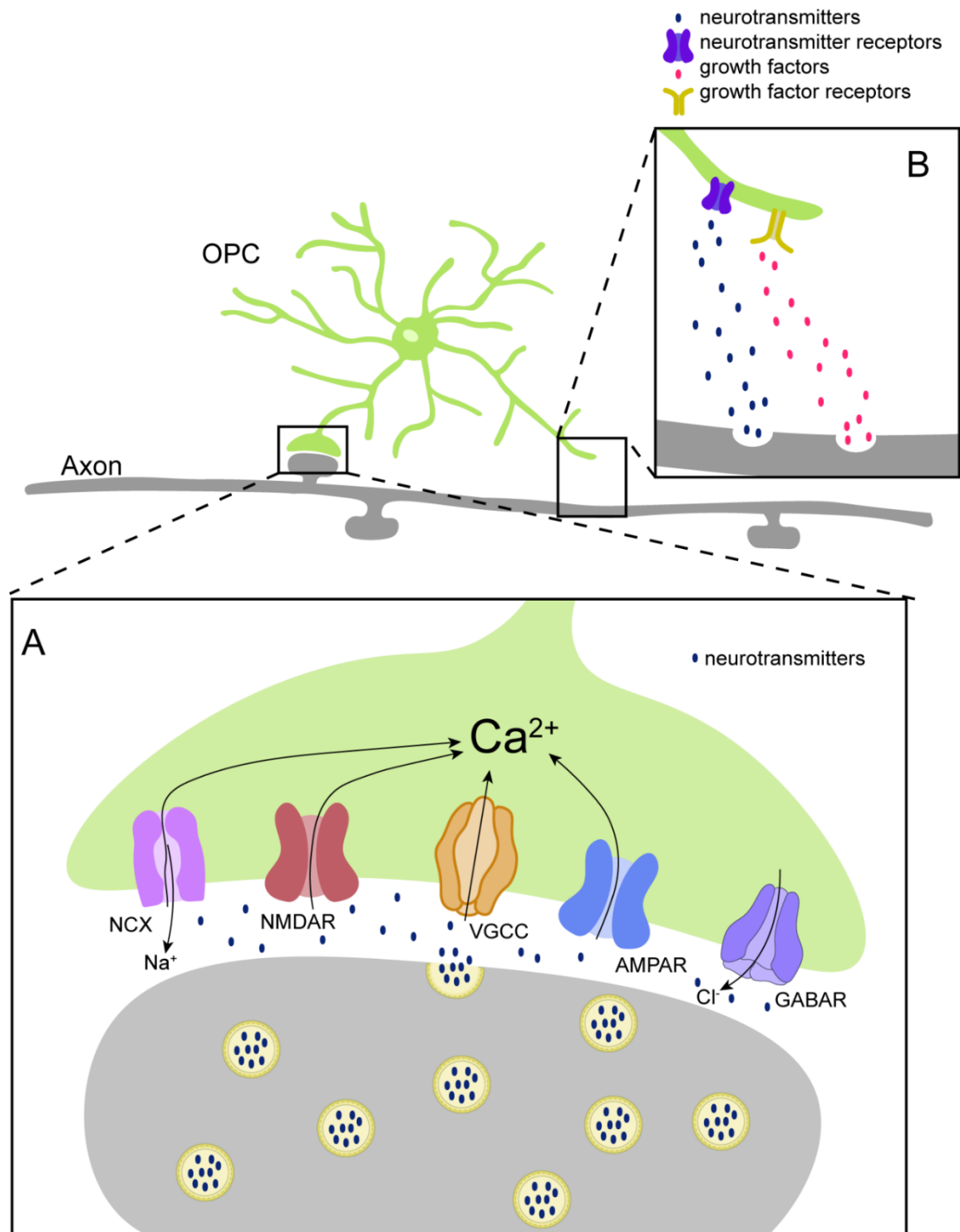


Fig. 1.5 Calcium in axon-OPC contacts

Upper schematic: Axon-OPC synaptic contacts. **a)** zoom in of the axon-OPC synapse. OPCs receive both glutamatergic and GABAergic synaptic inputs from neurons through the expression of several neurotransmitter receptors. AMPAR (α -amino-3-hydroxy-5-methyl isoxazole propionic acid receptor), NMDAR (N-methyl-D-aspartate receptor), GABAR (gamma-aminobutyric acid receptor). Through these receptors, intracellular calcium rises in OPCs as well as through VGCC (voltage gated calcium channel) and the NCX (Na⁺/Ca²⁺ exchangers). Black arrows indicate the direction of ion flux through channels. **b)** zoom in of the axon-OPC non-synaptic contact. Active axons can also signal to OPCs via non-synaptic contacts, through vesicular release of neurotransmitters or growth factors, indeed OPCs express also growth factor receptors. Adapted from Paez and Lyons, 2020 and Faria et al., 2019.

1.6.2 Visualising calcium signalling dynamics in oligodendrocyte lineage cells

Different mechanisms can regulate changes in intracellular Ca^{2+} but it is still unclear how this can affect aspects of OPC function. This section will highlight the effects of calcium changes during oligodendrocyte formation and myelin formation. At the beginning of my PhD, no data on calcium imaging in oligodendrocyte lineage *in vivo* were available. Recently, *in vivo* calcium imaging studies in zebrafish showed that the characteristics of calcium transients in myelin sheaths of newly formed oligodendrocyte correlated with their behaviour (Baraban et al., 2018; Krasnow et al., 2018). High-amplitude, long-duration Ca^{2+} transients preceded retraction of sheaths mediated by calpain, a Ca^{2+} -dependent non-lysosomal protease (Baraban et al., 2018). In contrast, lower-amplitude, shorter-duration calcium events were indicative of sheath elongation, and their frequency correlated with sheath growth speed (Baraban et al., 2018; Krasnow et al., 2018). In the study from Krasnow and colleagues, calcium activity in developing oligodendrocytes was analysed, starting with pre-myelinating oligodendrocytes. Process and cell soma calcium transients decreased while maturation towards oligodendrocytes occurred. Moreover, calcium transients correlated with neuronal electric stimulation and their firing rates were reduced by approximately 50% after Tetrodotoxin (TTX) injection which blocks action potentials (Krasnow et al., 2018). Another recent work examined calcium transients in myelin sheath formation in the mouse somatosensory cortex. The authors similarly identified high-rate spontaneous calcium transients propagating along the myelin sheaths which decreased with sheath maturation, but which were again more active during remyelination following cuprizone-induced demyelination. In contrast to the previous work, microdomain Ca^{2+} transients in myelin sheaths did not correlate with neuronal activity, but they were almost completely abolished when the mitochondrial permeability transition pores have been pharmacologically inhibited (Battefeld et al., 2019). The mechanisms that regulate calcium-mediated myelin formation and elongation need to be further explored to clarify the role of neuronal activity and the other factors involved in this process. Furthermore, a complete calcium activity description of oligodendrocyte lineage cells is still missing, since the calcium response profile of OPCs that receive synaptic contacts from axons has been not described in the previous *in vivo* studies.

As OPCs receive both glutamatergic and GABAergic synaptic inputs from neurons and express various voltage gated ion channels, it would be interesting to characterise their calcium transients as well as to evaluate their connection to neuronal activity in regulating myelin dynamics.

1.7 Summary

CNS myelin, formed by oligodendrocytes, allows fast and precise axon conduction to fine tune neural circuits. In the last twenty years, oligodendrocyte precursor cells (OPCs) have been widely studied for different reasons: they constitute one of the major cell population in the CNS, their density is maintained constant throughout life and some, but not all, OPCs differentiate into myelinating oligodendrocytes. Previous studies have demonstrated that myelin can be modulated throughout life, and have identified several cues that can influence myelination, such as neuronal activity, learning and social experiences. OPCs integrate neuronal activity by expression of different neurotransmitter receptors and voltage gated ion channels. A key role in sensing neuronal activity is played by calcium. Indeed, intracellular calcium rises have been detected in OPCs upon neuronal activity. Axon-OPC interactions modulate changes in the oligodendrocyte lineage cell fate, but it is still unclear how this is regulated since increased neuronal activity triggers both proliferation and differentiation of OPCs. One possible explanation is based on the heterogeneity found across the OPC population, especially with regard to their differential ability in sensing axonal activity through the appearance of diverse electrophysiological properties. This would consequentially affect OPC cell fate response to axonal activity. Moreover, differences amongst OPCs have already been described across several brain regions and time windows, arising the question of whether OPCs being intrinsically diversified or if they are at differential states during their lineage progression but not functionally different.

A work that combines the study of OPC heterogeneity together with functional readouts of their role in integrating axonal activity, and their differing potential to contribute to myelination is still missing.

1.8 Aims and experimental strategy

Oligodendrocyte precursor cells (OPCs) represent a heterogeneous population with different gene expression profiles, physiological properties and behavioural fates. However, these features have not yet been directly correlated. In particular, neuronal activity appears to have different effects on OPCs by promoting both proliferation and differentiation. This arises the question whether amongst OPCs are indeed subtypes, some of which proliferate in response to neural activity while others differentiate, or whether the apparent OPC diversity reflects other features that cells can have or acquire. Therefore, the general aim of my thesis was to investigate mechanisms of axon-OPC interactions to understand whether all OPCs similarly sense neural activity and if they all contribute to myelination.

In order to address this question, the aims of my PhD project were the following:

- 1) To characterise OPC cell morphology and position in the zebrafish spinal cord, and to identify synapse-like axon-OPC contacts *in vivo* focusing on possible differences between OPCs.
- 2) To describe OPC calcium dynamics at both single cell and population levels in order to identify potential differing calcium properties amongst OPCs.
- 3) To explore neuronal-induced effects on OPC calcium dynamics and cell fates to define possible differential responses amongst OPCs in sensing neural activity.

To address these aims, I used zebrafish as a model organism considering its well-known advantages. Zebrafish larvae are optically transparent and permit non-invasive in-vivo imaging of OPC morphology, physiology and fate over time using transgenic reporters and biosensors. Moreover, it is a relatively small animal model, allowing large volume imaging in a short amount of time with a light-sheet microscopy. This animal model is also ideal for pharmacological manipulations permitting a precise control of drug delivery and dosage. Furthermore, up to 70% of human genes are conserved, and zebrafish has been previously used to study myelination.

2 MATERIAL AND METHODS

2.1 Cloning

The cloning performed for this study was done in collaboration with Dr. Tim Czopka, Wenke Barkey, Tobias Hoche and Dr. Laura Hoodless. The entry clones generated are listed below and their respective primers are in Table 2.1.

p5E_mfap4: The 5' entry clone p5E_mfap4 was generated by PCR amplification of a 1.5 kb DNA fragment of mfap4 upstream regulatory sequence (Walton et al., 2015) from zebrafish AB wild-type genomic DNA and subsequently recombined with a pDONRP4P1R plasmid using a BP-reaction.

pME_GCaMP6m: To generate the middle entry clone pME_GCaMP6m the coding sequence was PCR amplified from a template plasmid (Chen et al., 2013) and subsequently recombined with a pDONR221 plasmid using a BP-reaction.

pME_GCaMP6m-CAAX: To generate the middle entry clone pME_GCaMP6m-CAAX the coding sequence was PCR amplified from a template plasmid (Chen et al., 2013) and subsequently recombined with a pDONR221 plasmid using a BP-reaction.

pME_mCherry-CalEx: To generate the middle entry clone pME_mCherry-CalEx the coding sequence was PCR amplified from a template plasmid (Yu et al., 2018) and subsequently recombined with a pDONR221 plasmid using a BP-reaction.

pME_mScarlet: The middle entry clone pME_mScarlet was generated using a BP-reaction, the coding sequence with appropriate sites for recombination with pDONR221 was commercially synthesized by BioCat.

pME_PSD95_nostop: To generate the middle entry clone pME_PSD95_nostop the coding sequence was PCR amplified from a template plasmid (Niell et al., 2004) and subsequently recombined with a pDONR221 plasmid using a BP-reaction.

pME_synaptophysin-nostop: To generate the middle entry clone pME_synaptophysin-nostop the coding sequence was PCR amplified from a template plasmid (Meyer et al., 2006) and subsequently recombined with a pDONR221 plasmid using a BP-reaction.

p3E_tagRFPt-pA: To generate the 3' entry clone p3E_tagRFPt-pA the coding sequence was PCR amplified using the primer combination attB2_tagRFPt_F and attB3R_pA_R and subsequently recombined with a pDONR_P2P3R plasmid using a BP-reaction.

pME_CaMPARI: To generate the middle entry clone pME_CaMPARI the coding sequence was PCR amplified from a template plasmid (Fosque et al., 2015) and subsequently recombined with a pDONR221 plasmid using a BP-reaction.

pME_TRPV1-tagRFPt: The middle entry clone pME_TRPV1-tagRFPt was generated using a BP-reaction, the coding sequence with appropriate sites for recombination with pDONR221 plasmid was commercially synthesized by BioCat.

pME_jRGECO1a: To generate the middle entry clone pME_jRGECO1a the coding sequence was PCR amplified from a template plasmid (Dana et al., 2016) and subsequently recombined with a pDONR221 plasmid using a BP-reaction.

pTol2_olig1(4.2):nls-mApple: The expression construct pTol2_olig1(4.2):nls-mApple was generated with the 5' entry clone p5E_olig1(4.2) (Auer et al., 2018) and the Tol2Kit entry clones pME_nls-mApple, p3E-pA and pDestTol2_pA (Kwan et al., 2007) using Multisite LR recombination reactions.

pTol2_elavl3:mCherry: The expression construct pTol2_elavl3:mCherry was generated with the 5' entry clone p5E_elavl3 (Mensch et al., 2015) and the Tol2Kit entry clones pME_mCherry, p3E-pA and pDestTol2_pA (Kwan et al., 2007) using Multisite LR recombination reactions.

pTol2_elavl3:synaptophysin-tagRFP: The expression construct pTol2_elavl3:synaptophysin-tagRFP was generated with the 5' entry clone p5E_elavl3 (Mensch et al., 2015), the generated middle entry clone pME_synaptophysin-nostop, the 3'

entry clone tagRFP and the Tol2Kit entry clones p3E-pA and pDestTol2_pA (Kwan et al., 2007) using Multisite LR recombination reactions.

pTol2_olig1(4.2):KalTA4: The expression construct pTol2_olig1(4.2):KalTA4 was generated with the 5' entry clone p5E_olig1(4.2) (Auer et al., 2018), the middle entry clone pME_KalTA4 (Almeida et al., 2015) and the Tol2Kit entry clones p3E-pA and pDestTol2CG2 (Kwan et al., 2007) using Multisite LR recombination reactions.

pTol2_UAS:PSD95-YFP: The expression construct pTol2_UAS:PSD95-YFP was generated with the 5' Tol2Kit entry clone p5E_UAS(10x) (Kwan et al., 2007), the generated middle entry clone pME_PSD95_nostop, the 3' entry clone p3E_EYFPpA (Auer et al., 2018) and the Tol2Kit plasmid pDestTol2_pA (Kwan et al., 2007) using Multisite LR recombination reactions.

pTol2_olig1(4.2):GCaMP6m: The expression construct pTol2_olig1(4.2):GCaMP6m was generated with the 5' entry clone p5E_olig1(4.2) (Auer et al., 2018), the generated middle entry clone pME_GCaMP6m and the Tol2Kit entry clones p3E-pA and pDestTol2_pA (Kwan et al., 2007) using Multisite LR recombination reactions.

pTol2_olig1(4.2):GCaMP6m-CAAX: The expression construct pTol2_olig1(4.2):GCaMP6m-CAAX was generated with the 5' entry clone p5E_olig1(4.2) (Auer et al., 2018), the generated middle entry clone pME_GCaMP6m-CAAX and the Tol2Kit entry clones p3E-pA and pDestTol2_pA (Kwan et al., 2007) using Multisite LR recombination reactions.

pTol2_olig1(4.2):CaMPARI: The expression construct pTol2_olig1(4.2):CaMPARI was generated with the 5' entry clone p5E_olig1(4.2) (Auer et al., 2018), the generated middle entry clone pME_CaMPARI and the Tol2Kit entry clones p3E-pA and pDestTol2_pA (Kwan et al., 2007) using Multisite LR recombination reactions.

pTol2_UAS:TRPV1-tagRFPT: The expression construct pTol2_UAS:TRPV1-tagRFPT was generated with the 5' Tol2Kit entry clone p5E_UAS(10x) (Kwan et al., 2007), the generated middle entry clone pME_TRPV1-tagRFPT, the 3' entry clone p3E-pA (Auer et al., 2018) and

the Tol2Kit plasmid pDestTol2_pA (Kwan et al., 2007) using Multisite LR recombination reactions.

pTol2_cntn1b:jRGECO1a: The expression construct pTol2_cntn1b:jRGECO1a was generated with the 5' entry clone p5E_cntn1b (Czopka et al., 2013), the generated middle entry clone pME_jRGECO1a and the Tol2Kit entry clones p3E-pA and pDestTol2_pA (Kwan et al., 2007) using Multisite LR recombination reactions.

pTol2_elavl3:jRGECO1a: The expression construct pTol2_elavl3:jRGECO1a was generated with the 5' entry clone p5E_elavl3 (Mensch et al., 2015), the generated middle entry clone pME_jRGECO1a and the Tol2Kit entry clones p3E-pA and pDestTol2_pA (Kwan et al., 2007) using Multisite LR recombination reactions.

pTol2_mfap4:memCerulean: The expression construct pTol2_mfap4:memCerulean was made with the generated 5' entry clone p5E_mfap4, the middle entry clone pME_memCerulean (Auer et al., 2018) and the Tol2Kit entry clones p3E-pA and pDestTol2_pA (Kwan et al., 2007) using Multisite LR recombination reactions.

pTol2_UAS:mCherry-CalEx: The expression construct pTol2_UAS:mCherry-CalEx was generated with the 5' Tol2Kit entry clone p5E_UAS(10x) (Kwan et al., 2007), the generated middle entry clone pME_mCherry-CalEx, and the Tol2Kit entry clones p3E-pA and pDestTol2_pA (Kwan et al., 2007) using Multisite LR recombination reactions.

pTol2_UAS:mScarlet: The expression construct pTol2_UAS:mScarlet was generated with the 5' Tol2Kit entry clone p5E_UAS(10x) (Kwan et al., 2007), the generated middle entry clone pME_mScarlet, and the Tol2Kit entry clones p3E-pA and pDestTol2_pA (Kwan et al., 2007) using Multisite LR recombination reactions.

Table 2.1 Primers used for cloning

| Primer name | Sequence |
|-------------------------------|--|
| attB1_GCaMP6m_F | GGGGACAAGTTTGTACAAAAAAGCAGGCTGCCACCATGGGTTCTCATC |
| attB2R_GCaMP6m_R | GGGGACCACTTTGTACAAGAAAGCTGGGTCTCACTTCGCTGTCATCATTTGTA |
| CAAX-GCaMP6m_R | TCAGGAGAGCACACACTTGCAGCTCATGCAGCCGGGGCCACTCTCATCAGGAGGGTTCAGCTTTCCTCACTTCGCTGTCATCATTTGTAC |
| attB2R_CAAX_R | GGGGACCACTTTGTACAAGAAAGCTGGGTCTCAGGAGAGCACACACACTTGC |
| attB1_synaptophysin_F | GGGGACAAGTTTGTACAAAAAAGCAGGCTGCCACCATGGATGTTGCC |
| attB2R_synaptophysin_nostop_R | GGGGACCACTTTGTACAAGAAAGCTGGGTCCATCTCGTTGGAGAAGGATG |
| attB2_tagRFpT_F | GGGGACAGCTTTCTTGTACAAAGTGGTAATGGTGTCTAAGGGCGAAGAGC |
| attB3R_pA_R | GGGGACAACCTTTGTATAATAAAGTTGAAAAACCTCCCACACCTCCC |
| attB1_mCherry_F | GGGGACAAGTTTGTACAAAAAAGCAGGCTGCCACCATGGTGAGCAAGGGCGAG |
| attB2R_CalEx-R | GGGGACCACTTTGTACAAGAAAGCTGGGTCCCTAAAGCGACGTCTCCAG |
| attB4_mfap4 | GGGGACAACCTTTGTATAGAAAAGTTGGCGTTTCTTGGTACAGCTGG |
| attB1R_mfap4 | GGGGACTGCTTTTTTGTACAACTTGCTTCTCACTCTCTCCTCAAC |
| attB1_PSD95_F | GGGGACAAGTTTGTACAAAAAAGCAGGCTGCCACCATGCCTCTCAACGAGAAG |
| attB2R_PSD95_nostop_R | GGGGACCACTTTGTACAAGAAAGCTGGGTCCAGTCTCTCTCGTGTGG |
| attB1_CaMPARI_F | GGGGACAAGTTTGTACAAAAAAGCAGGCTGCCACCATGCTGCAGAAC |
| attB2R_CaMPARI_R | GGGGACCACTTTGTACAAGAAAGCTGGGTCTTATGAGCTCAGCCGACC |
| attB1_jRGecko1a_F | GGGGACAAGTTTGTACAAAAAAGCAGGCTGCCACCATGCTGCAGAAC |
| attB2R_jRGecko1a_R | GGGGACCACTTTGTACAAGAAAGCTGGGTCTCACTTCGCTGTCATCATTTGTA |

att recombination site, Kozak sequence, coding sequence

2.2 Transgenic lines

All animals were kept at 28.5° with a 14/10 hour light/dark cycle according to local animal welfare regulations. AB and nacre wild-type animals were used for this study. All transgenic lines used are listed in Table 2.2.

Table 2.2 Transgenic lines used

| Line | Reference |
|---------------------------------|----------------------------------|
| Tg(olig1:memEYFP) | generated (Marisca et al., 2020) |
| Tg(olig1:nls-mApple) | generated (Marisca et al., 2020) |
| Tg(mbp:memCerulean) | (Auer et al., 2018) |
| Tg(mbp:EGFP-CAAX) | (Almeida et al., 2011) |
| Tg(elavl3:synaptophysin-tagRFP) | generated (Marisca et al., 2020) |
| Tg(mbp:nls-EGFP) | (Karttunen et al., 2017) |
| Tg(cntn1b:KaTA4) | (Mensch et al., 2015) |
| Tg(olig1:KaTA4) | generated (Marisca et al., 2020) |
| Tg(UAS:GCaMP6s) mpn101 | (Thiele et al., 2014) |
| Tg(olig1:GCaMP6m) | generated (Marisca et al., 2020) |
| Tg(mbp:KillerRed) | (Auer et al., 2018) |
| Tg(olig1:CaMPARI) | generated |
| Tg(mfap4:memCerulean) | generated (Marisca et al., 2020) |
| Tg(elavl3:h2b-GCaMP6s) | (Freeman et al., 2014) |

2.3 mRNA transposase synthesis and DNA microinjection for sparse labelling

Transposase plasmid (Tol2Kit) (Kwan et al., 2007) was linearized with NotI (New England BioLabs). Afterwards, it was purified with a PCR purification kit (Qiagen) following the protocol. The mRNA synthesis was done with the mMessage mMachine SP6 kit (Invitrogen) and then purified with an RNAeasy Mini kit (Qiagen) according to the protocol. RNA concentration was then measured at the spectrophotometer and stored at -80°C.

One cell stage eggs were microinjected with 1nl of injection solutions containing 5-25 ng/ µl DNA, 25-50 ng/ µl Tol2 transposase mRNA and 10 % phenol red (Sigma Aldrich). The needle for microinjection was always calibrated using a micrometer and injecting the solution in a drop of mineral oil.

Generation of new transgenic lines

A fluorescent dissecting microscope (Nikon SMZ18) was used to screen embryos for the expression of the injected construct. Injected animals were used for single cell experiments or raised to generate the full transgenic line. To generate stable transgenic lines, injected F0 embryos were raised and when they reached adulthood were outcrossed to wild-type zebrafish. F1 generation was screened for germline transmission of the fluorescent transgene and raised.

2.4 Immunostaining and imaging of fixed samples

Tissue preparation and cryosectioning

5-7 days post fertilisation zebrafish larvae were euthanised with 4mg/ml tricaine (MS-222) and then fixed overnight at 4°C in 4% paraformaldehyde (PFA). Fixed animals were incubated for a minimum of three days in an increasing concentration of sucrose (10%, 20%, 30%), until the larvae sank to the bottom of the well plate. Afterwards zebrafish larvae were embedded in OCT medium (Tissue-Tek) and frozen on dry ice. The samples were then stored at -80°C until sectioning. Transversal section of the spinal cord with a thickness of 14-16 µm were obtained using a Leica CM1850UV cryostat. Sections were stored at -80°C until needed for immunostaining.

Immunostaining

Slides were kept at RT 1 hour before starting the washes to remove the residual OCT medium. Afterwards, sections were washed three times with PBS and then were blocked for 1.5 hour at room temperature in PBS, 0.1% Tween20, 10% FCS, 0.1% BSA and 3% normal goat serum. Sections were placed in a humid chamber and incubated in primary antibodies diluted in blocking solution overnight at 4°C. Subsequently, sections were washed three times in PBS, 0.1% Tween20 and then incubated for 2 hours at RT in the dark with the corresponding Alexa Fluor-conjugated secondary antibodies (Invitrogen). Antibodies and dilutions are listed in Table 2.3. Stained sections were washed two times in PBS, 0.1% Tween20 and once in PBS and subsequently mounted with ProLong Diamond Antifade Mountant with DAPI (Thermo Fisher Scientific). Nail polish was applied at the border of the coverslip to prevent the embedding medium to evaporate. Sections were stored at 4°C.

Table 2.2 Antibodies used

| Name | Organism / type | Dilution | Company |
|----------------------------------|------------------------|-----------------|--------------------------------------|
| anti-DSRed | polyclonal rabbit IgG | 1:1000 | Takara/Clontech |
| anti-mCherry | polyclonal chicken IgY | 1:1000 | Novus Biologicals |
| anti-GFP | polyclonal chicken IgY | 1:2000 | Abcam |
| anti-3A10 | monoclonal mouse IgG1 | 1:10 | Developmental Studies Hybridoma Bank |
| anti-acetylated tubulin | monoclonal mouse IgG2b | 1:2000 | Sigma-Aldrich |
| anti-MAP2 | monoclonal mouse IgG1 | 1:5000 | Abcam |
| anti-gephyrin | monoclonal mouse IgG1 | 1:500 | Synaptic systems |
| anti- PSD95 | polyclonal rabbit IgG | 1:1000 | Abcam |
| anti-chicken Alexa Fluor 488 | polyclonal goat IgG | 1:1000 | Thermo Fisher |
| anti-chicken Alexa Fluor 555 | polyclonal goat IgG | 1:1000 | Thermo Fisher |
| anti-rabbit AlexaFluor 555 | polyclonal goat IgG | 1:1000 | Thermo Fisher |
| anti-rabbit Alexa Fluor 633 | polyclonal goat IgG | 1:1000 | Thermo Fisher |
| anti-mouse Alexa Fluor 633 | polyclonal goat IgG | 1:1000 | Thermo Fisher |
| anti-mouse IgG1 Alexa Fluor 555 | polyclonal goat IgG | 1:1000 | Thermo Fisher |
| anti-mouse IgG2b Alexa Fluor 633 | polyclonal goat IgG | 1:1000 | Thermo Fisher |

EDU incorporation assay

At 4 dpf Tg(olig1:nls-mApple, mbp:nls-EGFP) zebrafish embryos were incubated in 0.4 mM 5-ethynyl-2'-deoxyuridine (EDU) in Danieau's solution. After 6 h incubation, embryos were incubated for 15 minutes in 2mg/ml Pronase (Sigma Aldrich) and subsequently fixed for 2h in 4% PFA. Whole embryos or spinal cord sections were stained for EDU using the Click-IT Alexa Fluor 647 Imaging Kit (ThermoFisher Scientific) as detailed in the kit protocol, with the exception of a 1.5h Click-IT reaction incubation time. Afterwards, immunofluorescence staining was performed for transgene detection.

Slide imaging

To image stained cryosections a Leica TCS SP8 confocal microscope was used. Images were acquired using 63x/1.3NA glycerol and 63x/1.2NA H₂O objectives with at least 100 nm pixel size (xy) and 1 µm z-spacing. When images were acquired for subsequent deconvolution, x/y/z parameters were adjusted to be suitable for processing with Huygens software. Overview images (i.e. EDU experiment) were taken using 10x/0.4NA (acquisition with 568nm pixel size (xy), 2 µm z-spacing) and 20x/0.7NA (acquisition with 142nm pixel size (xy), 1 µm z-spacing) objectives. 488nm excitation wavelength was used to detect DAPI; 488 nm for EGFP and Alexa Fluor(AF) 488; 514 nm for EYFP; 552 and 561 nm for Alexa Fluor 555; 633 nm for Alexa Fluor 633.

2.5 Live cell imaging

Zebrafish mounting for confocal imaging

Prior mounting, fish were screened at a fluorescent dissecting microscope (Nikon SMZ18). When specified, fish were treated with 1:200 BODIPY 630/650-X (Thermo Fisher) 1 hour before imaging. Fish were anaesthetized with 0.2mg/ml tricaine (PHARMAQ) in Danieau's

buffer and mounted laterally in 1% low melting point (LMP) agarose (Invitrogen) on a glass coverslip. The coverslip was flipped over on a glass slide with a ring of high-vacuum grease filled with 0.2mg/ml tricaine in Danieau's buffer to prevent drying out of the agarose. For confocal calcium imaging embryos were previously immobilised with 0.5 mg/ml mivacurium chloride (Abcam), a non-depolarising neuromuscular-blocking drug diluted in Danieau's buffer. Afterwards, animals were laterally embedded in 1% LMP agarose in a glass bottom dish filled with 0.5 mg/ml mivacurium chloride in Danieau's buffer.

Confocal imaging

Confocal z-stacks were acquired as 12bit images with a pixel size between 114 and 151 nm x/y and a z-spacing of 1µm on Leica TCS SP8 laser scanning microscopes. When images were acquired for subsequent deconvolution, resolutions were increased to be suitable for processing with Huygens software. 448 nm was used for excitation of Cerulean; 488 nm for EGFP; 514 nm for EYFP; 552 and 561 nm for mApple, mScarlet, mCherry, tagRFP; 633 nm for BODIPY630/650. Z-stacks of PSD95-positive cells were acquired every minute for 15-20 minutes to timelapse PSD95 puncta.

For calcium imaging single plane timelapses were acquired as a 12bit images with a pixel size between 114 and 151 nm x/y at 2Hz. 488nm excitation wavelength was used to detect GCaMP fluorescence. For fast confocal live cell imaging of cell motility and GCaMP imaging 8 kHz resonant scanner was used.

To test capsaicin (Csn, Sigma-Aldrich) effects on TRPV1-positive cells, a baseline timelapse of 5 minutes was acquired. Afterwards, Csn was added to the glass bottom dish to reach the indicated concentration (2.5-6 µM) and after 15 minutes a second timelapse was acquired.

To study the effects of 4-aminopyridine (4-AP, Sigma-Aldrich) on neurons, a baseline timelapse was acquired. Embryos were incubated overnight in 0.1 mM 4-AP. After 4-AP treatment, another timelapse was acquired. To study the effects of tetrodotoxin (TTX, Abcam)

on neurons, a baseline timelapse was acquired. Afterwards, 10 μ M TTX was added to the glass bottom dish and after 1 hour incubation a second timelapse was recorded.

To study the effects of the pharmacological manipulations on OPCs, a baseline timelapse was acquired. Afterwards 4-AP, was added to the glass bottom dish to reach the final concentration (0.5 mM) and after 15 minutes a second 5-10 minute timelapse was taken. Subsequently, 4-AP solution was removed and tetrodotoxin (TTX, Abcam) working solution was added. After 1 hour a third timelapse was recorded.

After imaging, the animals were either sacrificed or released from the agarose using microsurgery blades and kept individually in Danieau's buffer until further use.

Zebrafish mounting for light-sheet imaging

3 dpf fish were screened at a fluorescent dissecting microscope (Nikon SMZ18) for the expression of GCaMP6m. At 4dpf, before imaging, larvae were paralysed using mivacurium chloride at the final concentration of 0.5mg/mL diluted in Danieau's buffer. Fish were laterally or dorsally embedded in u-shaped glass capillary in 1% LMP agarose. The u-shaped glass capillary was placed in a glass bottom dish filled with Danieau's buffer.

Light-sheet imaging

To characterise GCaMP transients in OPCs light-sheet images were acquired at a Leica TCS SP8 DLS using a 2.5x/0.07NA illumination objective and 10X/0.3NA and 25X/0.95NA detection objectives with 2.5 mm deflection mirrors. GCaMP fluorescence was acquired using 488nm excitation wavelength. A ROI was drawn around either individual cells or a portion (5-7 somites) of whole zebrafish spinal cord tissue. Time-lapses of z-stacks were taken with a frame rate of 0.5-1Hz for 2x10 minutes, with a break of 10 minutes in between.

To explore neuron-OPC calcium transients, 4 dpf fish were screened for GCaMP6m expression in OPCs and RGECO expression in neurons. Selected fish were imaged using a 2.5x/0.07NA illumination objective and 10X/0.3NA detection objective with 2.5 mm deflection mirrors. A single plane ROI of 2-4 somites was recorded for 10 minutes at 2 Hz. When specified, fish were treated, 15 minutes prior imaging, with 0.5 mM 4-AP.

Tile scan images of CaMPARI fish were acquired using 10X/0.3NA detection objective with 5 mm deflection mirrors. CaMPARI green and red fluorescence were acquired using 488nm and 552 excitation wavelength respectively.

2.6 Assessment of zebrafish swimming behaviour

Single 4 dpf zebrafish were placed in a 3 cm dish in 3 ml Danieau's solution (\pm 0.1 mM 4AP and/or 50 μ M TTX) and imaged for two minutes at 16 frames per second using a Hamamatsu Orca-05G camera equipped with a Kowa LM35JC10M objective.

2.7 Mivacurium chloride treatment

Mivacurium chloride working solution was prepared prior imaging from the 100 μ M stock solution (Abcam). Mivacurium chloride was used at the final working concentration of 1 μ M (0.5 mg/mL) dissolved in Danieau's buffer. 4dpf zebrafish embryos were incubated in the solution for 5 minutes and subsequently embedded for imaging.

2.8 Capsaicin treatment

Capsaicin (Csn, Sigma) 1mM stock solution was prepared by dissolving the compound in dimethyl sulfoxide (DMSO). 2.5-6 uM Csn working solution was made from the stock solution and dissolved in Danieau's solution reaching 0.2 % DMSO.

2.9 4-amminopyridine treatment

4-amminopyridine (4-AP, Sigma-Aldrich) working solution was prepared prior imaging from the 500mM stock solution. 3 and 4 dpf were incubated in 4-AP dissolved in Danieau's solution. For long-term treatments (6-48 hours), 4-AP was used at 0.1 mM. For short-term treatments (<1 hour), 4-AP was used at 0.5 mM.

2.10 Tetrodotoxin treatment

Tetrodotoxin (TTX, Abcam) working solution was prepared from the 1mM stock solution. Zebrafish embryos at 3 and 4 dpf were incubated in TTX diluted in Danieau's solution. For long-term treatments (6-48 hours) TTX was used at 50 μ M. For short-term treatments (<1 hour), TTX was used at 10 μ M.

2.11 Splitomicin treatment

Splitomicin (Sigma Aldrich) working solution was prepared from the 10mM stock solution. Zebrafish embryos were incubated from 2/3 dpf in 4-5 uM Splitomicin until analysis.

2.12 UV-light treatment

Five embryos were placed into a glass bottom dish with a diameter of 2 cm. A 405 nm LED for photoconversion was placed above the dish at a fixed distance and evenly illuminated the entire dish. Light intensity was measured prior every UV-light treatment using a power meter. To test the CaMPARI technique various light intensities (50 to 800 mW/cm²) and exposure times (2-10 minutes) were used. For experiments an intensity of 100 mW/cm² and an exposure time of 5 minutes were applied. Fish were exposed to photoconversion light under various conditions, including freely swimming in Danieau's buffer, in 0.5 mM 4-AP, in 10 μ M TTX or anaesthetized in 0.2mg/ml tricaine.

2.13 Image processing

Images were analysed using Fiji and Imaris 8.4.2 (Bitplane). Deconvolution was done with the Huygens Essentials version 16.10 1p2 (Scientific volume imaging, the Netherlands, <http://svi.nl>). Fiji was used to adjust the brightness and to perform all measurements. The plugin StackReg was sometimes used to register the images and timelapses. Adobe Illustrator C6 was used to arrange the figures.

2.14 Data analysis

Cell reconstruction

OPC morphology reconstruction was done using the Imaris Filament Tracer. At first, OPC processes were traced using the automatic dendrite detection combined with manual correction. This analysis automatically provided the information about total process length. To quantify the process length only in the axo-dendritic areas, processes were traced taking into account the BODIPY staining and using the 3D viewer in Imaris.

Counting of cell and post-synaptic puncta

All cell number quantifications were done manually using Fiji. For a precise estimation cells were counted taking into account the z-stack images. To evaluate EDU positive cells, a transgenic line with a nuclear-targeted fluorescence protein was used. Macrophages and EDU positive cells were quantified using the Cell Counter Fiji plugin. Post-synaptic densities were manually quantified using the Point tool on Fiji.

Fluorescent intensity measurement

To measure the intensity of post-synaptic puncta, a rectangular ROI was drawn around a dendrite. The pixel intensity was measured using the Plot Profile in Fiji and the measurements were exported in Graphpad Prism to plot the graph.

GCaMP imaging analysis

To trace the GCaMP transients, for single cell analysis, regions of interest (ROIs) were drawn, using the Fiji ROI manager, around the somata and processes of single OPCs. To trace the GCaMP transients, for cell population analysis, ROIs were drawn only around OPC somata. Traces of individual ROI are shown as $\Delta F/F_0$ given by the maximum fluorescent intensity of individual ROI at each time point and normalised to the first 100 frames of each ROI using Matlab. To count GCaMP transients as events, a threshold of 40% above average fluorescence was established for the frequency of somatic transients, and of 30% for all other analysis. The duration of GCaMP transients was quantified considering the half-width of the maximum $\Delta F/F_0$ for each event.

To analyse dual color calcium imaging, ROIs were drawn around axons and neuron cell bodies (RGECO-positive) and around OPC somata (GCaMP-positive). Traces of individual ROI are shown as $\Delta F/F_0$ given by the maximum fluorescent intensity of individual ROI at each time point and normalised to the first 100 frames of each ROI using Matlab.

To assess changes in GCaMP after capsaicin treatment, I used maximum intensity of GCaMP fluorescence of ROI that were drawn around the same cells/processes in the baseline and in the capsaicin-treated timelapses. For each ROI, fluorescence was normalised to the first 100 frames in Matlab.

To analyse changes in GCaMP frequency after pharmacological treatments, I used mean intensity of GCaMP fluorescence traces in ROI that were drawn around the same cells/processes in each treatment condition (baseline, after 4-AP, after TTX). For each ROI, fluorescence was normalised to the first 100 frames using Matlab, and GCaMP events were determined using a threshold of 30% above average fluorescence change using the spike detrend function.

CaMPARI analysis

Quantification of red/green ratio was done using Fiji. ROIs were drawn, using ROI manager, around OPC somata and the mean fluorescence intensity was measured in the red and in the green channels of each ROI. An additional ROI was drawn as reference for the background subtraction and the mean fluorescence intensity was measured. All data were exported into Excel where background subtraction and red/green rate were calculated.

2.15 Statistics

Statistical analysis was done with Graphpad Prism. All data were tested for normal distribution using the Shapiro-Wilk normality test. In the figures, normally distributed data are shown as mean \pm standard deviation (SD) or 95% confidence intervals (CI), whereas non-normally distributed data are given as median with the 25% and 75% percentiles. When data were normally distributed to compare two groups unpaired t-test was performed. Non-normally distributed data were analysed for statistical significance using Mann-Whitney U test (unpaired data) and Wilcoxon signed-rank test (paired data). To compare multiple (>2) groups ANOVA was used in combination with Tukey's (paired data) or Kruskal-Wallis (unpaired data) multiple comparisons test. To analyse contingency tables, Fisher's exact test was used. P-values are indicated as *(p < 0.05), **(p < 0.01), ***(p < 0.001) in the figures.

2.16 Buffers and Solutions

Danieau's Buffer

| Reagent | Quantity for 900ml 30X stock solution |
|--|---------------------------------------|
| NaCl (Roth) | 91.52g |
| KCl (Roth) | 1.41g |
| MgSO ₄ (VWR Chemicals) | 2.66g |
| Ca(NO ₃) ₂ (Roth) | 3.83g |
| Hepes (Roth) | 32.17 |
| Distilled Water | Ad 900ml |
| Adjust pH to 7.6 | |

Working solution: 1x Danieau's 10ml 30x Stock solution plus 990ml distilled water

Tricaine

| Reagent | Quantity for xM Tricaine solution |
|------------------------------------|-----------------------------------|
| Tricaine/MS-222 (PharmaQ, UK) | 400mg |
| Distilled water | 100ml |
| Tris (Alfa Aesar) pH adjusted to 9 | 2ml |
| Adjust pH to 7 | |

Mivacurium Chloride

100x Stock solution

| Reagent | Quantity for 50mg/mL stock solutions |
|-----------------------------|--------------------------------------|
| Mivacurium Chloride (Abcam) | 25 mg |
| Distilled water | 500 μ l |

Working solution

| Reagent | Quantity for 400 μ l of 0.5mg/mL solution |
|--|---|
| Mivacurium chloride stock solution (100 μ M) | 4 μ l |
| Distilled water | 36 μ l |
| Danieau's | 360 μ l |

Capsaicin

Stock solution

| Reagent | Quantity for 100mM Stock solution |
|---------------------------|-----------------------------------|
| Capsaicin (Sigma Aldrich) | 50 mg |
| DMSO (Sigma Aldrich) | 1.637ml |

4-amminopyridine

Stock solution

| Reagent | Quantity for 500mM Stock solution |
|----------------------------------|-----------------------------------|
| 4-amminopyridine (Sigma-Aldrich) | 1 g |
| Distilled water | 21.2ml |

Tetrodotoxin

Stock solution

| Reagent | Quantity for 1mM Stock solution |
|----------------------|---------------------------------|
| Tetrodotoxin (Abcam) | 1 mg |
| Distilled water | 3.123ml |

Splitomicin

Stock solution

| Reagent | Quantity for 10mM Stock solution |
|-----------------------------|----------------------------------|
| Splitomicin (Sigma Aldrich) | 5 mg |
| DMSO (Sigma Aldrich) | 2.522ml |

3 RESULTS

3.1 OPC characterisation in the zebrafish spinal cord

3.1.1 OPC localisation in the zebrafish spinal cord

Oligodendrocyte Precursor Cells (OPCs) can differentiate to myelinating oligodendrocytes, which form electrically isolating myelin sheaths around axons and are essential for rapid nerve conduction. Myelination is a dynamic and activity-dependent process. OPCs sense axonal activity through the expression of neurotransmitter receptors and they form functional synaptic contacts with neurons (Bergles 2000). Neural activity regulates OPC fate, proliferation and differentiation, thereby controlling their potential contribution to myelination (Gibson et al., 2014).

To better understand the mechanisms by which neural activity is integrated by OPCs, I started characterising the OPC population within the zebrafish spinal cord, with regard to OPC morphology and position. The main purpose of these experiments was to define OPC position in the zebrafish spinal cord at different developmental ages to study if OPCs in different locations in the spinal cord have the same morphology. Moreover, I also characterised the environment and different cell types by which OPCs are surrounded. As in the mammalian CNS, differences in OPC ability to differentiate have been identified between white and grey matter. White matter OPCs in the cerebral cortex have a higher differentiation and proliferation rate than grey matter ones suggesting that the environment surrounding OPCs plays an important role in determining their behaviour (Viganó and Dimou 2016). Therefore, the description of OPC position in the spinal cord, related to their surroundings, is necessary to delineate any type of analogy with the mammalian CNS and to highlight possible location and environmental differences between OPCs.

I labelled OPCs using a double transgenic line in which nuclear- and membrane-targeted fluorescence proteins (nls-mApple and memEYFP, respectively) were expressed in OPCs under control of *olig1* gene regulatory sequences (oligodendrocyte transcription factor 1)

(Schebesta et al., 2009). Whole animal imaging of this OPC line revealed that OPCs constitute a dense population throughout the zebrafish CNS (Fig. 3.1A).

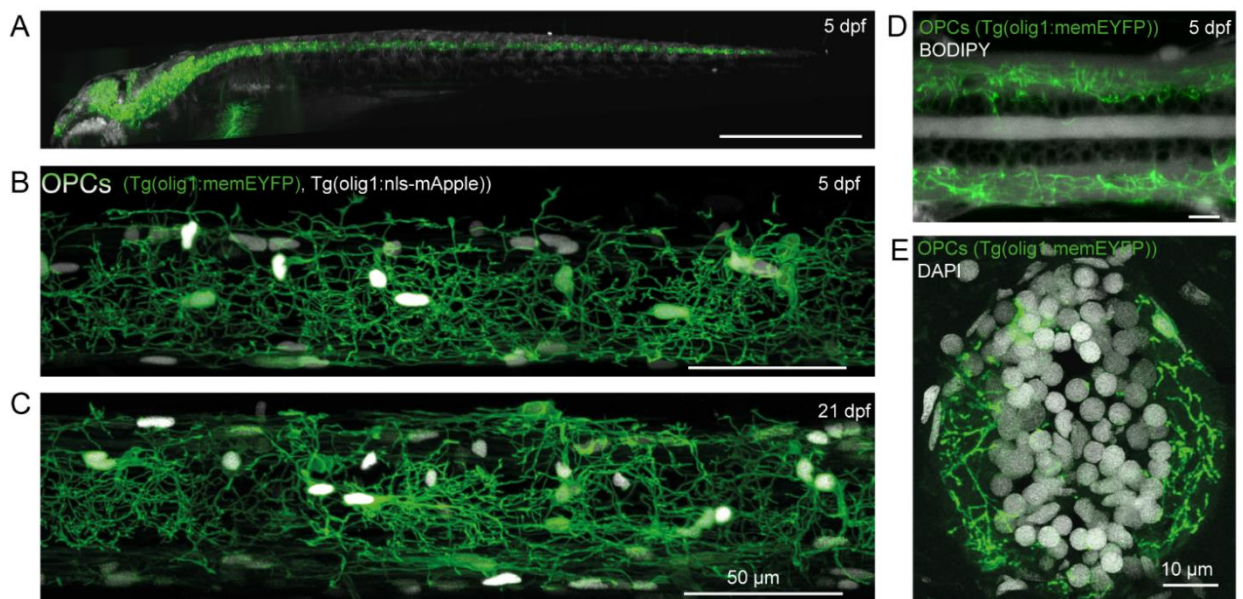


Fig. 3.1 Oligodendrocyte Precursor Cells in the zebrafish spinal cord

A) Lightsheet microscopy image of whole *Tg(olig1:memEYFP)* transgenic animal at 5 days post-fertilisation (dpf). Scale bar: 1mm. **B)** Confocal image of a *Tg(olig1:memEYFP)*, *Tg(olig1:nls-mApple)* zebrafish, lateral view of the spinal cord at 5 dpf. Scale bar: 50 μ m. **C)** Confocal image of a *Tg(olig1:memEYFP)*, *Tg(olig1:nls-mApple)* zebrafish, lateral view of the spinal cord at 21 dpf. Scale bar: 50 μ m. **D)** Dorsal confocal image of a *Tg(olig1:memEYFP)* zebrafish stained with BODIPY showing OPC processes projecting in the lateral side of the spinal cord at 5 dpf. Scale bar: 10 μ m. **E)** Cross-sectional view of the spinal cord showing the distribution of OPC processes in *Tg(olig1:memEYFP)* at 7dpf. Scale bar: 10 μ m. (Marisca et al., 2020)

Higher magnification imaging highlighted a dense network of OPC processes in the zebrafish spinal cord at 5 days post fertilisation (dpf) (Fig. 3.1 B). This network was maintained at the later age of 21 dpf (Fig. 3.1 C).

Furthermore, I combined OPC dorsal imaging with BODIPY (4,4-Difluoro-4-Bora-3a,4a-Diazas-Indacene) staining to delineate the outlines of the different parts of the spinal cord. The medial part is recognisable by the central canal and the area where all neuron cell bodies are, identified by the incorporation of BODIPY in the cell membrane. The lateral side of the spinal cord is where most of OPC processes reside (Fig. 3.1 D). Cross section images of the membrane targeted OPC line, stained also with DAPI (4',6-diamidino-2-phenylindole) a nuclear dye, confirmed that OPCs project their processes into the lateral spinal cord and almost no processes were found in the cell body region of the medial spinal cord (Fig. 3.1 E).

To describe the area where OPCs extend their processes and what they contact, I also wanted to look at axons and co-label them using a myelin and an axon labelling.

The axons in the zebrafish spinal cord run in stereotypic position along the lateral side with the myelinated axons located mostly in the ventral and dorsal spinal cord tracts.

To identify myelinated axons, I used a transgenic line where a fluorescence protein (memCerulean) was driven by the promoter mbp (myelin basic protein) (Auer et al., 2018) combined with an OPC line. Lateral spinal cord imaging allowed me to observe myelinating oligodendrocytes mostly at the ventral and dorsal side of the spinal cord (Fig. 3.2 A).

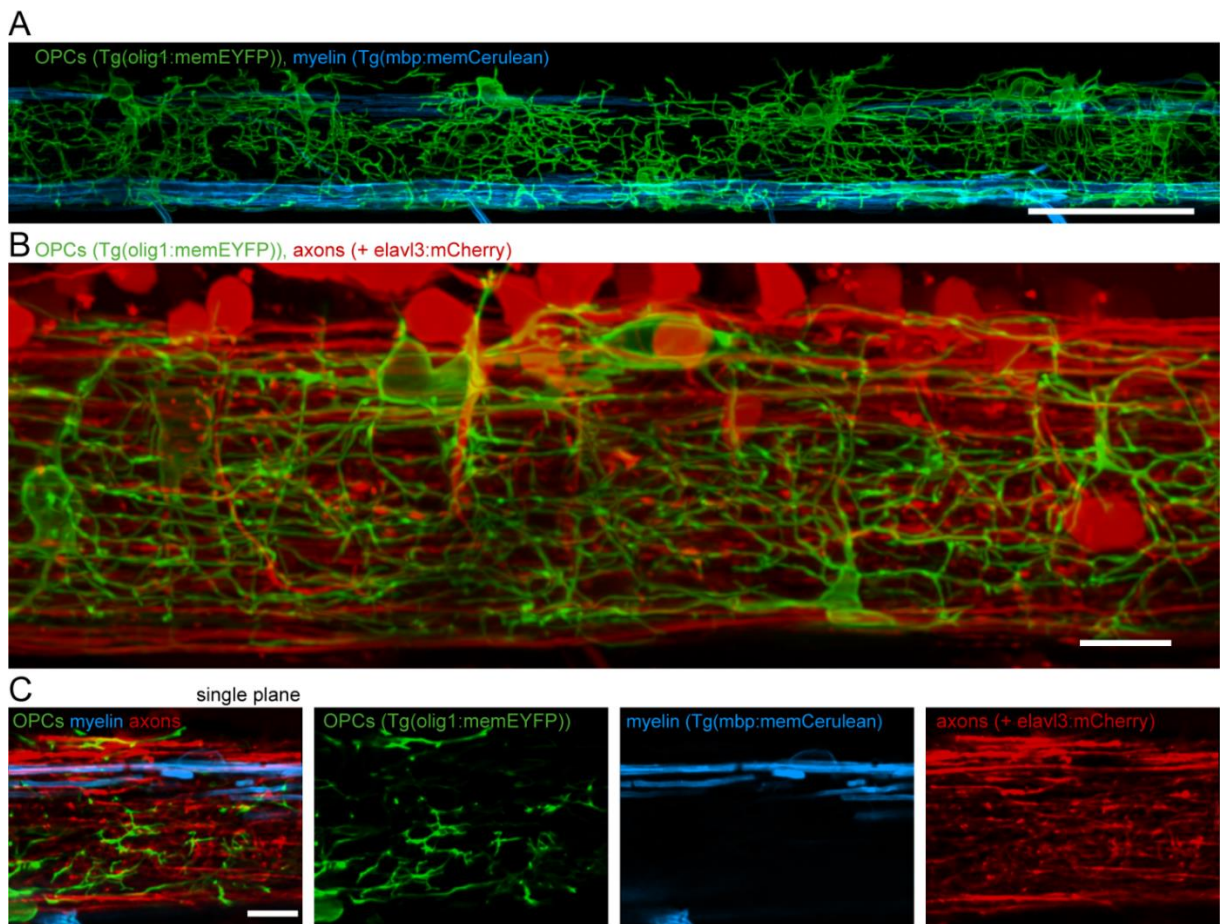


Fig. 3.2 OPCs, axons and myelin in the zebrafish spinal cord

A) Confocal image of a Tg(olig1:memEYFP), Tg(mbp:memCerulean) zebrafish, lateral view of the spinal cord at 5 dpf. Scale bar: 50 μ m. **B)** Confocal image of a Tg(olig1:memEYFP) fish injected with elavl3:mCherry, lateral view of the spinal cord at 4 dpf. Scale bar: 10 μ m. **C)** Single plane confocal images of a Tg(olig1:memEYFP), Tg(mbp:memCerulean) + elavl3:mCherry lateral view of the spinal cord at 5 dpf, showing that OPC processes are located in the lateral spinal cord with myelinated and unmyelinated axons. Scale bar: 10 μ m.

Furthermore, I injected mCherry under the *elavl3* promoter, a neuron-specific RNA-binding protein (Coolen et al., 2012), into *Tg(olig1:memEYFP)* to transiently label axons and OPCs. OPCs form a dense network in the lateral spinal cord where also axons are (Fig. 3.2 B). The combination of axons, OPCs and myelin labelling in the same animal and high-resolution single plane images revealed that OPC processes reside in the same region as myelin and axons (Fig. 3.2 C). In addition to lateral views which highlight the process network that OPCs create within the lateral axonal tract, I used cross sectional immunostaining to identify the position of myelinated and unmyelinated axons within the spinal cord volume. Myelinated axons, labelled by using the *Tg(mbp:EGFP-CAAX)* line, were located mostly ventrally and dorsally in both side of the spinal cord stained with DAPI (Fig. 3.3 A). To have a closer analysis of the axonal tracks, to further describe the environment where OPC processes project, I labelled axons and dendrites using antibodies against acetylated tubulin and MAP2 (microtubules-associated protein 2) respectively. Both of them constituted the lateral spinal cord. The DAPI staining highlighted the position of the cell bodies in the central part of the spinal cord (Fig. 3.3 B). As both OPC processes and axons create a dense network in the lateral spinal cord and they also form synaptic contacts (Bergles et al., 2000), I also wanted to visualise synapse position in the zebrafish spinal cord using pre- and post-synaptic markers. I generated the *Tg(elavl3:synaptophysin-tagRFP)* transgenic line to label the presynaptic site in neuron under the *elavl3* promoter, a widely used pan-neuronal marker. Synaptophysin is a synaptic vesicle protein which localises to pre-synaptic sites. I performed immunostaining using gephyrin as a post-synaptic marker to detect synaptic structures which were also located in the lateral spinal cord (Fig. 3.3 C).

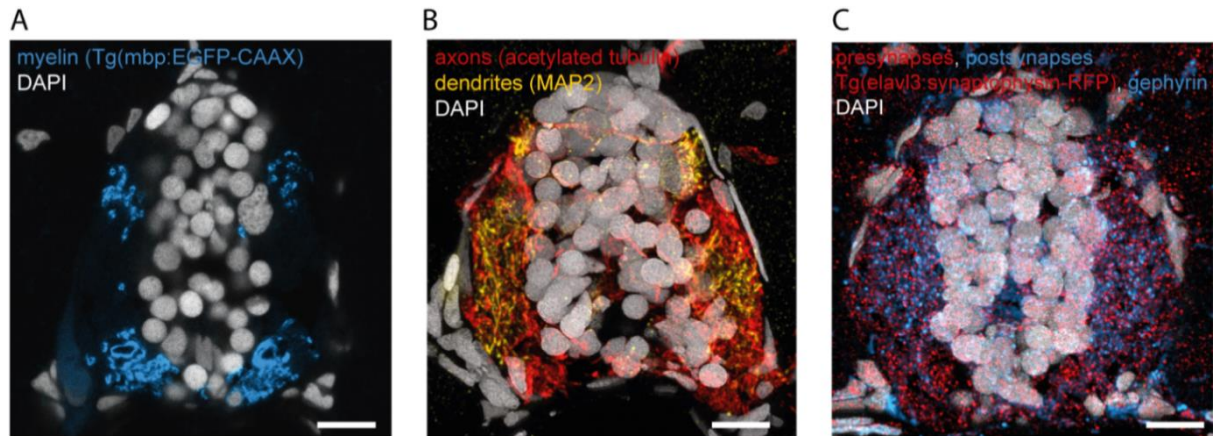


Fig. 3.3 Lateral spinal cord consists of myelinated and unmyelinated axons and synapses

A) Cross-sectional view of the spinal cord showing the distribution of myelin in Tg(mbp:EGFP-CAAX), stained with DAPI. Scale bar: 10 μ m. **B)** Cross-sectional view of the spinal cord showing the distribution of axons and dendrites stained respectively with anti-acetylated tubulin and anti-MAP2 and DAPI at 7dpf. Scale bar: 10 μ m. **C)** Cross-sectional view at the level of the spinal cord showing the distribution of pre- and post-synapses (Tg(elavl3:synaptophysin-RFP) and anti-gephyrin). Scale bar: 10 μ m. (Marisca et al., 2020)

To summarise, OPCs have a characteristic morphology with several process ramifications that form a dense network within the lateral spinal cord. Myelinated and unmyelinated axons have stereotypical positions in the lateral spinal cord with the myelinated axons occupying mostly the ventral and dorsal axonal tracks. The lateral spinal cord includes also pre- and post-synaptic sites as well as dendrites, axons and OPC processes suggesting that most of the contacts can be found in the lateral spinal cord. The lateral spinal cord, where OPC processes reside, is constituted of myelinated, unmyelinated axons, dendrites and synapses and I will refer to it as ‘axo-dendritic areas’. The medial region of the spinal cord is mostly composed of cell bodies, highlighted by DAPI staining, and I will describe it as ‘neuron-rich areas’ throughout this thesis.

OPCs extend several processes in the axo-dendritic area of the zebrafish spinal cord which is composed of myelinated as well as unmyelinated axons. To further investigate single OPC morphology and to look at possible differences in terms of shape and position amongst OPCs in the zebrafish spinal cord, we transiently injected olig1:memYFP to sparsely label OPCs (Fig. 3.4 A). In the image example presented here, five distinct OPCs were detected using transient injections. 3D reconstruction of two OPCs (cell#1 – cell#2) using Imaris software allowed us to

discriminate between these cells that were located in the same area and to define their process ramification. Cell#1 presented a relatively simpler process ramification compared to cell#2 (Fig. 3.4 A). Images taken were rotated for 90 degrees and combined with BODIPY staining to analyse OPC soma position of cell#1 and cell#2 in the spinal cord. The rotation showed that one OPC cell body (cell#1) resides in the axo-dendritic areas and the other one (cell#2) in the neuron-rich areas (Fig. 3.4 B). Independent of soma position, all OPC processes projected into the axo-dendritic areas. There was no difference in the percentage of OPC processes occupying the axo-dendritic areas between OPCs with their somata in the axo-dendritic areas and OPCs with their somata residing in the neuron-rich areas (mean $91.3\% \pm 2.3$ SD neuron-rich vs. $98.9\% \pm 0.7$ SD axo-dendritic; $n=5$ cells/condition from 6 animals) (Fig. 3.4 C).

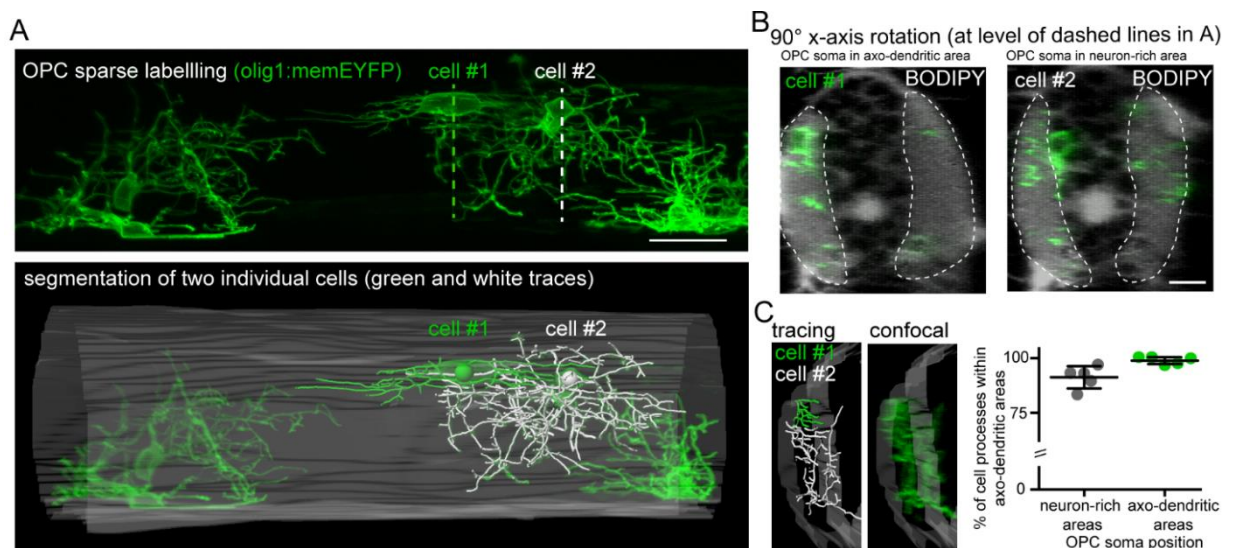


Fig. 3.4¹ OPC processes reside in the axo-dendritic areas of the spinal cord, independent of OPC soma position

A) Top: sparse labelling of olig1:memEYFP expressing OPCs at 4dpf. Bottom: Tracing of two neighbouring exemplary OPCs and the spinal cord outlines. Dotted lines indicate the position of the y-axis rotations shown in B. **B)** 90° y-axis rotations of at the level of the soma of each of the two cells shown to the left with a BODIPY counterstain to reveal the position of OPC somata in axo-dendritic (cell #1) and neuron-rich (cell#2) regions. Dotted lines indicate axo-dendritic areas. Scale bar: 20 μ m. **C)** High-magnification view showing the proximity of the processes made by the two OPCs shown in panel A within axo-dendritic areas. Quantification shows the percentage of cell processes resident in axo-dendritic areas formed by OPCs with their soma in neuron-rich and axo-dendritic regions at 4-5dpf. (mean $91.3\% \pm 2.3$ SD neuron-rich vs. $98.9\% \pm 0.7$ SD axo-dendritic); $n=5$ cells/condition from 6 animals. (Marisca et al., 2020)

¹ All images in this figure are from the work of my colleague Tobias Hoche. Tracing and quantification of OPCs in the graph of panel C were done by me.

Therefore, even if OPC processes were found in the same local environment, we found differences in morphology and process dynamics and the different features corresponded to OPC soma position localised to different areas within the spinal cord. One hour time-lapse of single labelled OPCs revealed that axo-dendritic area OPCs continuously remodelled all their processes, whereas neuron-rich area OPCs remodelled only the terminal portion of their processes maintaining stable their main branches. Neuron-rich area OPCs had stable and highly ramified processes. On the other hand, axon-dendritic area OPCs presented highly dynamic processes and simpler morphology (Fig. 3.5) (Marisca et al., 2020).

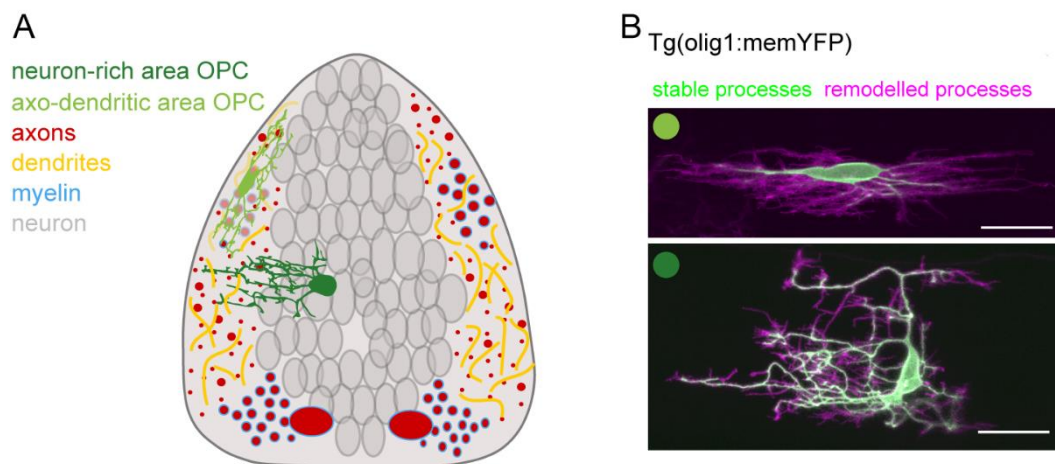


Fig. 3.5 OPC process remodelling

A) Schematic overview depicting the positioning of OPCs in the zebrafish spinal cord. **B)** ²Projections of 60 minutes time-lapse imaging of olig1:memYFP positive cells to show remodelled and stable processes of OPCs with their soma in different regions. (Marisca et al., 2020)

To summarise, single OPC labelling showed that OPC cell bodies can have different soma position either in the axon-dendritic areas or in the neuron-rich areas. However, all OPC processes projected in the axo-dendritic areas, sharing the same environment. The two different OPC cell body positions correlated with differences in morphology and process dynamics. OPCs with their soma residing in the axo-dendritic areas showed simpler process ramification and faster process remodeling compared to OPCs with their soma located in the neuron-rich areas. This suggested the presence of two different subgroups showing different morphology and soma position in the zebrafish spinal cord.

² Images from the work of my colleague Tobias Hoche

3.1.2 OPC properties within the zebrafish spinal cord and their contribution to myelination

The previous descriptive experiments and analyses showed that in the zebrafish spinal cord OPCs can be grouped in two categories. OPCs that have their somata located in the neuron-rich areas, which have a rather complex morphology and more stable processes compared to OPCs with their somata located in the axo-dendritic areas that have a simpler morphology and dynamic processes. Both OPC types extended their processes in the same axo-dendritic areas in the lateral spinal cord (Fig. 3.6 A).

Longitudinal studies, done by my colleague Tobias Hoche, following single OPCs, investigated the contribution of these two different groups of OPCs to myelination. It was shown that neuron-rich area OPCs usually do not differentiate directly to myelinating oligodendrocytes. In contrast, axo-dendritic area OPCs can directly differentiate to generate myelinating oligodendrocytes. However, neuron-rich area OPCs can also contribute to myelination but only after a recent cell division. Therefore, these data highlight two factors, one extrinsic and one intrinsic, that define the differentiation potential of the two OPC subgroups. The extrinsic determinant is represented by the local environment surrounding the cell body. Neuron-rich area OPCs have their somata surrounded by other cell bodies. On the other hand, the environment surrounding the somata of axo-dendritic area OPCs is constituted by the neuropil. The intrinsic determinant is characterised by the recent cell division which is necessary to enable a neuron-rich area OPCs to indirectly contribute to myelination. Moreover, these analyses defined the interrelation between the two OPC subgroups. Neuron-rich area OPCs need to divide to give rise to new daughter cells which could have axo-dendritic OPC features and be primed to differentiation. After acquiring one of the two OPC subgroup features, OPCs do not switch towards the other group (Marisca et al., 2020) (Fig. 3.6 B).

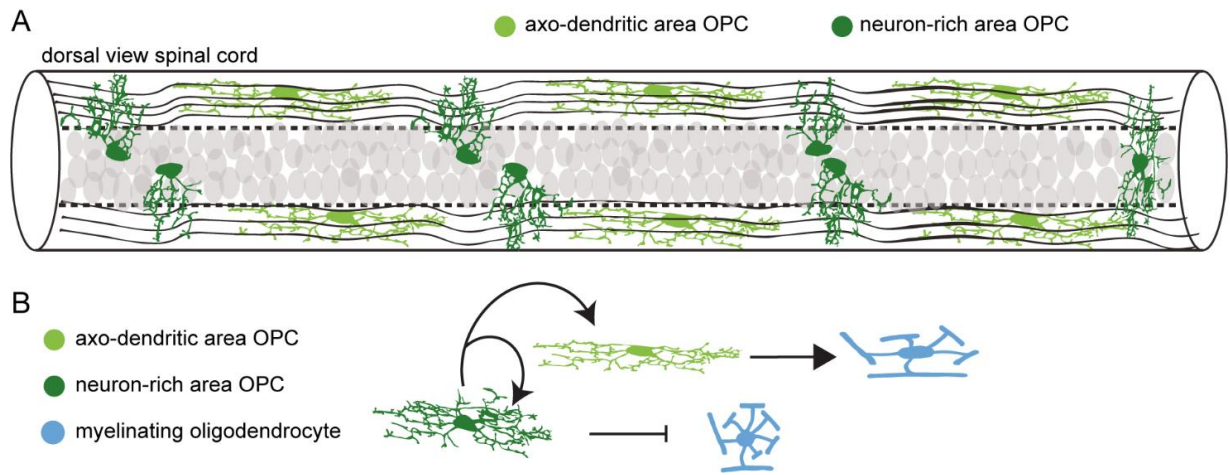


Fig. 3.6 Schematic of OPC subgroups properties

A) Cartoon representing the location of the two groups of OPCs in spinal cord from the dorsal view. OPCs with their somata in the axon-dendritic area and OPCs which somata reside in the neuron-rich area. Both OPC groups expand their processes in the axo-dendritic area. **B)** Schematic representing the relationship between the two OPC groups and their behaviour. Neuron-rich area OPCs, which have a more complex morphology, do not directly differentiate but they can proliferate to give rise to a axo-dendritic area OPCs. Axo-dendritic areas OPCs, have a simpler morphology and are the cells that more likely differentiate to give rise to myelinating oligodendrocytes. (Marisca et al., 2020)

To further study how necessary division events to form OPCs that can differentiate into myelinating oligodendrocytes are, we increased oligodendrocyte differentiation using splitomicin. Splitomicin is a selective inhibitor of the Sir2p, a NAD⁺-dependent histone deacetylase (HDAC), which was identified in an automated screen in zebrafish as a compound that increments oligodendrogenesis and myelination (Early et al., 2018). This is important to understand whether neuron-rich area OPCs in an enhanced oligodendrogenesis condition, behave differently and if they differentiate directly into myelinating oligodendrocytes or if they need to divide before. As increases in oligodendrogenesis are often combined also with an increase in OPC proliferation, several different outcomes are expected from this experiment. On the one hand, neuron-rich area OPCs, treated with splitomicin, could differentiate directly into myelinating oligodendrocyte, which would suggest that neuron-rich area OPCs do have the intrinsic potential to directly form new myelinating oligodendrocytes if oligodendrogenesis is increased. On the other hand, these OPCs could still need a preceding division event before they can differentiate into oligodendrocytes. The latter would strengthen the differential

differentiating potential of the two OPC subgroups and would create a link as well between the two subgroups.

At first, we tested splitomicin effects in our system, and incubation with splitomicin (4-5 μM) , from 2 to 4 dpf indeed had a 1.5-fold increase of myelinating oligodendrocyte number (13.6 ± 0.9 cells/field vs. 20.4 ± 1.0 cells/field, $p<0.001$, unpaired t-test) (Fig. 3.7 A). Then, I followed individual neuron-rich area OPCs from 3 to 5 dpf in control condition or treated with splitomicin (4-5 μM) to test which OPCs account for the increase in myelinating oligodendrocyte formation. The daily imaging is a good temporal resolution to detect division or differentiation events of sparsely labelled OPCs. More OPCs in control condition were quiescent compared to the ones treated with splitomicin (control vs splitomicin: 64% (21/33) vs. 45% (15/33) quiescent, $p=0.22$, two-tailed Fisher's exact test). Neuron-rich area OPCs treated with splitomicin gave rise to myelinating oligodendrocytes only after a cell division and their contribution to myelination was significantly higher than the control neuron-rich area OPCs (control vs splitomicin: 0% (0/33) vs. 18% (6/33) differentiation following division, $p= 0.02$, two-tailed Fisher's exact test). None of the neuron-rich area OPCs directly differentiated into a myelinating oligodendrocyte (Fig. 3.7 B). From these cell fate data, I confirmed that neuron-rich area OPCs do not directly contribute to myelination but they can proliferate and one or both daughter cells can have the ability to differentiate into a myelinating oligodendrocyte. Moreover, the increase in myelinating oligodendrocytes, triggered by splitomicin treatment, derives from recently divided neuron-rich area OPCs.

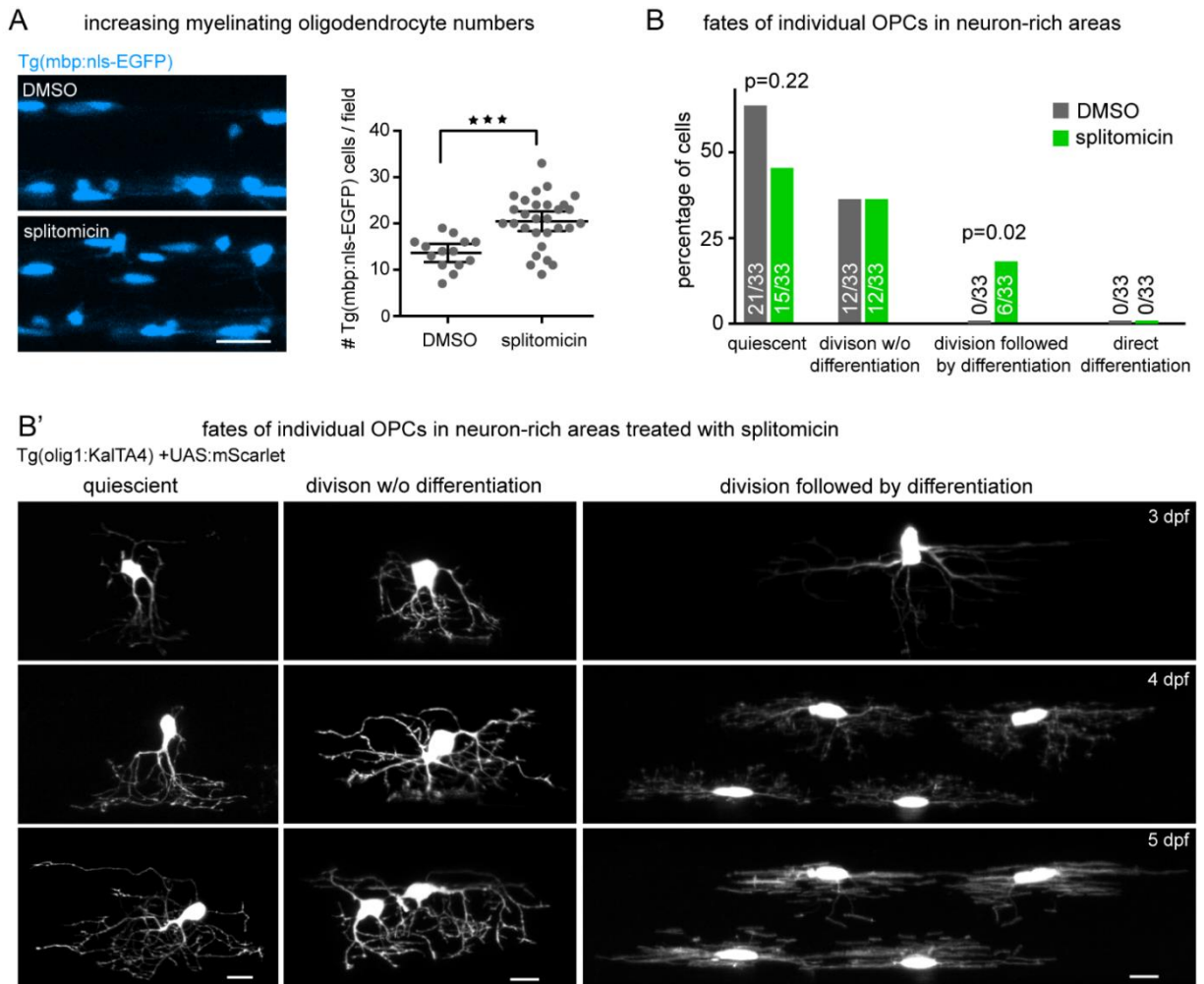


Fig. 3.7 Neuron-rich area OPCs contribute to myelination only after a division event

A) ³Representative images and quantification of increased oligodendrocyte differentiation in control upon splitomicin treatment from 2 to 4 dpf. Data shown as mean \pm 95% confidence interval (13.6 ± 0.9 cells/field vs. 20.4 ± 1.0 cells/field, $p < 0.001$ (unpaired t-test, two tailed, $t = 4.184$, $df = 41$), $n = 14/29$ animals. Scale bar: 20 μ m. **B)** Quantification of fates of OPCs in neuron-rich areas between 3-5 dpf, with and without splitomicin (control vs splitomicin: 64% (21/33) vs. 45% (15/33) quiescent, $p = 0.22$ (two-tailed Fisher's exact test); 0% (0/33) vs. 18% (6/33) differentiation following division, $p = 0.02$ (two-tailed Fisher's exact test); $n = 23$ animals per group. **B')** Example confocal images of possible fates of individual neuron-rich area OPCs after splitomicin treatment. Scale bar: 10 μ m. (Marisca et al., 2020)

³ Data shown in panel A are from the work of my colleague Laura Hoodless

3.1.3 Axon-OPC synaptic contacts in zebrafish

In the previous section, I showed that OPCs with their soma in the neuron-rich areas have a complex morphology, show slow process remodelling and they need to proliferate before differentiating into myelinating oligodendrocytes. Conversely, OPCs with their soma residing in the axo-dendritic areas, have a simpler morphology, show faster process remodelling and can differentiate directly into myelinating oligodendrocytes (Marisca et al., 2020). Oligodendrogenesis and OPC proliferation are regulated by axon activity, OPCs integrate the neural signalling through the expression of neurotransmitter receptors (Lin and Bergles, 2004; Káradóttir et al., 2005; Kukley et al., 2007). Indeed, OPCs interact with axons through synaptic contacts, which were for the first time described by electron microscopy (Bergles et al., 2000). The functions of these contacts are not yet clear; although one hypothesis is that such axon-OPC contacts are involved into regulating activity-dependent adaptive myelination.

Since we identified two different OPC subpopulations, I wondered whether they also had distinct ability to form synaptic contacts. Since synapses should be quite stable, I would expect that OPCs that show less process remodelling dynamics and that do not directly differentiate are potentially the cells able to form such contacts. In contrast, OPCs primed for differentiation are very motile which could prevent the formation of stable synaptic contacts with axons.

Before looking at differences between the two OPC subpopulations, I needed to address if zebrafish OPCs form synapses at all and if I could identify them in the spinal cord. To label synapse-like sites, I used histological analysis to localise the post-synaptic marker PSD95 (postsynaptic density protein 95) in OPCs of the zebrafish spinal cord. Cross section immunostaining of olig1:memEYFP fish with anti-PSD95 revealed that PSD95 expression was found in the somata of the medial as well as in the lateral spinal cord (Fig. 3.8 A). By looking at the 3D stack images, it was difficult to localise PSD95 expression in OPC processes as most of the PSD95 puncta were probably expressed in neurons. Some of them may also be found inside OPC processes, however it was not possible to draw a clear conclusion from this type of analysis (Fig. 3.8 B).

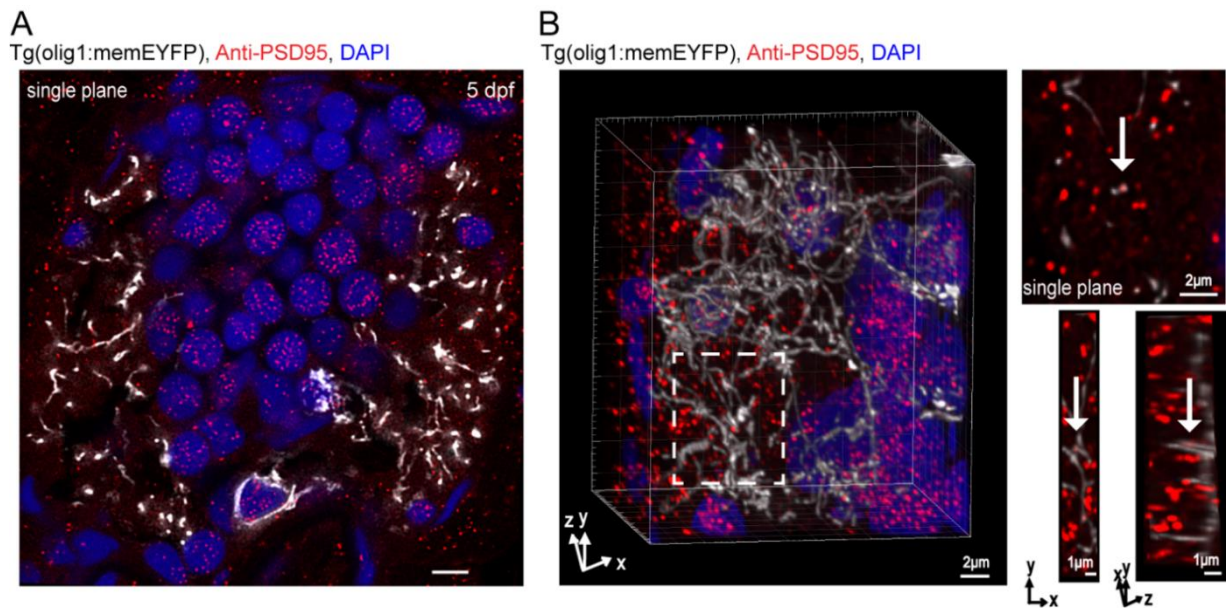


Fig. 3.8 Post-synaptic expression in the zebrafish spinal cord revealed by immunostaining

A) Single plane cross-sectional view of the spinal cord showing an overview of the distribution of PSD95 (anti-PSD95) in Tg(olig1:memEYFP) and DAPI staining at 5 dpf. Scale bar: 10 μm . **B)** Left: Higher resolution and deconvolved 3-D representation of Tg(olig1:memEYFP) spinal cord cross-section stained with anti-PSD95 and DAPI. Scale bar: 2 μm . Top right: single plane of the area indicated on the left by a dashed rectangle, showing a PSD95 puncta in a OPC process (white arrow). Scale bar: 2 μm . Bottom: projection and 3-D rotation of the puncta indicated in the top panel inside the OPC process. Scale bar: 1 μm .

Therefore, I used the UAS:PSD95-EYFP construct where PSD-95 is linked to a fluorescent protein (EYFP) to localise PSD95 *in vivo* (Niell et al., 2004). I transiently injected this construct into a gal4 line to get sparse cell labelling in zebrafish spinal cord. As a control, I injected the PSD95 construct into a neuronal gal4 line, under the contactin 1b promoter (cntn1b) which labels a subset of neurons. PSD95 expression in neurons *in vivo* was characterised by several PSD95 puncta in the soma but also along the dendrites (Fig. 3.9 A).

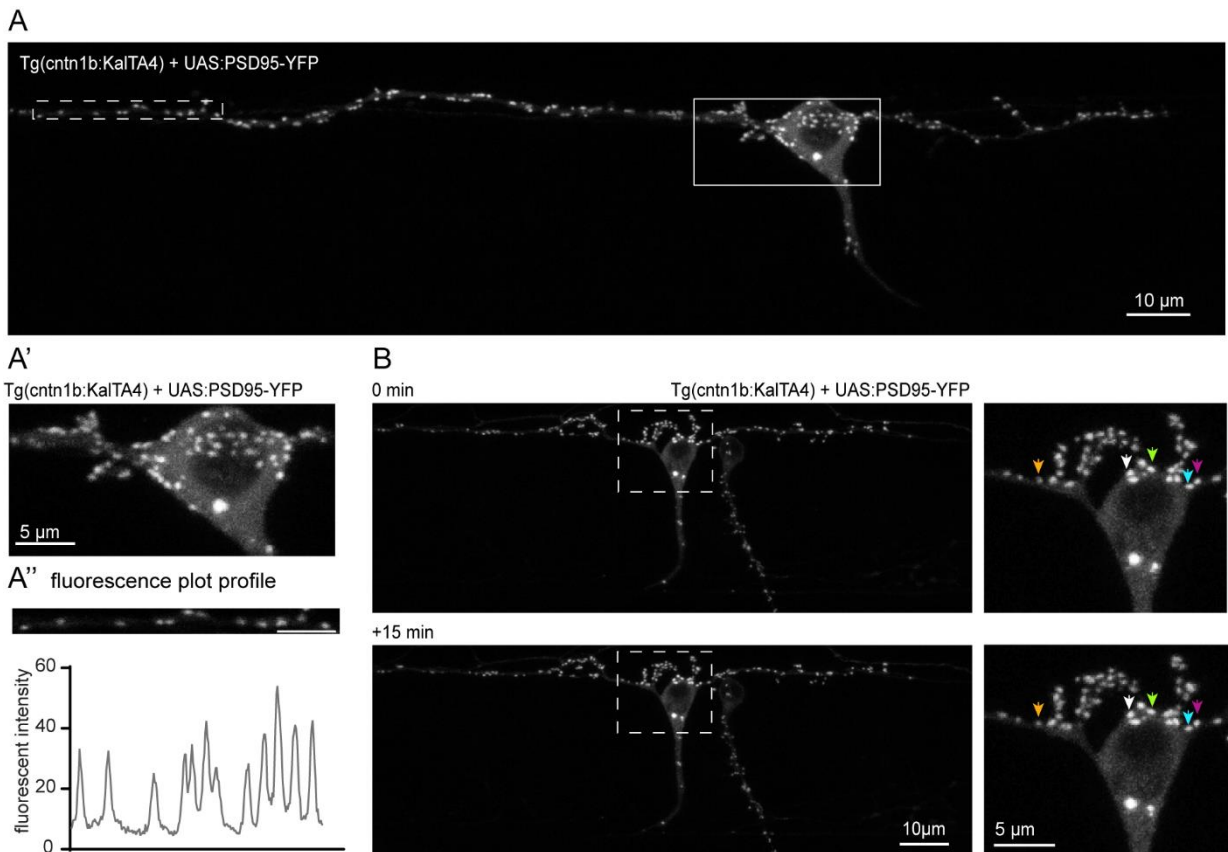


Fig. 3.9 PSD95 expression is stable in neurons

A) Projection of Tg(cntn1b:KalTA4) +UAS:PSD95-YFP showing PSD95-positive neuron in the zebrafish spinal cord. Scale bar: 10 µm. **A')** Close up of the box area expressing PSD95 in the neuron somata. Scale bar: 5 µm. **A'')** Close up of the dashed box area in A and fluorescence plot profile. Scale bar: 5 µm. **B)** Left: confocal images of the first and the last frame of a 15 minutes of PSD95 puncta in neurons (Tg(cntn1b:KalTA4) +UAS:PSD95-YFP) confirming that PSD95 puncta are stable. Scale bar: 10 µm. Right: close up of the dashed box area on the right to highlight the position of PSD95 puncta before and after 15 minutes, same coloured arrow depicts the same puncta. Scale bar: 5 µm.

PSD95 sites appeared quite clear, thus allowing to almost always discriminate between neighbouring puncta, this is highlighted by the close up and the fluorescence plot profile (Fig. 3.9 A'-A''). To confirm that indeed the PSD95 expression was reliable and that the PSD95-positive puncta were not moving vesicles, I performed single cell short timelapses to assess the stability of PSD95, since synaptic sites are known to be stable in a cell. In a 15 minute timelapse I verified that PSD95 puncta were quite stable in neurons (Fig. 3.9 B). I therefore expressed PSD95 also in OPCs to verify the stability of PSD95 puncta also in these cells. PSD95 puncta appeared less dense as well less bright and clear in OPCs compared to neurons, but most of them were stable during the timelapses (Fig. 3.10).

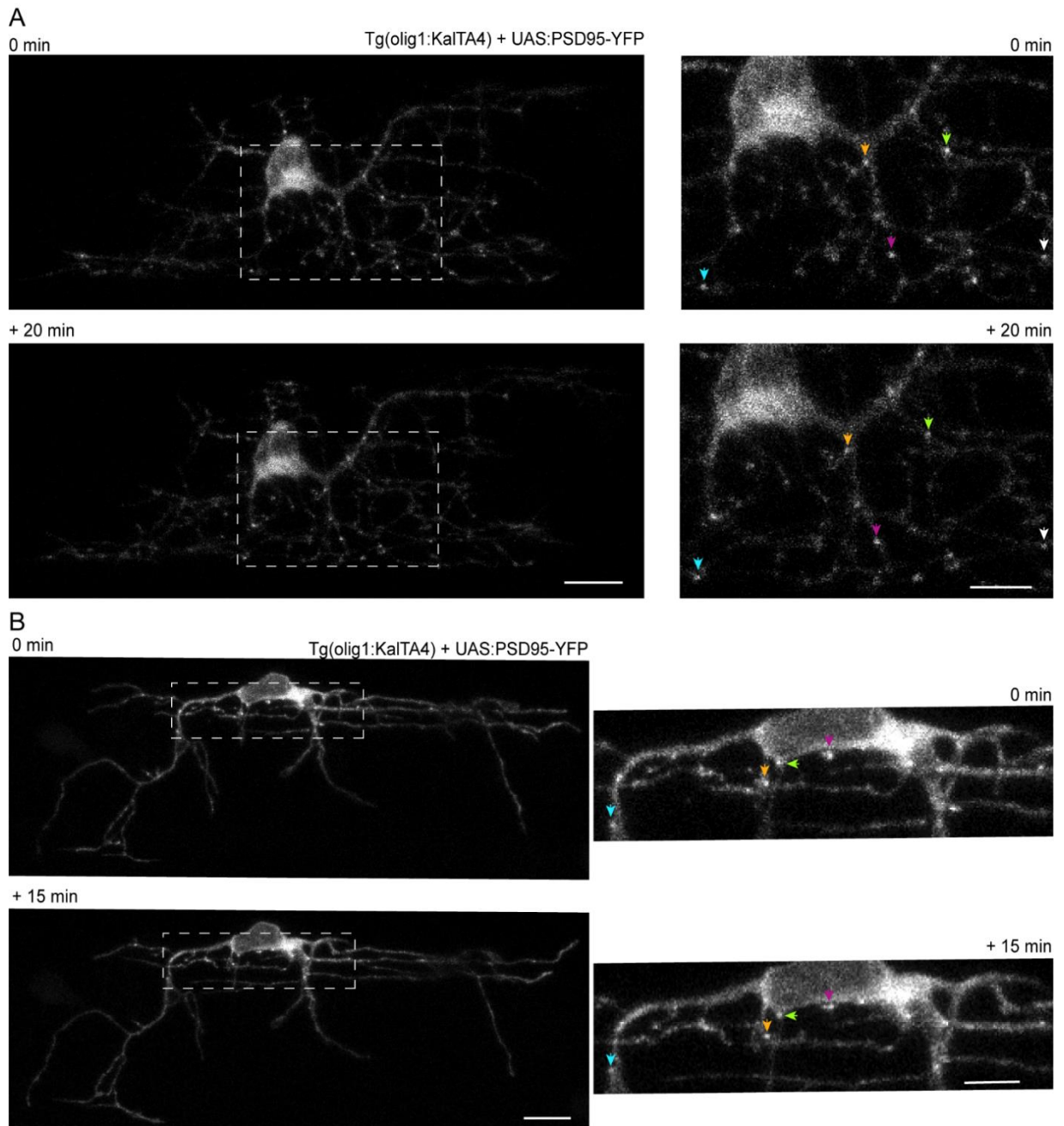


Fig. 3.10 PSD95 expression is stable in OPCs

A-B) Two timelapse examples of PSD95 in OPCs. Left: confocal images of the first and the last frame of a 15 minutes of PSD95 puncta expression in OPCs (Tg(olig1:KalTA4) +UAS:PSD95-YFP) confirming that PSD95 puncta are stable. Scale bar: 10 μ m. Right: close up of the dashed box area on the right to highlight the position of PSD95 puncta before and after 15 minutes, same coloured arrow depicts the same puncta. Scale bar: 5 μ m

The utilisation of a post-synaptic labelling alone is meaningless to identify synaptic contacts if this does not appose a pre-synapse. Hence, I used a pre-synaptic labelling in neurons to identify axon-OPC contacts. I injected the UAS:PSD95-YFP construct into the OPC Gal4, Tg(olig1:KalTA4) and I crossed it with the Tg(elavl3:synaptophysin-tagRFP) line that I have

generated. Therefore, I could label axon-OPC synaptic contacts expressing a pre-synaptic marker in neurons and a post-synaptic marker in OPCs. PSD95 expression in OPCs was characterised by puncta, as well, which were less dense along the cell compared to neurons. Going through single planes of the z-stacks I identified sites in which the pre- and post-synaptic markers were in close proximity (Fig. 3.11).

This suggests that I could detect potential axon-OPC synaptic contacts in the zebrafish spinal cord using synaptophysin and PSD95 as pre- and post-synaptic markers, respectively.

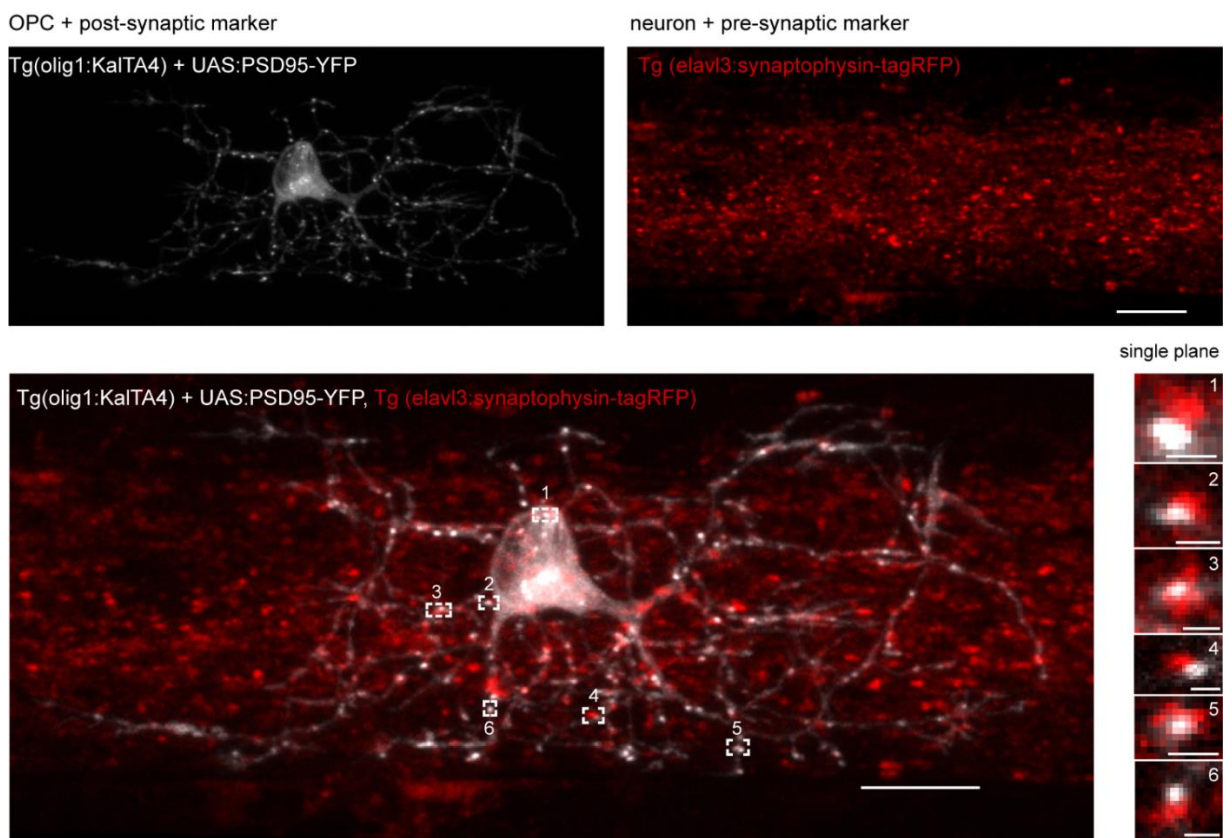


Fig. 3.11 Axon-OPC synaptic-like contacts in vivo

Top panel: confocal single channel projection of PSD-95 positive OPC (left) and Tg(elavl3:synaptophysin-tagRFP) line (right) labelling pre-synaptic sites in neurons at 5 dpf. Scale bar: 10 µm. Bottom panel: Confocal image of the two merged channels in the upper panel showing expression of pre-synaptic marker in neurons and a post-synaptic marker in OPC Scale bar: 10 µm. Bottom-right: Close up and single plane of the dashed box area showing close proximity of the pre- and post-synaptic markers. Scale bar: 1 µm.

Since we previously found differences in terms of morphology and fate amongst OPCs in the spinal cord, I wondered whether the post-synaptic marker PSD95 was also differentially expressed in the two types of cells. The hypothesis would be that axo-dendritic area OPCs which showed fast remodelling would have less chances to form a stable synaptic contact with neurons compared to the neuron-rich area OPCs which have instead stable processes.

Axo-dendritic and neuron-rich area OPCs differ in cell morphology and soma position, but another hallmark to distinguish these two OPC subgroups is their cell body shape. Using an OPC nuclear-membrane labelling combination, I identified examples for each OPC subgroup within the spinal cord. The cell body shape of neuron-rich area OPCs (cell#1), characterised by a complex process morphology, presented a round morphology. Instead, the soma of axo-dendritic area OPCs (cell#2), delineated by the typical simple process morphology, had an elongated shape (Fig. 3.12 A). To confirm the correlation between soma shape and position, I combined OPCs labelling with BODIPY staining and 90° rotations to localise the soma position of the two previous cells within the spinal cord (Fig. 3.12 B).

OPCs with their cell body in the axo-dendritic areas of the spinal cord presented an elongated cell body shape. In contrast, OPCs with their cell body in the neuron-rich areas showed a rounded soma shape.

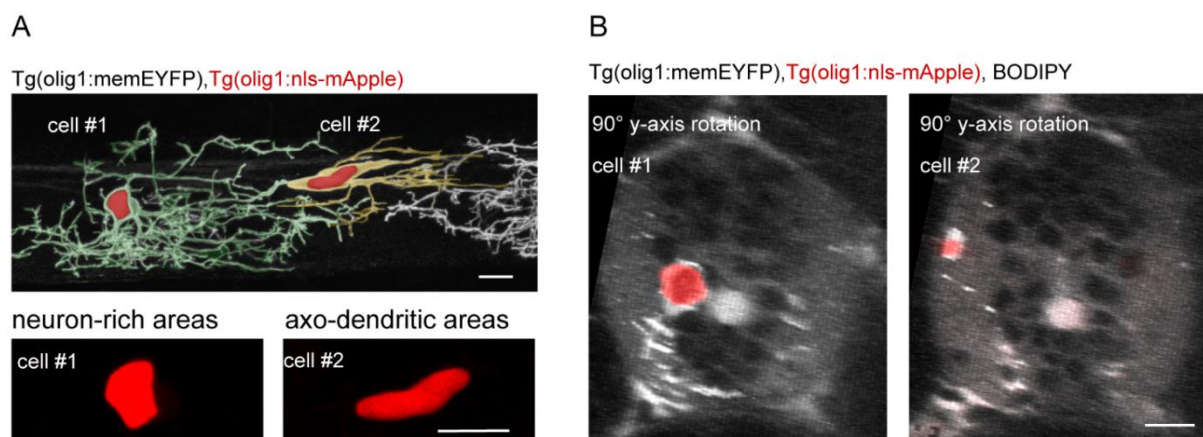


Fig. 3.12 Neuron-rich and axo-dendritic area OPCs are distinguished by their cell body shape

A) Example image of two neighbouring OPCs labelled with a membrane and a nuclear fluorescent proteins (Tg(olig1:memEYFP), Tg(olig1:nls-mApple)) showing that OPCs with their soma in neuron-rich (cell #1) and axo-dendritic areas (cell #2) can be distinguished by the shape of their cell body. Scale bar: 10 μ m. **B)** 90° rotation of the two cells labelled in A to correlate the soma shape with the soma position using BODIPY staining. Scale bar: 10 μ m.

To test whether there was any difference between PSD95 expression in axo-dendritic area and neuron-rich area OPCs, I injected the UAS:PSD95-EYFP construct into Tg(olig1:KaITa4) line. To discriminate between the axo-dendritic area and the neuron-rich area OPCs I looked at the cell body shape that, as I illustrated in the previous paragraph, was elongated in the axo-dendritic area OPCs and round in the neuron-rich area ones. Confocal imaging of sparsely labelled PSD95-positive cells revealed that PSD95 expression was mostly punctate and variable among different cells (Fig. 3.13A, B). PSD95 puncta were mostly restricted to OPC processes and a few of them were also localised in the cell soma (Fig. 3.13A', B'). In one cell, PSD95 expression spread in the whole cell without showing the typical punctate labelling (Fig. 3.13B). Moreover, manual quantification analysis in ImageJ to count PSD95 puncta in each OPCs combined with cell reconstruction done with the Imaris software showed that neuron-rich area OPCs have more PSD95 puncta/100 μ m compared to axo-dendritic area OPCs ($2.9 \pm 2.6/7.0$ neuron-rich areas vs $2.2 \pm 0.5/2.5$ axo-dendritic areas, $p=0,01$, Mann Whitney t-test) (Fig. 3.13C).

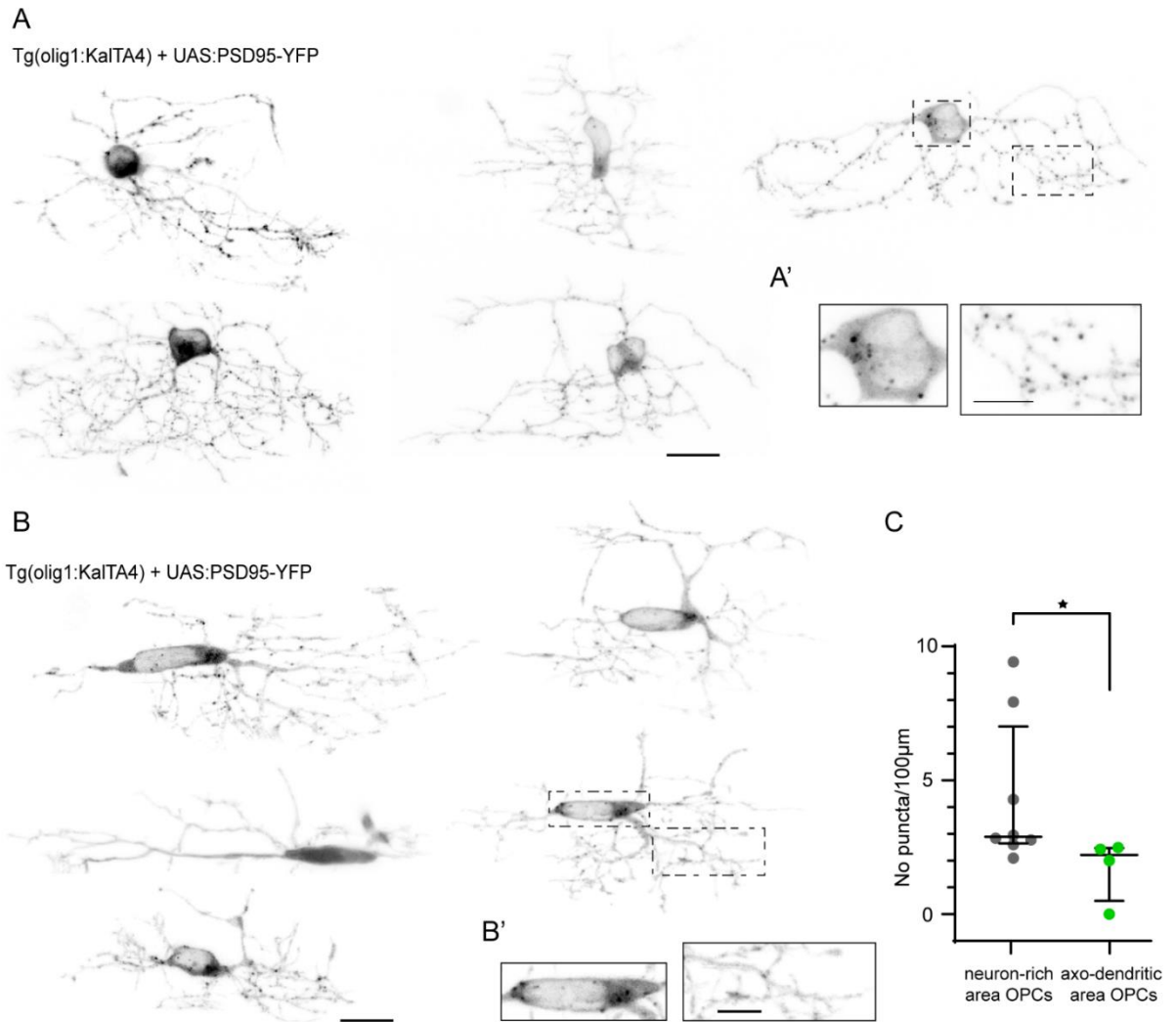


Fig. 3.13 PSD95 expression in OPCs

A) Example images of PSD95 expression in neuron-rich area OPCs (tg(olig1:KalTA4) +UAS:PSD95-EYFP) Scale bar: 10 μ m. **A')** Close up of PSD95 expression in soma and processes of neuro-rich area OPCs. Scale bar: 5 μ m. **B)** Example images of PSD95 expression in axo-dendritic area OPCs (tg(olig1:KalTA4) +UAS:PSD95-EYFP) Scale bar: 10 μ m. **B')** Close up of PSD95 expression in soma and processes of axo-dendritic area OPCs. Scale bar: 5 μ m. **C)** Graph showing the quantification of number of puncta/100 μ m, each data point represents a cell. Data are expressed as median \pm interquartile range (2.9 \pm 2.6/7.0 neuron-rich areas vs 2.2 \pm 0.5/2.5 axo-dendritic areas, p=0,01, Mann Whitney t-test).

In this section, I showed that OPCs have a typical morphology with process ramification. OPCs extend their processes in the zebrafish lateral spinal cord which is characterised by myelinated and unmyelinated axons that are in a stereotypical position. Looking at single OPC morphology, position and dynamics we could categorise OPCs in two subgroups. Axo-dendritic area OPCs with elongated somata that reside in the lateral spinal cord, present a simple morphology and fast process remodelling. Neuron-rich area OPCs with rounded somata localise to the medial spinal cord, they have a complex morphology and show slow process remodelling. These two OPC subgroups have also different potential to give rise to myelinating oligodendrocytes. Axon-rich area OPCs can differentiate directly into myelinating oligodendrocytes, instead neuron-rich area OPCs do not differentiate directly but they can proliferate to form a cell with differentiation potential. Moreover, I could identify axon-OPC synaptic-like contacts in the zebrafish spinal cord. Differences in post-synaptic marker expression were also found between OPCs, neuron-rich area OPCs showed more post-synaptic sites compared to the axo-dendritic area ones.

3.2 OPC calcium dynamics

3.2.1 GCaMP transients of individual OPCs

In the previous sections, I showed that the zebrafish spinal cord presents two groups of OPCs. The cells with their somata in the axo-dendritic areas with a simpler morphology which are more likely to differentiate into myelinating oligodendrocytes, and the OPCs with their somata in neuron-rich areas with a more stable and complex morphology which do not directly differentiate. The latter seem to form more synapses than the other group. Moreover, from our RNA single-cell sequencing data we found that neuron-rich area OPCs are enriched in genes involved in neurotransmitter signalling (Marisca et al., 2020). Hence, we wondered if OPCs differently sense neuronal activity. In particular, neuron-rich area OPCs which showed less process remodelling and more synaptic sites might be able to integrate more signals from neurons. To investigate this hypothesis, I decided to use a genetically encoded calcium indicator (GECI) in OPCs and perform GCaMP imaging to establish calcium activity of OPCs. This method enables non-invasive measurements of cell activity *in vivo*. Specifically, I used the green fluorescent protein (GFP)-based GECIs GCaMP6m which has a good signal-to-noise ratio (Chen et al., 2013).

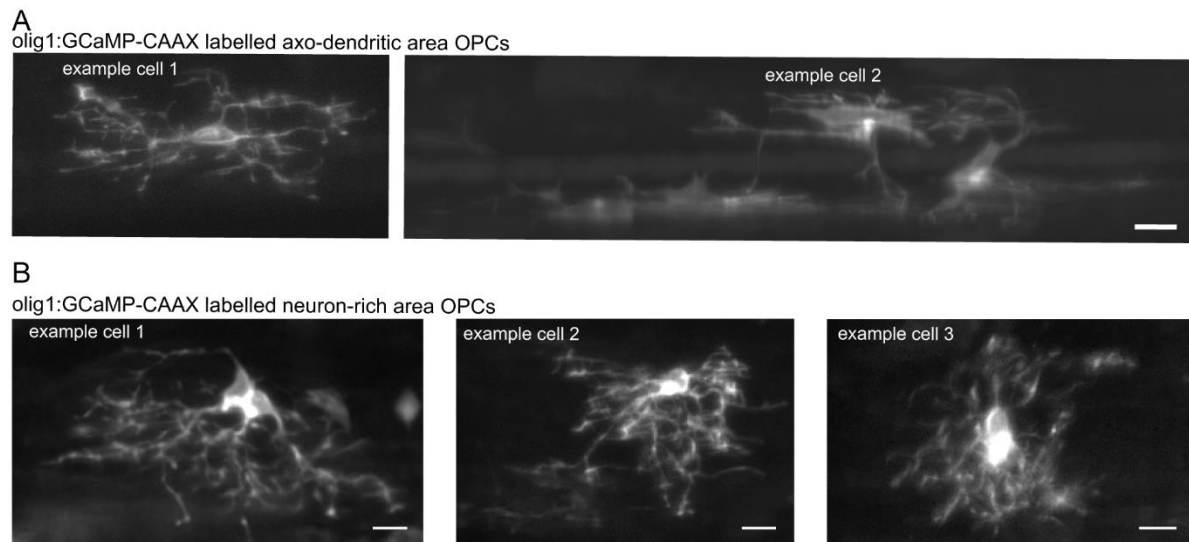


Fig. 3.14 GCaMP-positive cells show typical OPC morphology and consequently no myelin sheaths

A) Example light-sheet image of GCaMP6m-CAAX labelled axo-dendritic area OPCs showing no sign of myelinating sheaths. Scale bar: 10 μm . **B)** Example light-sheet images of GCaMP6m-CAAX labelled neuron-rich area OPCs showing no sign of myelinating sheaths. Scale bar: 10 μm . (Marisca et al., 2020)

To describe GCaMP dynamics in single cell OPCs, I expressed GCaMP6m-CAAX, a membrane targeted GCaMP, under the olig1 promoter. GCaMP6m-CAAX positive OPCs in both axo-dendritic and neuron-rich areas, do not have any signs of early myelination, no myelin sheaths were detectable in z-stacks projection of example cells (Fig. 3.14 A-B).

My first aim was to investigate the duration of calcium transients in OPCs using GCaMP6m to adjust the frequency imaging setting in order to detect all GCaMP transients without neglecting any signals. GCaMP transient duration can be variable depending on the different cell types and on the calcium indicators. In neurons, GCaMP transients can last from 0.2 until 3 seconds, whereas in astrocytes the mean duration is 8.5 seconds (Chen et al., 2013, Agarwal et al., 2017). Therefore, I performed single plane fast calcium imaging (10 Hz) using light-sheet microscopy to understand the average duration of calcium transients in OPCs and to establish the appropriate imaging setting to look at OPC GCaMP events (Fig. 3.15 A). GCaMP transient dynamics in OPC processes and somata were variable. After rising, some GCaMP transients remained elevated for several seconds, forming a plateau, and then descending smoothly afterwards. Some others rose and decayed shortly afterwards, thus creating a sharper peak (Fig. 3.15 C). Similarly, the duration of GCaMP transients also displayed variability. Overall,

OPCs showed slow calcium transients at the level of the processes as well as at the soma which lasted for 2-4 seconds (average duration= 2.95 ± 0.5 SD) (Fig. 3.15 B-D).

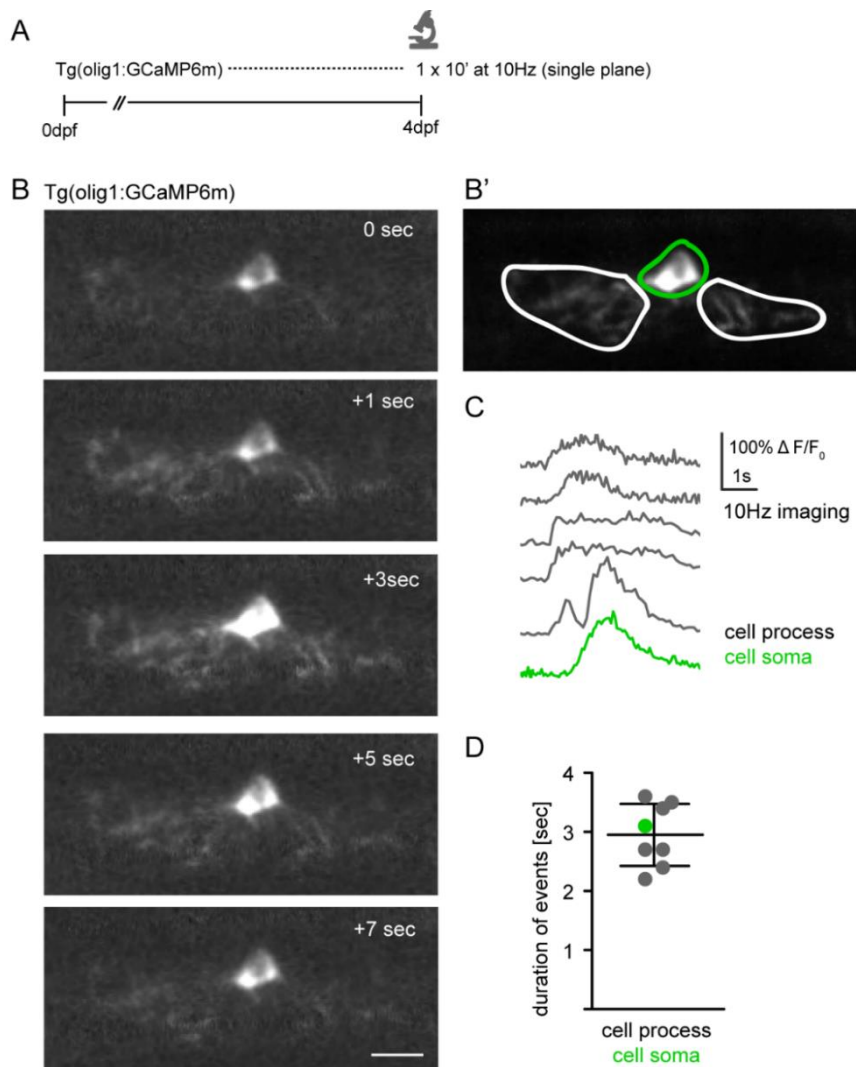


Fig. 3.15 Duration of OPC GCaMP events

A) Experiment paradigm **B)** Different timepoints of a single GCaMP6m-positive OPC at 4 dpf showing calcium transient going through the all cell. Scale bar: 10 μ m. **B')** ROIs analysed of OPC in **B.** **C)** Example traces of GCaMP transients in cell processes and soma of Tg(olig1:GCaMP6m) animals at 4 dpf (n=6 ROI from 2 animals). **D)** Quantification of the duration of GCaMP transient in OPC soma and processes (average duration= 2.95 ± 0.5 SD). (Marisca et al., 2020)

OPC GCaMP transients of both somata and processes showed slow kinetics, suggesting that 0.5 Hz imaging frequency will be sufficient to detect all GCaMP events.

Next, I wanted to focus on single OPCs to describe more in details the dynamics of GCaMP transients at a single cell resolution and identify possible differences between OPC subgroups. To characterise single cell GCaMP activity in OPCs, I injected the olig1:GCaMP6m-CAAX construct into nacre fish to sparsely label individual cells and I took 10 minute timelapses for each sample using a slower imaging frequency (0,5-1 Hz) at the light-sheet microscope(Fig. 3.16 A). Often, during 10 minutes of timelapse imaging, GCaMP transients were restricted to process subdomains (cell #1). Sometimes, the cells remained silent showing no signs of GCaMP activity (cell #2) (Fig. 3.16 B). Interestingly, two neighbouring cells did not show the same degree of GCaMP activity in the processes, suggesting that their calcium activity in the processes is unrelated to OPCs in their vicinity. The GCaMP activity of whole cells was described by taking a volumetric timelapse. GCaMP transients in OPCs were analysed manually drawing ROIs around processes and somata (Fig. 3.16 B'). Looking at the GCaMP traces of these two neighbouring OPCs, calcium transients appeared to be of different shapes and amplitudes. A clear peak was detectable in all GCaMP transients, higher amplitude and longer duration were visible comparing one transient (in magenta) with the other (in green) (Fig. 3.16 B'').

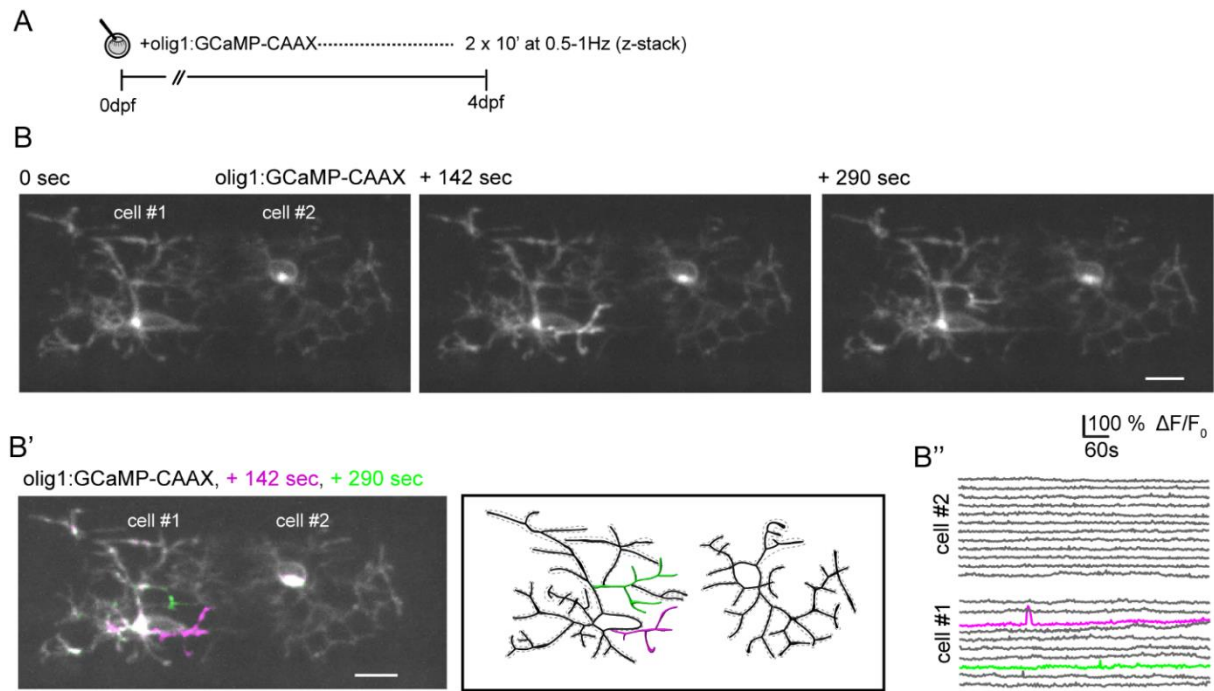


Fig. 3.16 GCaMP transients restricted to process subdomains

A) Experiment paradigm **B)** Three time points of two individual olig1:GCaMP-CAAX expressing cells showing transients in the process subdomain (cell#1) or being silent (cell#2). Scale bar: 10 μm . **B')** Left: projection of the three timepoints of two olig1:GCaMP-CAAX expressing cells at 4dpf. Scale bar: 10 μm . Right: measured ROI indicated by the dotted lines around the reconstructed cells, active ROI are highlighted in green and magenta. **B'')** Traces of cells in B-B'. (Marisca et al., 2020)

In a few cases, the GCaMP transients spread also throughout the whole cell (Fig. 17). Somatic GCaMP transients lasted for several seconds and even after 4 seconds elevated GCaMP levels were detectable in the somata of the cells compared to baseline (time 0), suggesting that the transients were slow and gradually decreasing. Moreover, in this example, the somatic calcium transient did also spread into the neighbouring cell (Fig. 3.17).

olig1:GCaMP-CAAX

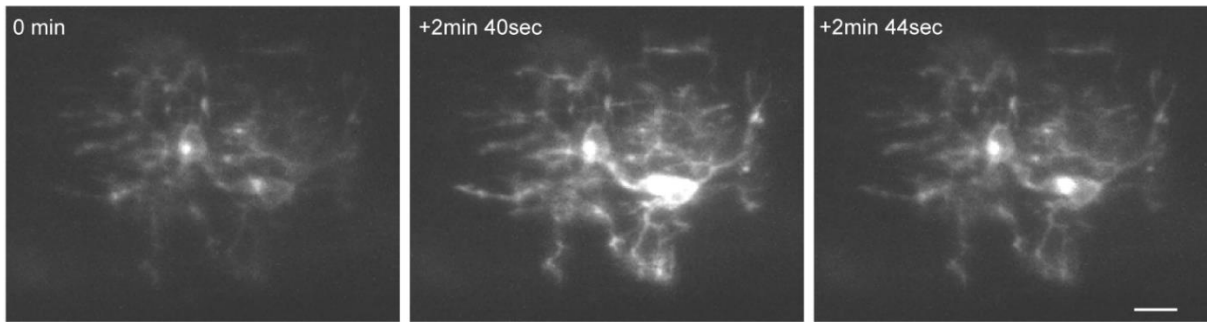


Fig. 3.17 GCaMP transients spreading through the whole cells

Three time points of two individual olig1:GCaMP-CAAX expressing cells showing transients spreading throughout the cells. Scale bar: 10 μ m.

Within the 10 minute timelapse of about 50 single OPCs, the majority (67%) showed GCaMP transients that were restricted to process subdomains. Whole cell GCaMP transients were very rare (6%) and the rest of the cells (27%) did not have any GCaMP transients during the timelapse (Fig. 3.18 A).

I classified GCaMP data obtained from single OPCs in the two groups based on cell morphology and soma position. Most of the cells analysed were neuron-rich area OPCs (39 cells), which have a complex morphology, more stable processes and do not directly differentiate into myelinating oligodendrocytes. The rest of the cells (12 cells) were axo-dendritic area OPCs which have a simpler morphology, more dynamic processes and the potential to differentiate in myelinating oligodendrocytes. Both neuron-rich area and axo-dendritic area OPCs presented mostly GCaMP transients in the process subdomains (61% neuron-rich areas; 83% axo-dendritic areas), fewer cells were completely silent (31% neuron-rich areas; 17% axo-dendritic areas). GCaMP events that spread throughout the entire cell were rare (8%) and only detected in the neuron-rich area OPCs (Fig. 3.18 A').

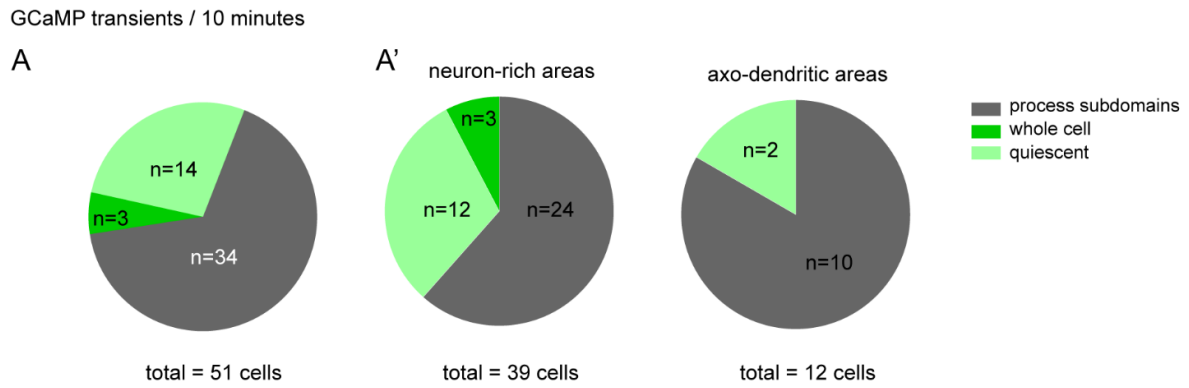


Fig. 3.18 GCaMP transients in single OPCs

A) Quantification of different types of GCaMP transients observed during 10 minutes timelapse in individual olig1:GCaMP-CAAX expressing cells. **A')** Pie charts with cells from A split between neuron-rich area and axo-dendritic area OPCs indicating absolute numbers of olig1:GCaMP-CAAX expressing cells showing GCaMP transients at the level of process subdomains, entire cells or being silent during a 10 minutes timelapse. (Marisca et al., 2020)

To summarise, single cell GCaMP imaging revealed that OPCs can show two different types of GCaMP transients restricted to process subdomains or spreading through the whole cell. Both types of GCaMP transients display slow dynamics and long duration.

Both neuron-rich and axo-dendritic area OPCs mostly presented GCaMP transients restricted to process subdomains. Sometimes OPCs were completely quiescent, showing no signs of GCaMP events. Whole cell GCaMP transients were detected only in neuron-rich area OPCs suggesting that there might be differences in somatic GCaMP transients between the two OPC subpopulations.

3.2.2 Somatic GCaMP transients at the cell population level

After characterising GCaMP activity in single OPCs, I wondered how calcium dynamics are in neighbouring OPCs, as this information is not achievable from the single cell resolution imaging. As I previously described, axons run along the whole length of the spinal cord in a stereotypic lateral position where also OPCs extend their processes suggesting that neighbouring OPCs could contact the same axons. Moreover, OPC processes form a dense network in the lateral spinal cord being in close proximity to each other, suggesting also possible OPC-OPC interactions. Therefore, I sought to analyse a population of cells to study how they relate to neurons and to each other. To investigate GCaMP transients at the cell population level and study whether groups of OPCs show different pattern of calcium transients, I analysed only somatic calcium events in large volumes of spinal cord. As when imaging a tissue where all cells are labelled it would not be possible to have a single cell resolution of the calcium transients. I generated a full transgenic line in which cytoplasmic GCaMP6m was expressed in OPCs under the olig1 promoter Tg(olig1:GCaMP6m). Analysis of the OPCs GCaMP line crossed to a mbp line, where a red fluorescent protein was expressed in myelinating oligodendrocytes (Tg(mbp:KillerRed), confirmed that GCaMP6m positive cells were OPCs and not myelinating oligodendrocytes, while only 3 out of 360 (1%) cells were double positive suggesting they were newly differentiated oligodendrocytes (Fig. 3.19A, B). This experiment confirmed that Tg(olig1:GCaMP6m) line is specific to analyse GCaMP transient in OPCs.

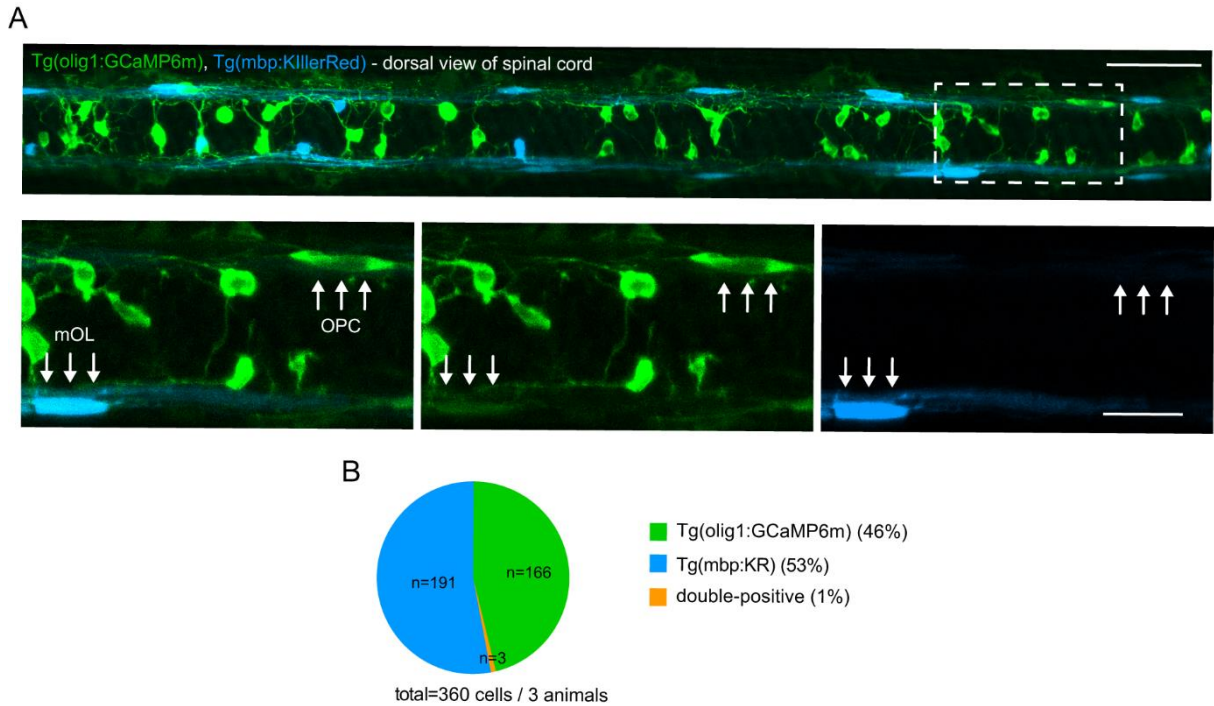


Fig. 3.19 Characterisation of Tg(olig1:GCaMP6m) line

A) Dorsal views of Tg(olig1:GCaMP6m), Tg(mbp:KillerRed) transgenic zebrafish at 4 dpf to label OPCs and differentiated oligodendrocytes. Dotted box indicates position of zoom-ins in bottom row. Scale bars: 50 μ m (top) and 20 μ m (bottom). **B)** Quantification of single and double-positive cells from images as shown in A. (Marisca et al. 2020)

To study GCAMP transients at the population level I performed light-sheet imaging of the spinal cord of a dorsally mounted 4 dpf zebrafish at 1 Hz frequency and I took 2 timelapses of 10 minutes for each sample (Fig. 3.20 A). High-resolution light-sheet imaging of a stretch of the spinal cord allowed the identification of all OPC somata morphology in the field of view (Fig. 3.20 B). By analysing the z-stack of the imaged spinal cord area, I was able to discriminate between neuron-rich and axo-dendritic area OPCs taking into account the soma position and shape (Fig. 3.20 B').

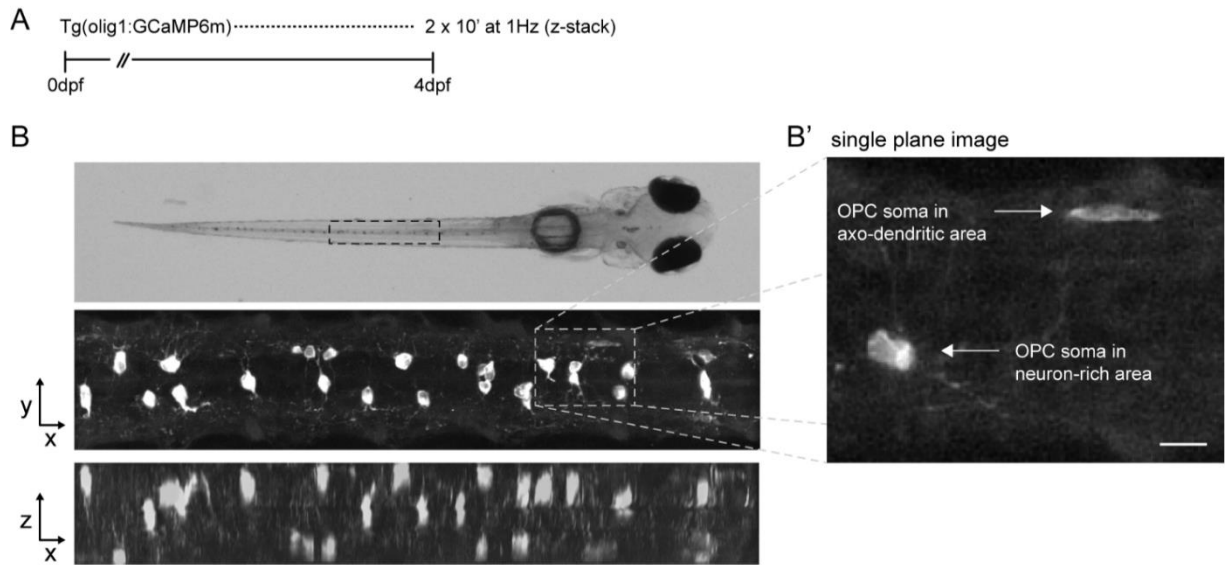


Fig. 3.20 OPC cell population GCaMP transients

A) Experimental paradigm. **B)** Top: Dorsal widefield view of a zebrafish at 4 dpf. Below: z-projection and z-rotation of Tg(olig1:GCaMP6m) in the spinal cord similar to as indicated by the boxed area above. Bottom: projection of 2 timepoints (baseline: grey, t1: green) showing a GCaMP transient restricted to a single cell in the spinal cord. Scale bar: 50 μ m. **B')** Single plane image taken as indicated by boxed area showing individual OPCs with their soma in neuron-rich and axo-dendritic areas. Scale bar: 10 μ m. (Marisca et al. 2020)

Population GCaMP imaging revealed different outcomes of somatic GCaMP transients. In some cases, during dorsal recording, somatic GCaMP transients could be restricted to a single cell in a large volume of zebrafish spinal cord (Fig. 3.21 A). The cell showing GCaMP activity was a neuron-rich area OPC, identified by the central cell body location in the spinal cord and a rounded shape (Fig. 3.21 A'). This single cell somatic GCaMP transient had a duration of a few seconds and from the traces a clear peak is discernible in the active OPC trace (Fig. 3.21 A').

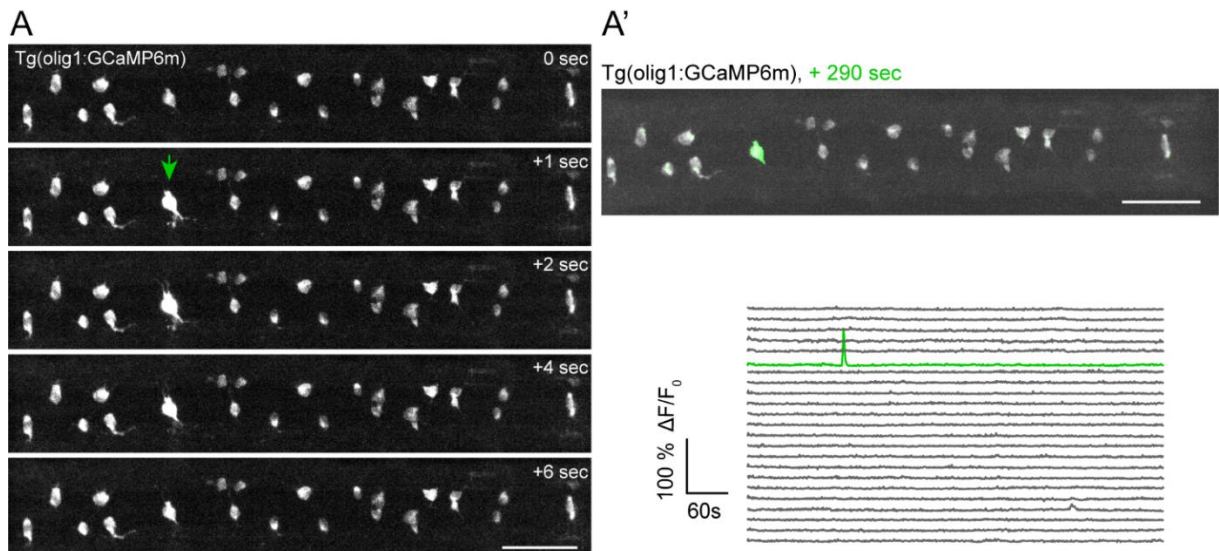


Fig. 3.21 Single cell somatic GCaMP transient amongst OPC population

A) Time points of Tg(olig1:GCaMP6m) line showing single cell GCaMP transient (green arrow). Scale bar: 50 μm .
A') Top: projection of 2 timepoints (baseline: grey, t1: green) showing the GCaMP transient restricted to a single cell in A. Scale bar: 50 μm . Bottom: $\Delta F/F_0$ GCaMP transients of all cells shown in the upper panel (in green the active soma). (Marisca et al., 2020)

Somatic GCaMP transients could also spread through a subgroup of OPCs that were close to each other. This could indicate that group of cells can be coupled amongst each other and that not all OPCs participate to this type of interconnection since not all of them showed GCaMP signal. GCaMP transients propagated in OPCs within the spinal cord with a head to tail direction. Also in this case, GCaMP dynamics were slow and spread in both neuron-rich and axo-dendritic areas of the spinal cord (Fig. 3.22).

A

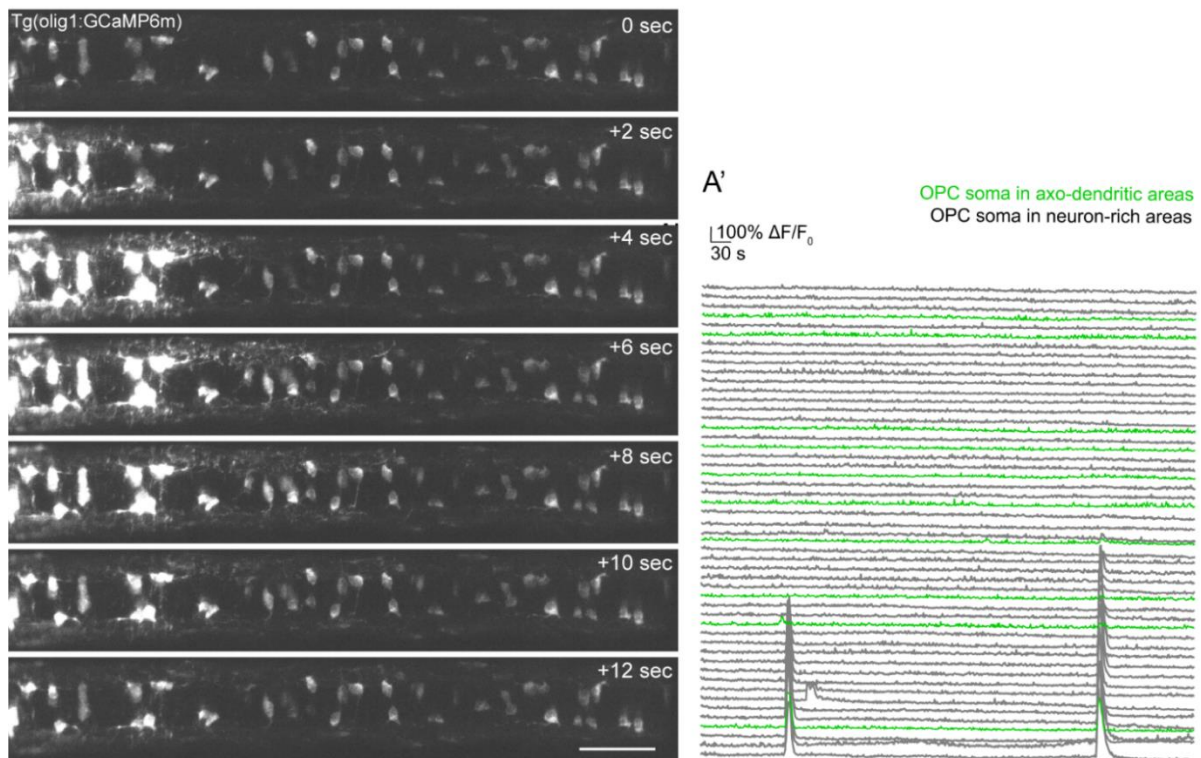


Fig. 3.22 Group of cell somatic GCaMP transient amongst OPC population

A) Time points of Tg(olig1:GCaMP6m) line showing GCaMP transient spreading throughout a group of neighbouring OPCs. Scale bar: 50 μm . **A')** $\Delta F/F_0$ GCaMP transients of all cells shown in A, in green axo-dendritic area OPCs and in grey neuron-rich area OPCs.

More rarely, I could also detect GCaMP transients propagating throughout the entire field of view. The directionality of the GCaMP events was always head to tail and GCaMP wave lasted for around 10 seconds. Somatic GCaMP transients started in OPCs closer to the head in the imaged area and then slowly expanded in the neighbouring OPCs towards the tail. GCaMP somatic transients showed all a clear peak and were detected in both OPC subpopulations (Fig. 3.23). Looking at this timelapse, one limitation stands out as I could analyse only the cells that were within the field of view, but very likely this GCaMP wave also involved OPCs outside the imaged area, as the wave involved all the cells in the field of view and presumably it would continue travelling further down the body of the fish (Fig. 3.23).

A

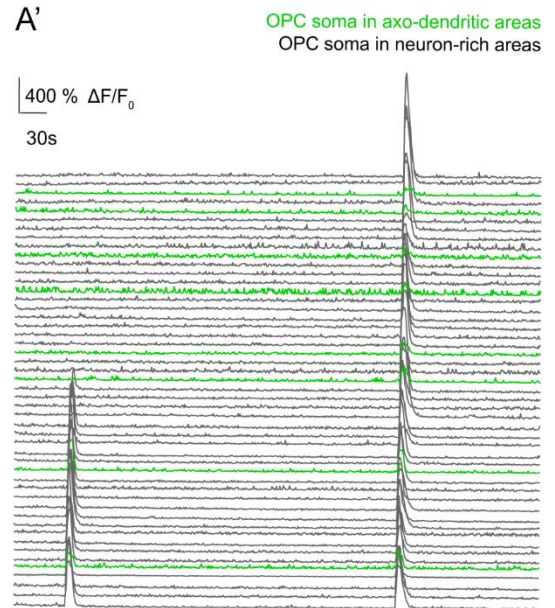
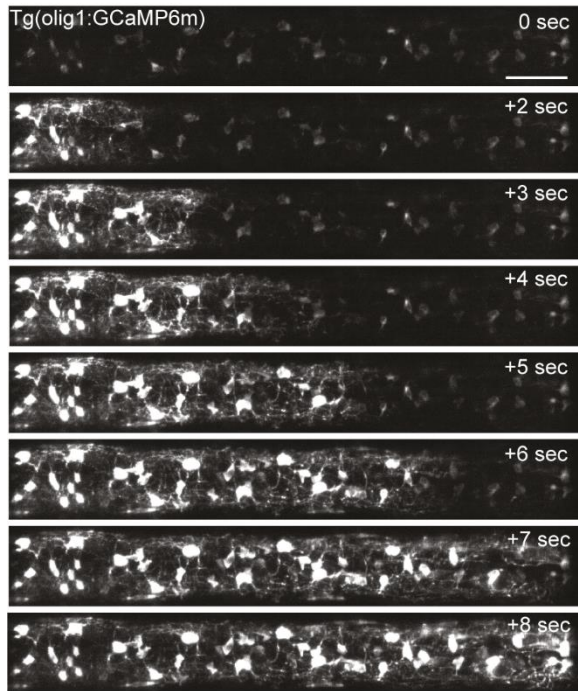


Fig. 3.23 GCaMP transient throughout OPC population in the spinal cord

A) Several timepoints of a OPC GCaMP6m timelapse showing GCaMP transient spreading throughout the spinal cord at 4 dpf. Scale bar: 50 μm . **A')** $\Delta F/F_0$ GCaMP transients of all cells shown in A, in green axo-dendritic area OPCs and in grey neuron-rich area OPCs.

Furthermore, looking at differences between the two OPC subgroups, OPCs with their somata in the neuron-rich areas had a higher probability to show somatic GCaMP compared to OPCs with their soma residing in the axo-dendritic areas (26% (73/285 cells) neuron-rich areas vs. 19% (9/48 cells) axo-dendritic areas, $p=0.007$, two-tailed Wilcoxon matched-pairs signed rank test) (Fig. 3.24 A). The percentage of somatic GCaMP transients in neuron-rich area OPCs was higher than the one of axo-dendritic area OPCs in all the analysed animals. In most timelapses, somatic GCaMP events were detected only in neuron-rich area OPCs suggesting that these cells extending their processes in the axonal tracts, might have an enhanced ability to sense neuronal activity (Fig. 3.24 A).

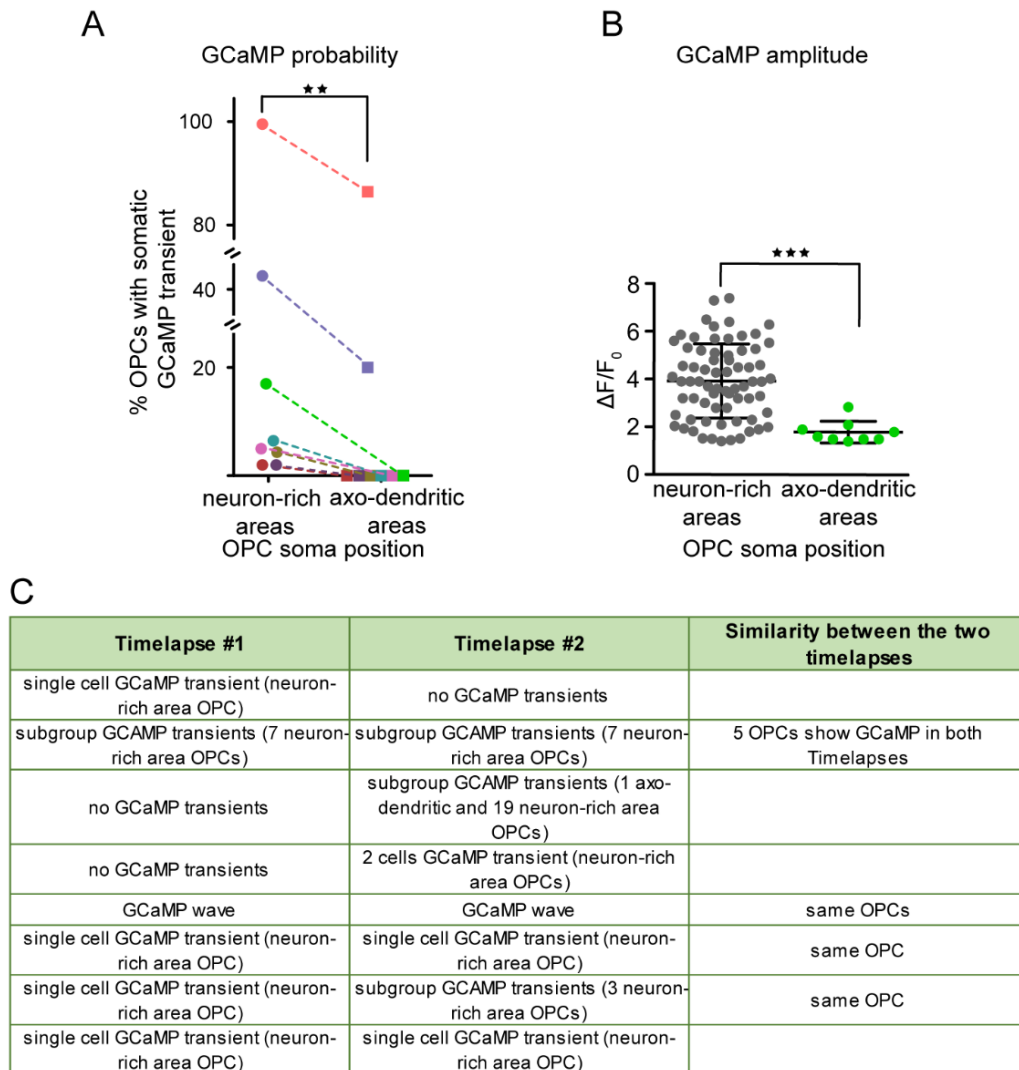


Fig. 3.24 GCaMP transient throughout OPC population in the spinal cord

A) Probability of somatic GCaMP transients of OPC in neuron-rich and axo-dendritic areas at 4 dpf (26% (73/285 cells) vs. 19% (9/48 cells), $p=0.007$ (two-tailed Wilcoxon matched-pairs signed rank test); $n=8$ animals. **B)** Quantification of GCaMP amplitudes measured in somata of OPCs in neuron-rich and axo-dendritic areas at 4 dpf. Data are expressed as mean \pm SD ($3.9 \pm 1.5 \Delta F/F_0$ vs. $1.8 \pm 0.4 \Delta F/F_0$, $p < 0.001$ (two-tailed Welch's t test), $n=81/9$ cells from 8 animals). **C)** Table to compare the first and second timelapse of the same OPCs analysed in A and B. (Marisca et al. 2020)

Moreover, amplitudes of somatic GCaMP transients were more than 2-fold higher in neuron-rich area OPCs compared to the axo-dendritic area OPCs ($3.9 \pm 1.5 \Delta F/F_0$ vs. $1.8 \pm 0.4 \Delta F/F_0$, $p < 0.001$, two-tailed Welch's t test). Somatic GCaMP events in neuron-rich areas had highly variable amplitudes, reaching in some cases a 7-fold increase compared to their baseline. Instead, somatic GCaMP amplitudes of axo-dendritic OPCs showed a maximum of 3-fold increase (Fig. 3.24 B). Interestingly, comparing the two 10 minute timelapses of the same stretch of the spinal cord, when a somatic GCaMP event was detected in both timelapses, it

appeared in the same OPCs (Fig. 3.24 C). This suggests that some OPCs are more sensitive than other OPCs to other signalling and show systematic calcium activity as they present somatic GCaMP transients at two different time points within 30 minutes.

In summary, OPCs which reside with their soma in the neuron-rich areas and that are not contributing directly to myelination but need to divide to give rise to a cell that can differentiate into myelinating oligodendrocytes, are more likely to show GCaMP events. When compared to the more rare GCaMP events of axo-dendritic areas, neuron-rich area OPCs have GCaMP transients of higher amplitude. This is consistent with the idea that neuron-rich area OPCs which have more stable processes, higher post-synaptic marker density and do not directly differentiate, are also the cells that display significantly higher and more frequent GCaMP transients.

3.2.3 Integrating calcium dynamics in OPCs using CaMPARI

GCaMP cell population analysis revealed that OPCs can have calcium transients spreading throughout a group of cells or all cells within the field of view. One limitation of the *in vivo* GCaMP imaging emerged when I focused on the GCaMP imaging timelapse of somatic GCaMP events expanding through the spinal cord (Fig. 3.23). Indeed, I could only analyse the cells that were in the field of view but it seemed that the GCaMP wave involved also OPCs outside this area. To overcome this limitation and to be able to have a wider overview of OPC calcium dynamics in the entire animal, I used CaMPARI (Calcium Modulated Photoactivatable Ratiometric Integrator). CaMPARI is a photoconvertible protein that enables imaging of the integrated calcium activity of large populations of cells over defined time windows (Fosque et al., 2015). This calcium integrator is based on a fluorescent protein that changes from green to red upon irradiation with UV-light only when high calcium concentration is present while the photoconversion light is applied (Fig. 3.25 A). The permanent conversion from green to red permits recording of the calcium activity during the UV light treatment time window.

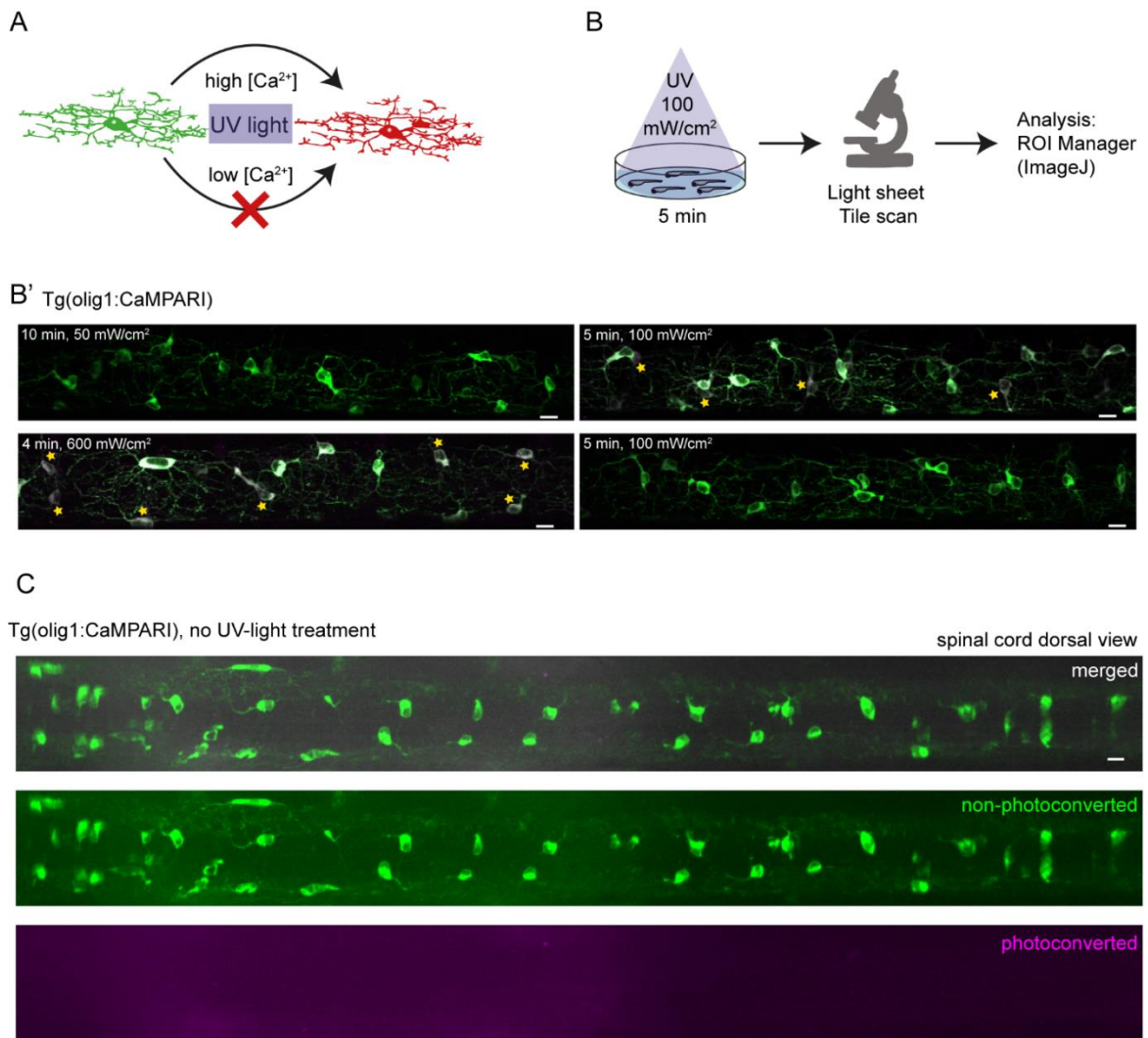


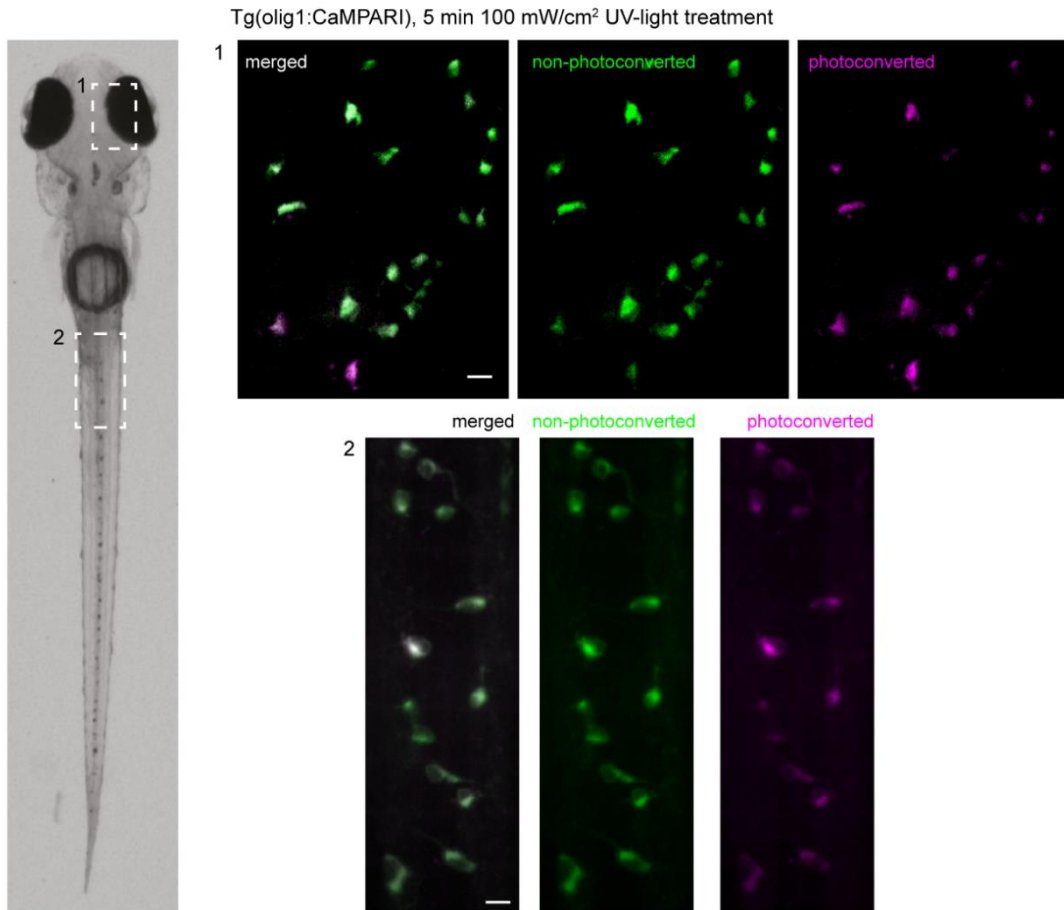
Fig. 3.25 CaMPARI technique in OPCs

A) Illustration showing how CaMPARI works. **B)** CaMPARI experiment paradigm. **B')** Example confocal images of Tg(olig1:CaMPARI) in different conditions. Right images are from the same group of experiments treated with 100mW/cm² UV light for 5 minutes and showing variable photoconversion. Stars depict some example cells that show signs of photoconversion. Scale bar: 10 μ m. **C)** Example light-sheet image of Tg(olig1:CaMPARI) line before UV-light treatment. Scale bar: 10 μ m.

The advantage of using CaMPARI as a tool is to image the total calcium activity of all OPCs during defined time windows, determined by the UV-light treatment duration. In addition, I can study calcium dynamics in all OPCs, illuminating the whole animal and more animals at a time, without having the restriction of a defined field of view as it happened during GCaMP imaging. The challenge of using CaMPARI was to establish a suitable setting to perform the experiment taking into account two main variables, the UV light intensity and the exposure time. A sufficient

UV light intensity to convert a cell from green to red without converting all cells and a UV-light treatment time window as wide as possible preventing overexposure were required. After trying different combinations and samples, I decided to use 100 mW/cm² light intensity for 5 minutes as there was variability amongst animals treated with the same amount of UV light within the same batch of experiment (Fig. 3.25 B-B'). To use CaMPARI and image the entire OPC population I made the transgenic line in which CaMPARI labelled all OPCs under the control of the *olig1* promoter. The untreated fish expressed the green fluorescent protein in all OPCs without having any sign of photoconversion (Fig. 3.25 C). Whereas, treated fish showed signal of photoconversion in different fish body regions (Fig. 3.26 A). I analysed OPCs located in 4 different anatomical regions: the telencephalon, the optic tectum, the hindbrain and the spinal cord. Animals were imaged and analysed from head to tail. Most OPCs had a red/green ratio between 0.3-0.6, while fewer between 0.7-1 and even fewer above 1 meaning that OPCs showed different degree of photoconversion and this can reflect different OPC calcium levels (Fig. 3.26 B). Variability was detected between different animals, in one case (animal #11) the rate of photoconversion was for most of the cells close to 0. In other cases, photoconversion was between 0 and 0.5 (animals #2, #4, #7, #9, #12) and in the rest of the animals, photoconversion rate resulted higher and close to 1 (animals # 1, #3, #5, #6, #8, #10). Interestingly, from the dot plot graph variability within individual animal was also detected, in particular some sample show a dot plot with an undulatory trend (Fig. 3.26 B'). One possible explanation is that this trend is caused by differences among diverse anatomical body regions since the fish was imaged and analysed from head to tail. Moreover, the photoconversion rate of neighbouring OPCs seemed to be in the same range reflecting the GCaMP transients in group of OPCs in close vicinity (Fig. 3.26 B-B').

A



B

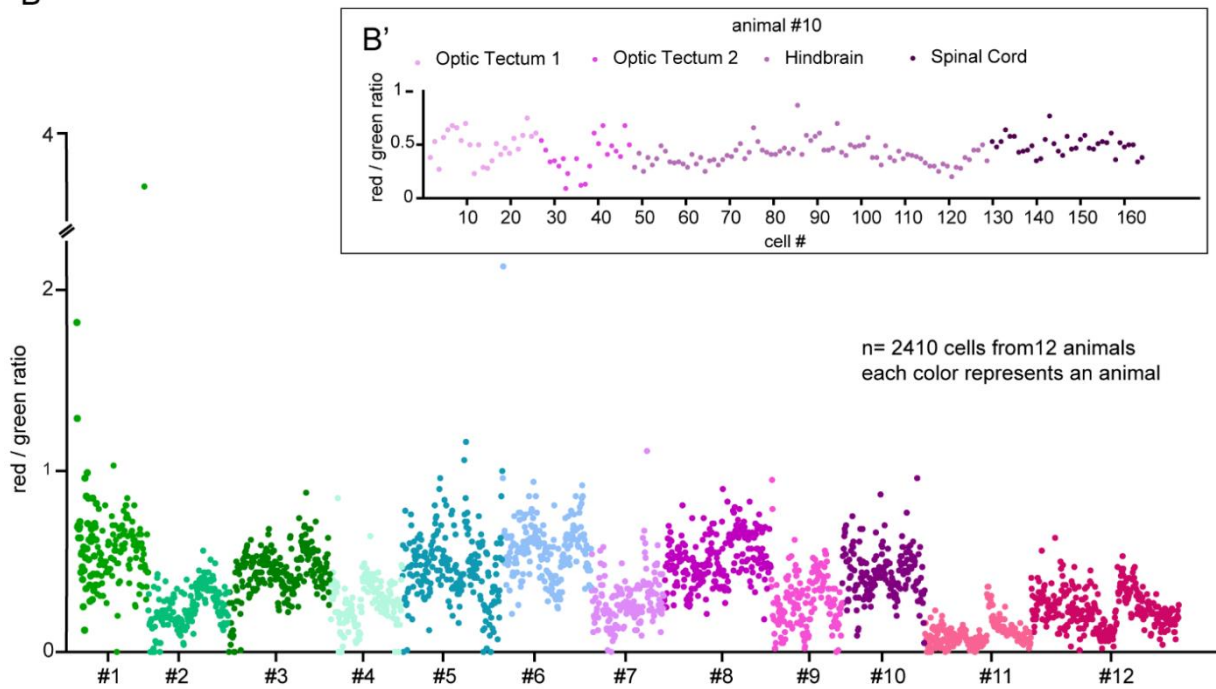


Fig. 3.26 Calcium dynamics using CaMPARI

A) Left: Dorsal widefield view of a zebrafish at 4 dpf with dashed box areas reported on the right. Right-top: projection of a light-sheet image showing degrees of photoconversion of the OPCs in the optic tectum after the UV-light treatment. Right-bottom: projection of a light-sheet image showing degrees of photoconversion of the OPCs in the spinal cord after the UV-light treatment. Scale bar: 10 μm . **B)** Dot-plot graph showing red/green ratio of each OPCs, each color represents and animal (n= 2410 cells from 12 animals). **B')** Close up of fish#10 dot plot to show the undulatory pattern of red/green ratio.

In summary, I demonstrated that CaMPARI can be used as a powerful technique instead of GCaMP imaging allowing us to detect the cumulative calcium levels of the entire animal during a determined time-frame and not only of a part of the spinal cord. Therefore, CaMPARI can be used to overcome the spatial limitation of *in vivo* GCaMP imaging and permit to analyse calcium activity of different body regions at the same time, resulting in a complete overview of OPC calcium dynamics.

3.3 Neuron – OPC interactions

3.3.1 Neural activity manipulation

Neuron-rich area OPCs presented higher probability of calcium events and higher amplitudes compared to the axo-dendritic area OPCs, which are more likely to differentiate. Moreover, cell population somatic GCaMP imaging revealed that neighbouring OPCs can show a rise in calcium at the same time and I even observed waves of GCaMP transients spreading through the whole field of view. Since OPCs extend their processes to the lateral side of the spinal cord where also axons run, it would be interesting to investigate whether OPC GCaMP transients result as a response to neural activity.

To study whether GCaMP transients in OPCs correlate with calcium transients in neurons, I injected the mApple-based GECIs, R-GECO under the neuron promoter *cntn1b* in the GCaMP6m OPC line (Zhao et al., 2011). I used a modified R-GECO version, jRGECO1a which has amplitudes and kinetics similar to that of GCaMP6f (Dana et al., 2016). Using light-sheet imaging, I detected a GCaMP wave going through the OPCs which was preceded by RGECO transients in the RGECO expressing neurons and axons (Fig. 3.27). The directionality of the transients was head to tail, as the one I described in the OPC population GCaMP analysis. Moreover, both GCaMP and RGECO transients showed slow kinetics and the transients lasted several seconds. This experiment suggests that there is a temporal correlation between the OPC somatic GCaMP transients and neural RGECO activity.

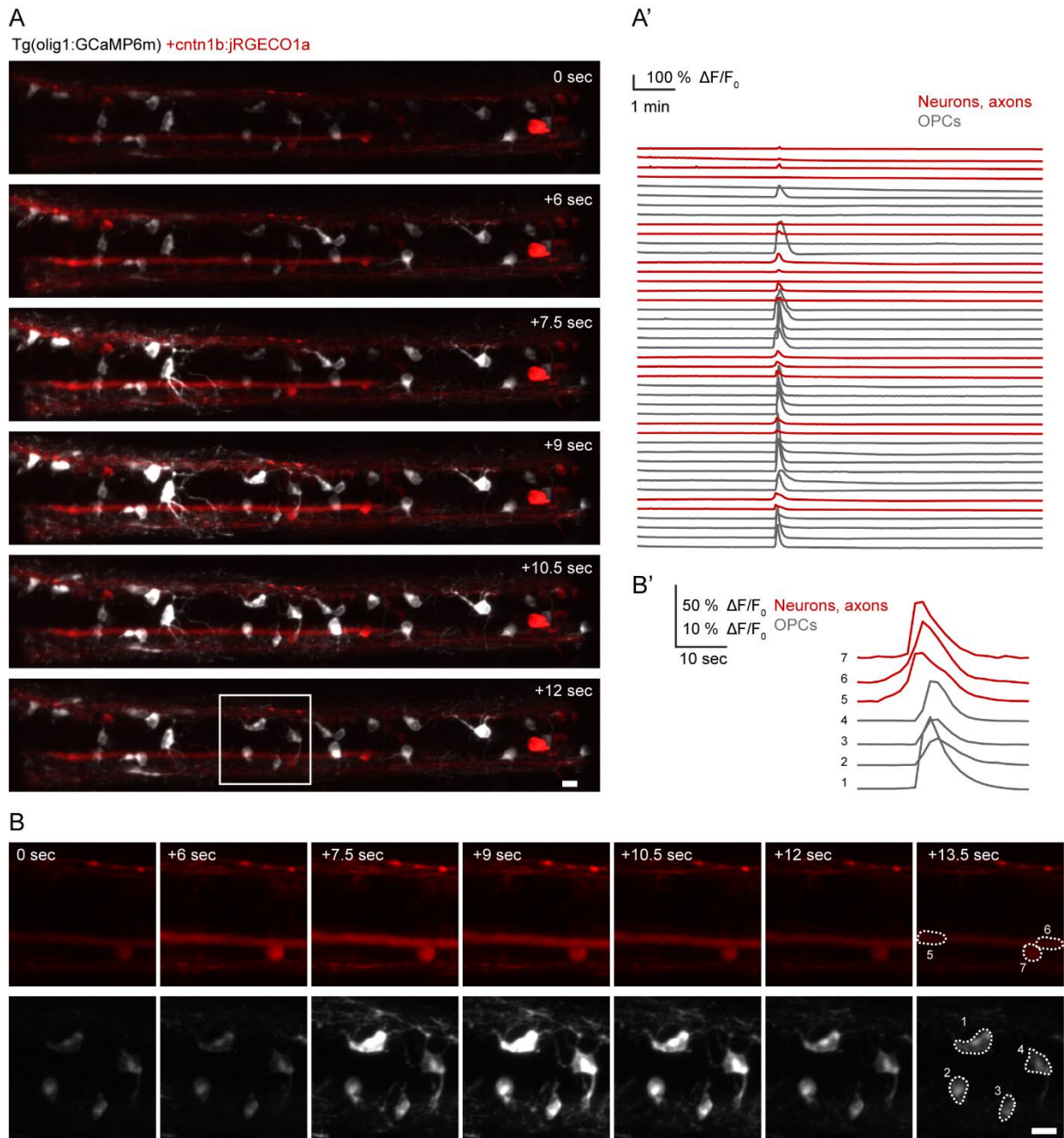


Fig. 3.27 Correlation between calcium transients in neurons and OPCs

A) Light-sheet images showing several time points of Tg(olig1:GCaMP6m) injected with cntn1b:jRGECO1a. Scale bar: 10 μm . **A')** Traces of OPC GCaMP transients and RGECO transients in neurons and axons. **B)** Light-sheet images showing several time points of the close up of the white box in A. GCaMP transients in OPCs arise right after calcium transients in neurons. Scale bar: 10 μm . **B')** Traces of B, traces are from ROI depicted in B (neurons/axons are in red and OPCs in grey). Scale bar: 10 μm .

To further study the correlation between these two cell types, neural activity can be manipulated to explore how this affects calcium transients and the fate of different OPCs.

There are different experimental approaches to manipulate neural activity: chemogenetic, optogenetic and pharmacological. At first, to induce neural activity, I tried a chemogenetic approach using Designer Receptor Exclusively Activated by a Designer Drug (DREADD) which are mutated muscarinic receptors that respond to a synthetic ligand called clozapine-N-oxide (CNO) and not to their natural ligand, acetylcholine. DREADDs are widely used in mice (Armbruster et al., 2007). Recently, a new study showed that it is clozapine, a CNO-derived metabolite (rather than CNO itself), which is the DREADD ligand *in vivo* in rodents (Gomez et al., 2017). I was not able to successfully use this chemogenetic approach in zebrafish, similar to previous studies, possibly because CNO cannot be metabolised by zebrafish (Chen et al., 2016).

Another chemogenetic tool to stimulate neural activity is the expression of the rat TRPV1 (transient receptor potential cation channel subfamily V member 1) channel in zebrafish, which is activated by capsaicin (Fig. 3.28 A) (Caterina MJ, et al. 1997; Chen et al., 2016). TRPV1 is a nonselective cationic ligand-gated channel located on cell membranes. It has high permeability to Ca^{2+} and once capsaicin is applied, the opening of the channel depolarises the cell and increases calcium influx (Fig. 3.28 A). This approach can be used in zebrafish as the endogenous TRPV1 channel of zebrafish is insensitive to capsaicin. The sites important for capsaicin binding are not conserved in zebrafish allowing the selective stimulation of the cell that express the rat TRPV1 channel after capsaicin application (Gau et al., 2013). To test functionality of the rat TRPV1 in zebrafish I performed single cell injection of UAS:TRPV1-tagRFP construct into neurons, using the *cntn1b:KaITa4*, UAS:GCaMP6s line. Consequently, I could follow the calcium activity of neurons before and after capsaicin application, combining the sparsely labelled TRPV1-positive neurons with GCaMP (Fig. 3.28 A'). Capsaicin induced neuronal depolarisation was restricted to the TRPV1-positive cells. After capsaicin application GCaMP activity of TRPV1-positive neurons gradually increased for several minutes until it reached a high plateau level where the trace appeared to be stable. The cell was constantly

depolarised without going back to basal calcium level, suggesting an unhealthy capsaicin effect on the neuron (Fig. 3.28 B-B'). Capsaicin application increased the GCaMP transients in the OPC processes. The rat TRPV1 positive OPCs showed more frequent GCaMP events within 5 minute timelapses compared to the same OPC processes before capsaicin application (Fig. 3.28 C-C'). However, the TRPV1-capsaicin tool was difficult to control, as it depends on the concentration of capsaicin as well as on the expression level of TRPV1 and high doses can be toxic, resulting in apoptosis upon prolonged activation (Chen et al., 2016). Indeed, upon prolonged exposure with capsaicin, OPCs showed cell death and defect in cell morphology appearing with shorter processes. Therefore, TRPV1 is not appropriate to activate neurons and study the effects on OPC fate since this would require a long incubation period.

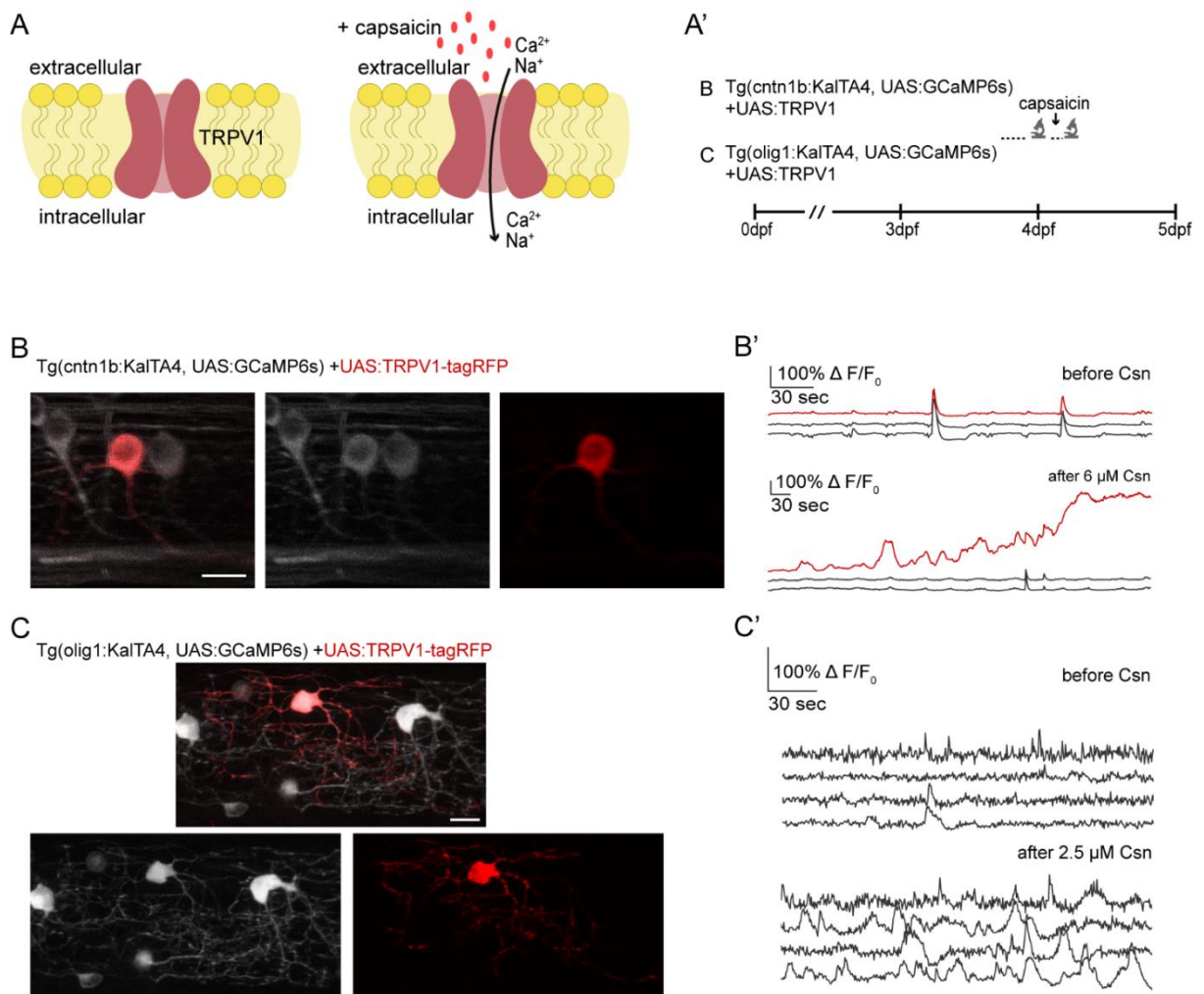


Fig. 3.28 Using TRPV1 in neurons and OPCs to manipulate Ca²⁺ signalling

A) Illustration explaining TRPV1 mechanism of action. **A')** TRPV1 experimental paradigm. **B)** Confocal image of a TRPV1-positive neuron (in red) in between two TRPV1-negative cells in the zebrafish spinal cord. All cells express also GCaMP6s (Tg(cntn1b:KaITa4, UAS:GCaMP6s)). Scale bar: 10 μ m. **B')** GCaMP traces of the neurons showed in B before and after capsaicin showing that the TRPV1-positive neuron (traces in red) is depolarised after the treatment. **C)** Confocal image of a TRPV1-positive OPC (in red) expressing also GCaMP6s (Tg(olig1:KaITa4, UAS:GCaMP6s)) in the zebrafish spinal cord. Scale bar: 10 μ m. **C')** Process GCaMP traces of the TRPV1-positive OPC in C before and after capsaicin showing that after capsaicin OPC processes were more active.

We decided to use a more general pharmacological approach, to globally enhance neuronal excitability by using 4-Aminopyridine (4-AP), a potassium channel blocker (Peña & Tapia, 1999). 4-AP has been also used to improve motor skills in MS patients (Goodman et al., 2013) and it has been shown to induce hyperactivity and seizure-like behaviour in zebrafish when used at high doses (Ellis et al., 2012; Winter et al., 2017).

To investigate the effect of 4-AP in neurons and OPCs I combined the GFP-based GECIs in OPCs using the GCaMP6m OPC line with R-GECO expressed in neurons. I generated the transgenic line Tg(elavl3:jRGECO1a) to express the m-Apple based calcium indicator in neurons. Light-sheet imaging of the double transgenic fish expressing GCaMP6m in OPCs and jRGECO1a in neurons, after 4-AP treatment showed a neuronal calcium transient going through the axonal tracts in the field of view and a subsequent calcium transient in OPC somata, displaying a temporal correlation of calcium activity between the two types of cells (Fig. 3.29). As 4-AP is a potassium channel blocker, it might act as well directly on OPCs since they also express potassium channels (De Biase et al., 2010; Kukley et al., 2010). However, neuronal R-GECO transients preceded the OPC GCaMP transients after 4-AP manipulation. The delay between neuron and OPC transients could highlight a functional connection between these two cell types, instead of OPC direct response to 4-AP (Fig. 3.29).

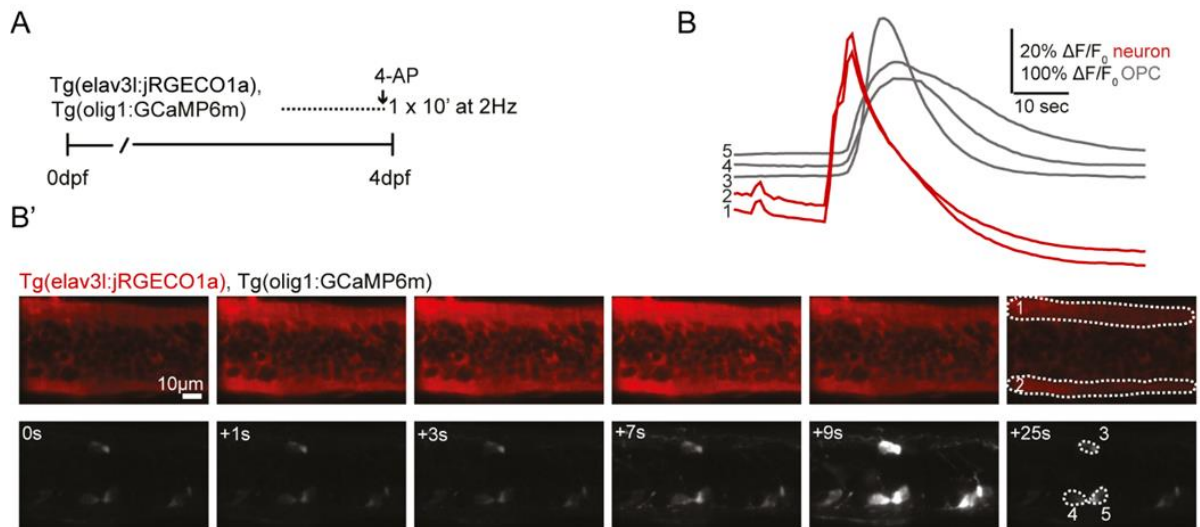


Fig. 3.29 Coupling between neurons and OPCs after 4-AP manipulation

A) Experiment paradigm. **B)** Traces of OPC GCaMP (Tg(olig1:GCaMP6m)) transients and neuron R-GECO(Tg(elav3l:jRGECO1a)) transients expressed in the same animal after 4-AP incubation, traces are from ROI depicted in B' (neurons are in red and OPCs in grey). **B')** Light-sheet images showing several time points of (Tg(elav3l:jRGECO1a), Tg(olig1:GCaMP6m)) double transgenic line after 4-AP. GCaMP transients in OPCs arise right after calcium transients in neurons. Scale bar: 10 μ m.

3.3.2 Calcium events in OPCs induced by neural stimulation

To further investigate the effects of neural manipulation on OPC calcium activity, I analysed calcium transients in OPC processes after 4-AP manipulation and I subsequently used another pharmacological approach to block neuronal activity. To prevent action potentials, I applied the voltage-gated sodium channel blocker tetrodotoxin (TTX) which has been widely used to block neural activity (Gnuegge et al., 2001; Miyazawa et al., 2018). Single plane confocal imaging of GCaMP6m expressed in OPCs under the olig1 promoter revealed that 15 minutes after application of 0.5 mM 4-AP increased in number of GCaMP events in OPC processes could be observed ($12.5\% \pm 9.5/18.3$ active ROI before 4-AP vs. $42.8\% \pm 28.6/78.0$ after 4-AP, $p=0.004$, Friedman with Dunn's multiple comparison test) (Fig. 3.30 A-B''). Almost all processes showed GCaMP events after 4-AP application compared to the baseline traces (Fig. 3.30 B-B'). This effect was partially blocked and reversed to control levels when subsequent $10 \mu\text{M}$ TTX to block action potentials was applied, suggesting that most of the 4-AP induced GCaMP transients were dependent on neural activity ($12.5\% \pm 9.5/18.3$ active ROI before 4-AP vs. $30\% \pm 14.1/44.1$ after 4-AP and subsequent TTX, $p=0.23$, Friedman with Dunn's multiple comparison test) (Fig. 3.30 B'').

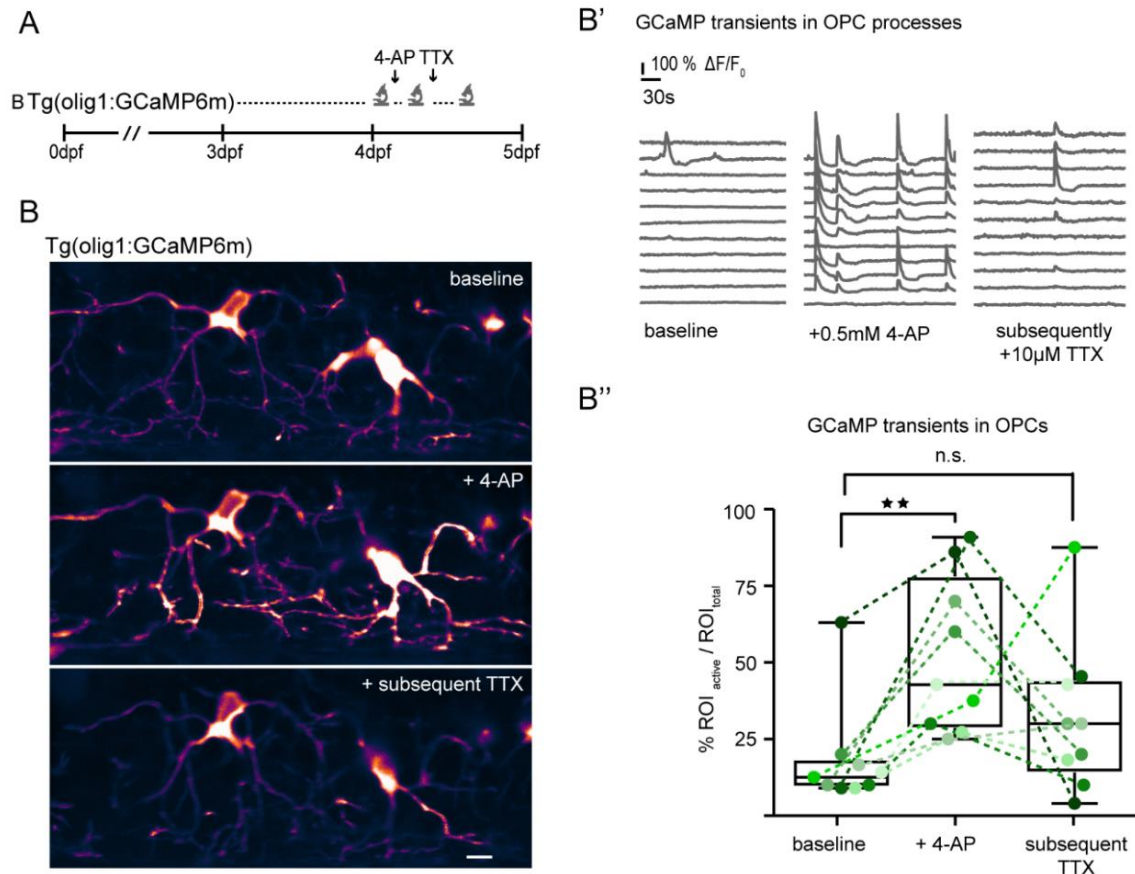


Fig. 3.30 Effects on OPC GCaMP transients after neural activity manipulation

A) Overview of experimental paradigm. **B)** Time projection timelapses traced in B' of OPCs expressing GCaMP Tg(olig1:GCaMP6m) before and after 4-AP or subsequent TTX incubation at 4 dpf. Scale bar: 10 μ m. **B')** Example GCaMP traces in Tg(olig1:GCaMP6m) before drug application, after treatment with 4-AP, and after addition of TTX. **B'')** Quantification of GCaMP events (ROI active / ROI total) per fish in the different treatment conditions as in B. Data are expressed as median \pm interquartile range (12.5% \pm 9.5/18.3 active ROI before 4-AP vs. 42.8% \pm 28.6/78.0 after 4-AP, $p=0.004$ vs. 30% \pm 14.1/44.1 after 4-AP and subsequent TTX, $p=0.23$ (Friedman with Dunn's multiple comparison test, test statistics=11.09), $n=9$ animals. (Marisca et al., 2020)

I could then replicate the effects of 4-AP and TTX on OPC calcium dynamics using CaMPARI. I treated animals with 4-AP, TTX or tricaine (MS-222), a fish anaesthetic which prevents Na^{2+} channel opening, prior and during the 5 minute UV light treatment. Tile scan images of the entire fish revealed that red/green ratio of OPCs was significantly higher in 4-AP treated animals (control 0.4 ± 0.21 vs 0.8 ± 0.36 4-AP, $p=0.04$, Kruskal-Wallis test) and lower in animals treated with TTX or tricaine compared to the control, confirming that CaMPARI is a valid technique to study cell resolution calcium dynamics also combined with a pharmacological manipulation approach (Fig. 3.31).

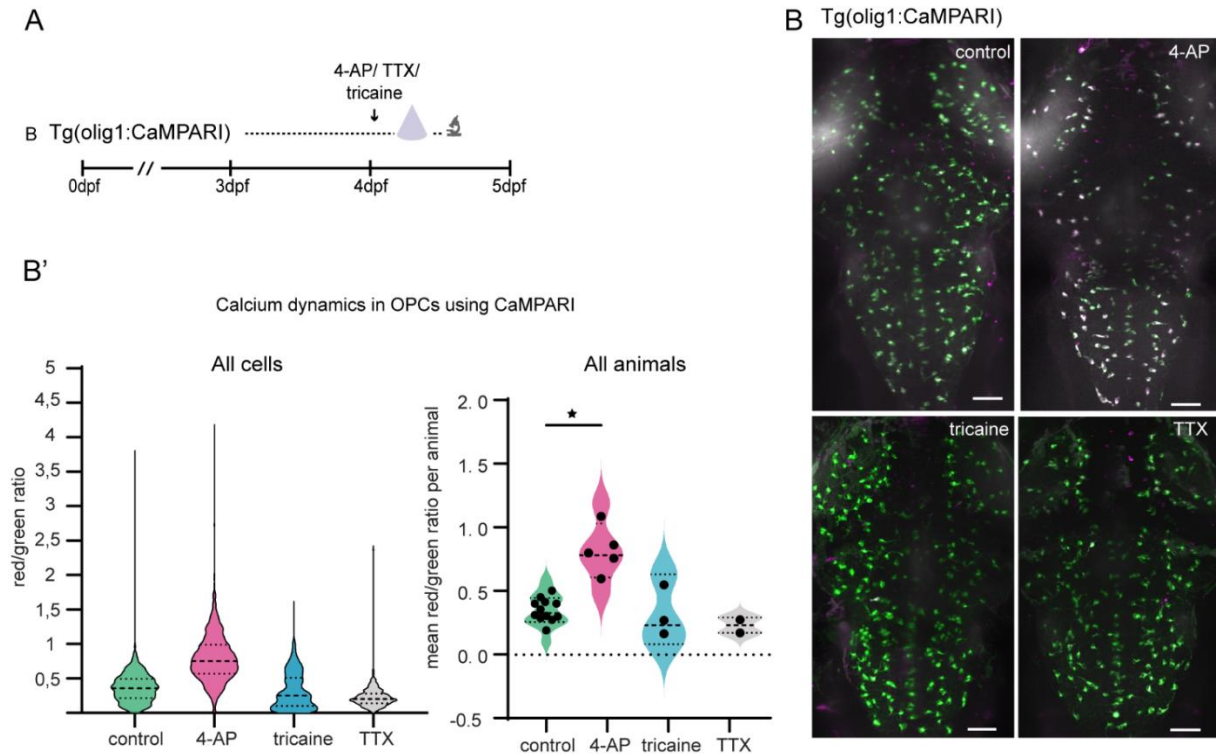


Fig. 3.31 Effects on OPC calcium activity after neural activity manipulation using CaMPARI

A) Overview of experimental paradigm. **B)** Example images of Tg(olig1:CaMPARI) animals in the four different conditions after UV light treatment. Scale bar: 50 μ m. **B')** left: red/green ratio of Tg(olig1:CaMPARI) animals after UV-light treatment and in different conditions (control, 4-AP, tricaine, TTX). Data are presented as median and interquartile range. Right: mean of red/green ratio per fish of control (0.4 ± 0.21), 4-AP (0.8 ± 0.36), tricaine (0.3 ± 0.26) and TTX (0.2 ± 0.14), each data point represents an animal. Data are presented as median and interquartile range. $p = 0.04$ (control vs. 4-AP) Kruskal-Wallis test, $n=12/5/3/2$ animals.

In summary, through *in vivo* GCaMP imaging I showed that some OPC calcium transients are induced by neural activity, since they were enhanced by 4-AP incubation and reverted using the action potential blocker TTX. Moreover, this result was confirmed using CaMPARI, showing that OPC intracellular calcium was increased and decreased applying 4-AP and TTX or tricaine respectively.

Fig. 3.32⁴ Macrophages infiltration after long term 4-AP incubation

A) Confocal images of Tg(mfap4:memCerulean), Tg(olig1:nls-mApple) zebrafish at 4 dpf after treatment with 0.1 mM 4-AP, 0.5 mM 4-AP, or Danieau's solution as control. Transmitted light images to show spinal cord morphology and tissue integrity following treatment. Scale bars: 100 μ m. The graph shows the number of macrophages which accumulate in 400 μ m length of spinal cord of Tg(mfap4:memCerulean) zebrafish after 1 day of control ($2 \pm 0.25/2$ cells), 0.1 mM ($2 \pm 1/2$ cells), and 0.5 mM ($3 \pm 0.25/2$ cells) 4-AP treatment (median (25%/75% percentiles); $p=0.43$ (control vs. 0.1mM 4-AP), $p=0.03$ (control vs. 0.5 mM 4-AP) (Kruskal-Wallis test), $n=16/19/8$ animals. (Marisca et al., 2020)

To test the efficacy of the long-term pharmacological treatment to induce activity, we first looked at swimming behaviour using 4-AP and TTX. We tested the swimming behaviour because 4-AP is a well-known convulsant used to induced seizures in mice (Yamaguchi and Rogawski, 1992). 4-AP and TTX application clearly increased and blocked respectively swimming activity compared to the control. TTX also prevented the effect of 4-AP when the two compounds were applied together (Fig. 3.33 A). To confirm 4-AP and TTX effects on neural calcium activity I performed single plane GCaMP imaging using GCaMP6s targeted to the nuclei and expressed in neuron under the *elavl3* promoter. As expected, 4-AP overnight application increased numbers of somatic GCaMP transients in neurons which showed mostly small and short GCaMP transients along the whole timelapse while before 4-AP incubation somata had less frequent GCaMP activity. Moreover, some of the somatic GCaMP transients appeared to be synchronised with other neurons both in control and after 4-AP incubation (Fig. 3.33 B-B'). Instead, TTX completely blocked somatic GCaMP transients in neurons which were almost completely silent compared to the ones before TTX incubation (Fig. 3.33 B-B').

⁴ Data shown in this figure are from the work of my colleague Laura Hoodless

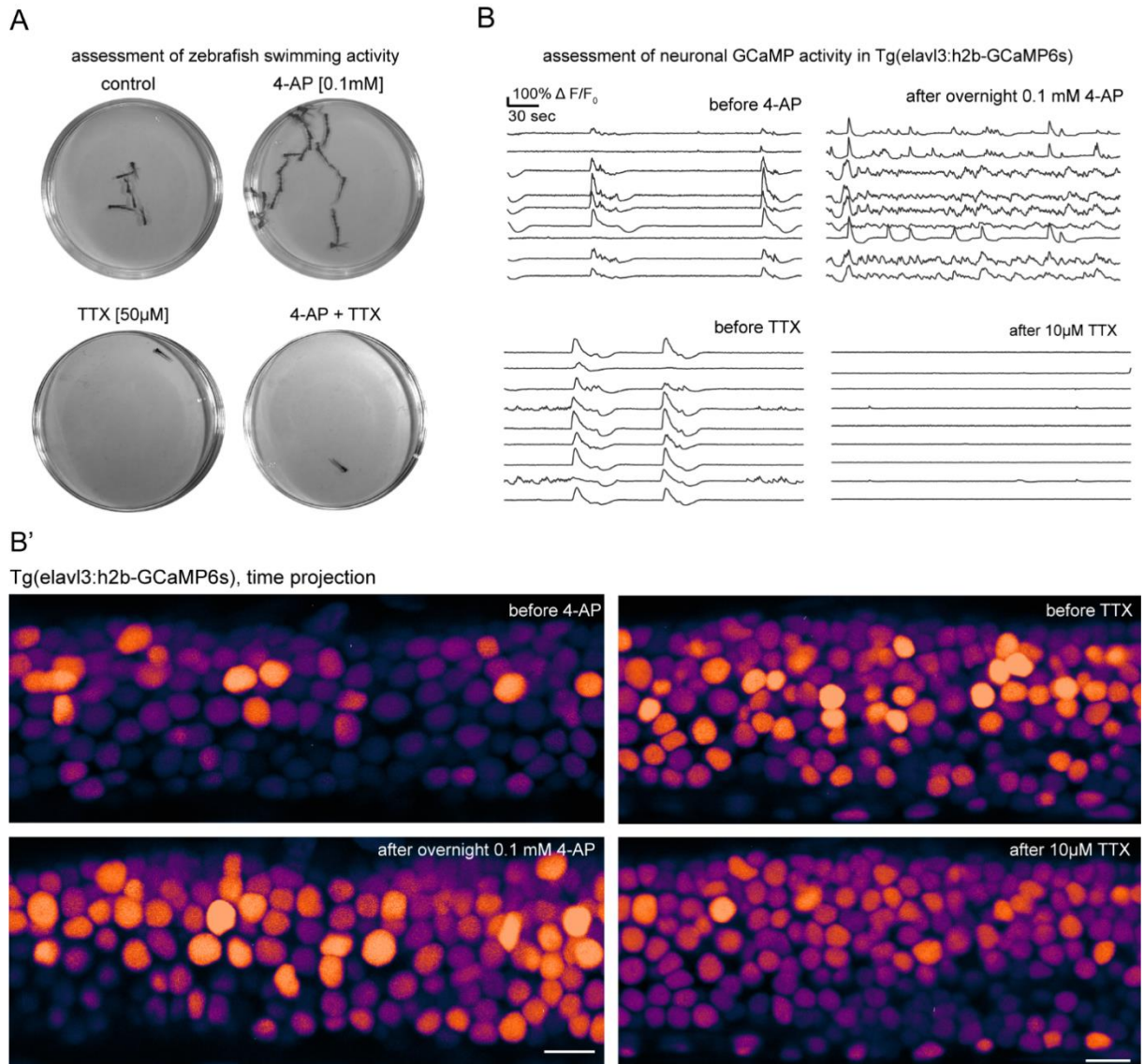


Fig. 3.33 Effects 4-AP treatment on zebrafish

A) ⁵Minimum intensity projections of a two-minute time-lapse of fish freely swimming in a 3 cm petri dish in different treatment conditions. **B)** Traces of GCaMP transients Tg(elavl3:h2b-GCaMP6s) zebrafish at 4 dpf and after overnight incubation in 0.1 mM 4-AP, and before / after 10 μM TTX. **B')** Time projection timelapses traced in B of neurons expressing GCaMP Tg(elavl3:h2b-GCaMP6s) before and after 4-AP or TTX incubation. Scale bar: 10 μm. (Marisca et al., 2020)

Now that we found the appropriate protocol for long term neural activity manipulation, we wanted to investigate the effect of neural activity on OPC cell fates. At this point, we could have different possible outcomes. Enhanced neural activity could increase OPC proliferation or OPC

⁵Data in panel A are from my colleague Laura Hoodless.

differentiation, or even both cellular behaviour responses at the same time. Moreover, we would expect that neuron-rich area OPCs are the cells affected the most as they integrate more neural activity compared to axo-dendritic area OPCs. To quantify OPC proliferation after neural manipulation, we used 5-ethynyl-2'-deoxyuridine (EdU). EdU is incorporated into the DNA of dividing cells during the S-Phase of the cell cycle. Using Tg(olig1:nls-mApple) transgenic fish after a 6 hours 4-AP incubation, we were able to identify an increase in EdU-positive OPCs, especially those residing in neuron rich areas ($9\pm 3.1\%$ vs. $0.08\pm 3.5\%$ increase, $p=0.02$ in neuron-rich areas, two-tailed unpaired t-test) (Fig. 3.34 A-B''). On the other hand, TTX treatment appeared to block the 4-AP effects on proliferation ($19.1\pm 1.1\%$ in control vs. $30.6\pm 1.5\%$ in 4-AP vs. $14.1\pm 2.2\%$ in 4-AP+TTX; $p<0.001$ (control vs. 4-AP), $p<0.001$ (4-AP vs. 4-AP+TTX), one-way ANOVA with Tukey's multiple comparisons test) (Fig. 3.34 B'). We also investigated subsequent changes in number of myelinating oligodendrocytes using the Tg(mbp:nls-EGFP) line after a two days of 4-AP treatment and we detected a small increase in the number of cells which did not reflect the more pronounced increase in OPC numbers (48.9 ± 2.4 cells/field in control vs. 54.6 ± 1.5 in 4-AP, $p=0.047$, two-tailed unpaired t-test) (Fig. 3.34 C).

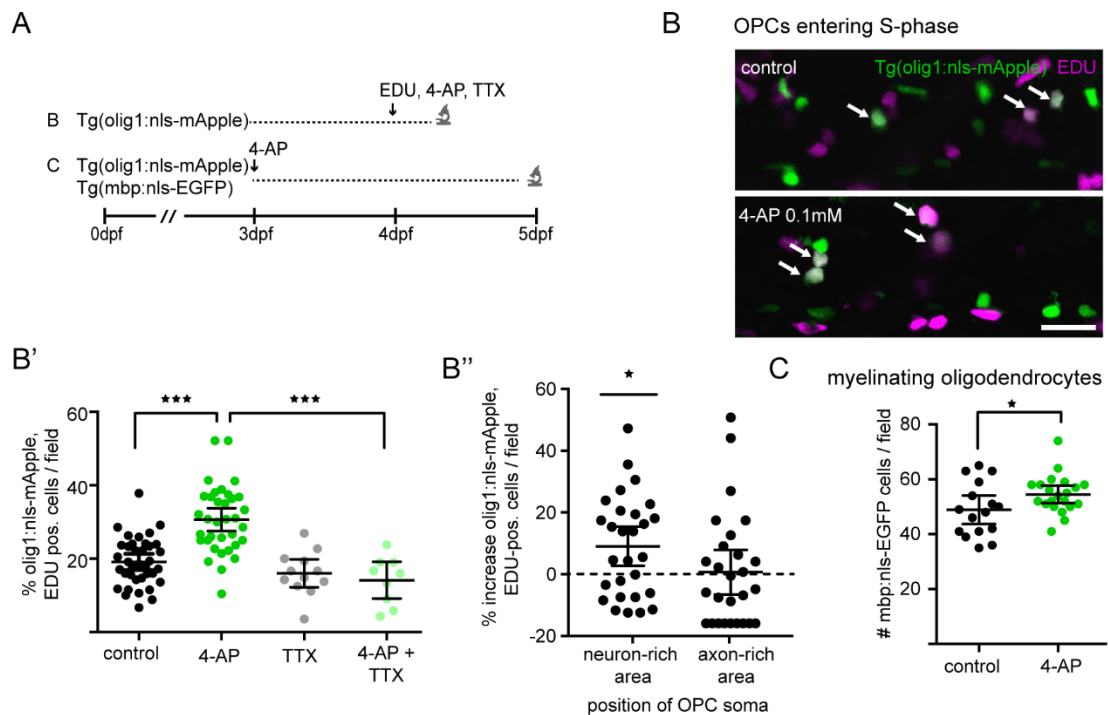


Fig. 3.34 ⁶Manipulation of neural activity increases proliferation of OPCs in neuron-rich areas.

A) Experiments paradigm. **B)** Representative confocal images of Tg(olig1:nls-mApple), EdU-labelled OPCs at 4 dpf. Arrows indicate double positive cells. **B')** Quantification shows olig1:nls-mApple/EdU double-positive cells in different treatment conditions. Data expressed as mean \pm 95% confidence interval, (19.1 \pm 1.1% in control vs. 30.6 \pm 1.5% in 4-AP vs. 14.1 \pm 2.2% in 4-AP+TTX; $p < 0.001$ (control vs. 4-AP), $p < 0.001$ (4-AP vs. 4-AP+TTX) (one-way ANOVA with Tukey's multiple comparisons test) $n = 37/35/9$ animals. Scalebar: 50 μ m. **B'')** Percentage increase in EdU-positive OPCs located in neuron-rich and axo-dendritic areas after 4-AP treatment. Data are expressed as mean \pm 95% confidence interval (9 \pm 3.1% vs. 0.08 \pm 3.5% increase, $p = 0.02$ in neuron-rich areas, two-tailed unpaired t-test), $n = 28$ animals. **C)** Myelinating oligodendrocyte numbers with and without 4-AP treatment. Data are expressed as mean \pm 95% confidence interval (48.9 \pm 2.4 cells/field in control vs. 54.6 \pm 1.5 in 4-AP, $p = 0.047$, two-tailed unpaired t-test), $n = 16/21$ animals. (Marisca et al., 2020)

Manipulation of neural activity affected OPC calcium levels and cellular behaviour. In particular, 4-AP-induced neural activity triggered frequent OPC GCaMP rises as well as OPC cell divisions. Therefore, we wondered how important the role of calcium signalling is in mediating proliferation induced by 4-AP. To investigate the importance of intracellular calcium rises, I expressed in OPCs the plasma membrane Ca^{2+} pump hPMCA2w/b (CaEx), previously used in astrocytes (Yu et al., 2018), which exports cytosolic calcium to reduce intracellular calcium signalling (Fig. 35 A). I expressed mCherry-CaEx in OPCs and followed their behaviour for 24h. CaEx-positive OPCs showed similar division rates as control,

⁶ Data shown in this figure are from the work of my colleague Laura Hoodless

UAS:mScarlet labelled OPCs. However, upon incubation with 4-AP for 24 hours, division events in OPCs of control animals were, as expected, significantly increased (15% (9/61 cells) in control vs. 45% (25/55 cells) in 4-AP-treated group, $p < 0.001$, two-tailed Fisher's exact test) whereas CalEx-positive OPCs did not show increased proliferation after 4-AP treatment (20% (7/35 cells) control vs. 24% (8/33 cells) 4-AP, $p = 0.77$, two-tailed Fisher's exact test) (Fig. 35 B-D). Neuronal activity-dependent OPC divisions triggered by 4-AP application relied on high OPC calcium levels. When intracellular calcium was extruded from OPCs, the activity-dependent proliferation enhancement was hindered. This highlights an important role for intracellular calcium to trigger OPC division induced by enhanced neural activity.

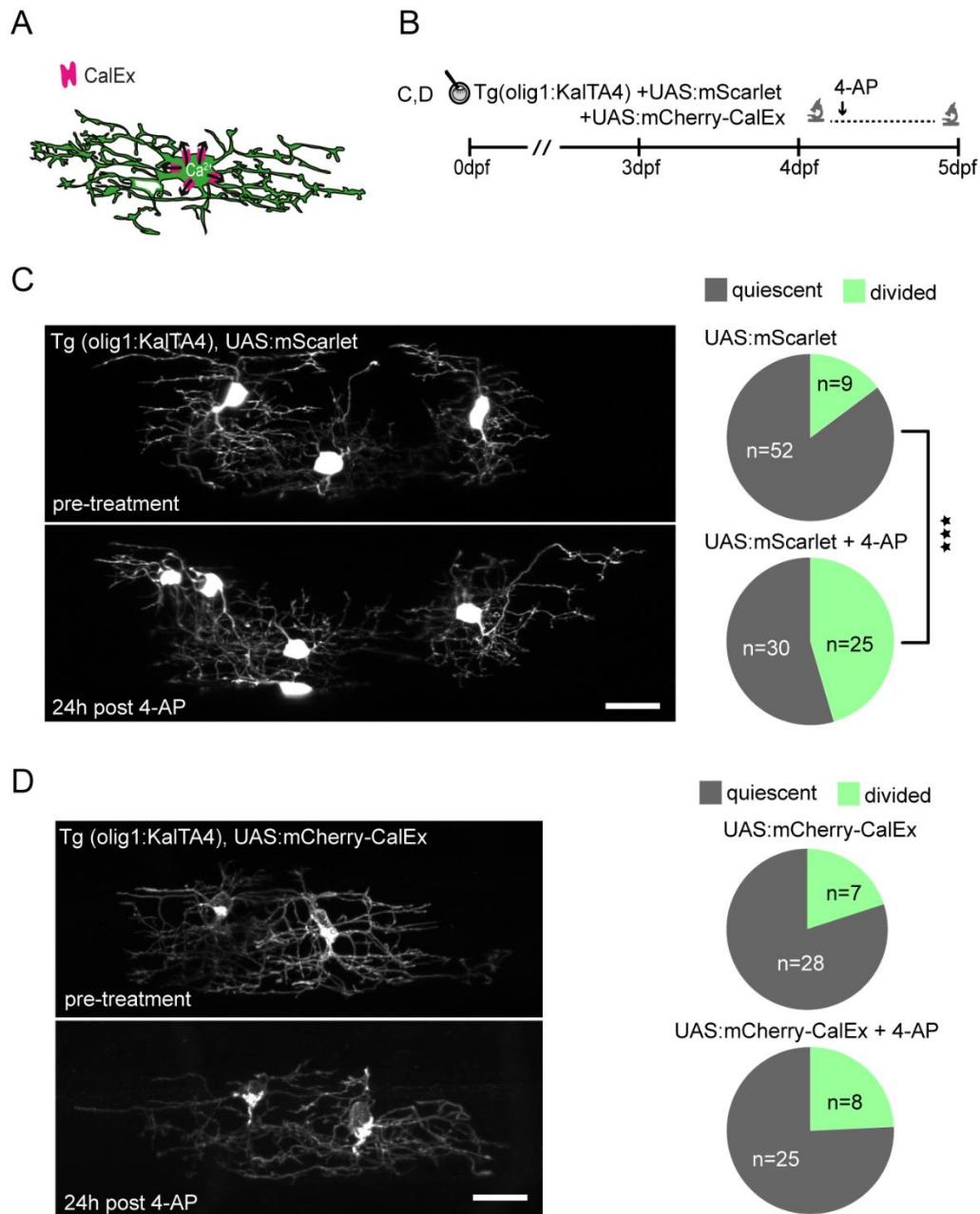


Fig. 3.35 OPC intracellular calcium signalling is necessary to induce proliferation generated by 4-AP incubation.

A) Illustration explaining CaMPARI. **B)** Experiments paradigm. **C)** Confocal images of individual OPCs at 4 dpf and 24h post 4-AP treatment. Scale bar: 20 μ m. Pie charts show the frequency of cell divisions observed in the different conditions. 15% (9/61 cells) in control vs. 45% (25/55 cells) in 4-AP-treated group, $p < 0.001$, two-tailed Fisher's exact test, $n = 18/24$ animals. **D)** Confocal images of individual CalEx expressing OPCs at 4 dpf and 24h post 4-AP treatment. Scale bar: 20 μ m. Pie charts show the frequency of cell divisions observed in the different conditions. 20% (7/35 cells) control vs. 24% (8/33 cells) 4-AP, $p = 0.77$, two-tailed Fisher's exact test, $n = 11/24$ animals. (Marisca et al., 2020)

Taken together, these data show that we can identify two different OPC types in the zebrafish spinal cord. OPCs with their somata residing in the neuron-rich areas of the zebrafish spinal cord and OPCs with their somata in the axo-dendritic areas. Neuron-rich area OPCs do not directly differentiate but they can contribute to myelination after a cell division event whereas, axo-dendritic area OPCs can directly differentiate into myelinating oligodendrocytes. Moreover, neuron-rich area OPCs are more sensitive to neural activity, they present more synaptic sites, have higher GCaMP amplitude and upon enhanced neural activity they proliferate more compared to the other group (Fig. 3.36 A). In addition, high intracellular calcium levels are necessary to trigger proliferation generated by neural activity via 4-AP treatment (Fig. 3.36 B).

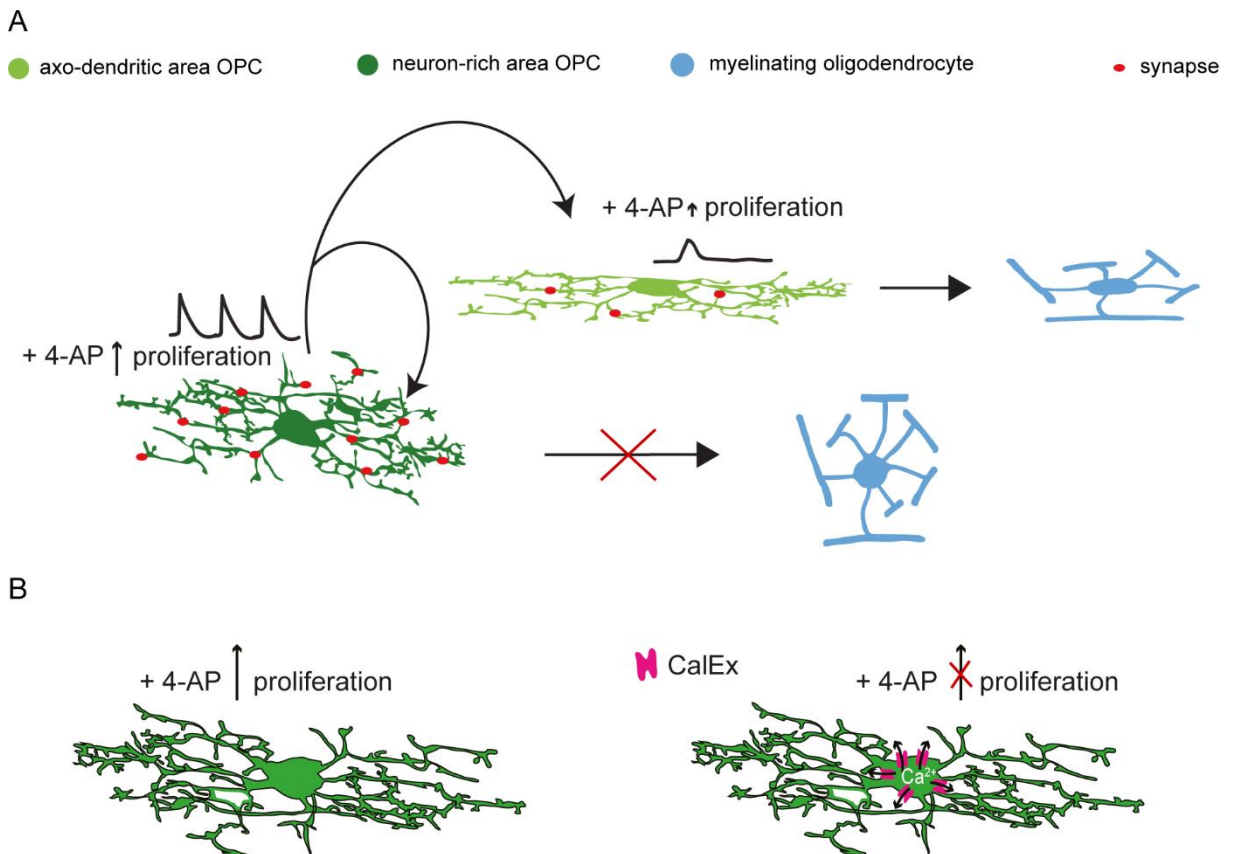


Fig. 3.36 Summary of OPC characteristic and behaviours in the zebrafish spinal cord upon stimulation of neural activity

- A)** Illustration summarising neuron-rich area and axo-dendritic area OPCs properties in the zebrafish spinal cord, including OPCs interrelation, synaptic densities, GCaMP transients and effect of neural manipulation on cell fate.
B) Illustration explaining 4-AP induced neural activity on OPCs expressing CalEx.

4 DISCUSSION

4.1 Key questions and findings

Myelination is important to modulate neural circuit function, allowing fast conduction between neurons. Myelin sheaths around the axons are made by oligodendrocytes which come from the differentiation of oligodendrocyte precursor cells (OPCs). OPCs represent one of the most abundant cell population of the central nervous system (CNS) and their number is constantly maintained during the whole life, considering that not all OPCs differentiate into oligodendrocytes. OPC proliferation and differentiation are both enhanced by several factors like social experience, learning and neuronal activity. Indeed, OPCs sense neural activity by expressing several neurotransmitter receptors and voltage gated ion channels. One important second messenger involved in neuron-OPC signalling is calcium which rises in OPCs in response to neural activity. Recently, OPCs have been recognised as a heterogeneous population, having diverse electrophysiological properties and different molecular signatures. This led to the question whether all OPCs communicate similarly with neurons, and how this interaction affects their behaviour and function in regulating myelination.

To study mechanisms of axon-OPC interaction, I used zebrafish spinal cord as a model system. Two distinct OPC subtypes were identified in the zebrafish spinal cord. One group of OPCs residing within axo-dendritic areas of the lateral spinal cord, which are characterised by a simple cell morphology, fast process dynamics and a high probability to differentiate. The other group of OPCs have their soma in the neuron-rich areas of the central spinal cord whilst extending their processes into axo-dendritic areas of the lateral spinal cord. These OPCs were characterised by a complex morphology, slow process dynamics and without direct differentiation potential. Moreover, neuron-rich area OPCs presented more post-synaptic densities and were more sensitive to neural activity compare to axo-dendritic OPCs primed to differentiation. In my PhD work, I have generated new reagents and lines to perform for the first time *in vivo* calcium imaging of OPC transients. I expressed the genetically encoded calcium sensor GCaMP in OPCs and I characterised OPC calcium transients at single and cell

population levels. OPCs can display different types of GCaMP transients: transients which are restricted to process subdomains, or which spread through the whole cell. Neuron-rich area OPCs had higher probability of showing somatic calcium transients and had higher amplitudes compared to axo-dendritic area OPCs. OPC population GCaMP imaging revealed that sometimes somatic calcium transients spread amongst neighbouring OPCs or even amongst all OPCs in the field of view, suggesting a sort of coupling between OPCs. Moreover, I set up another tool, CAMPARI, to study cell resolution somatic calcium dynamics amongst the entire OPC population of zebrafish. This method highlighted similar calcium concentration and boundaries between neighbouring OPCs comparable with the GCaMP imaging results. Finally, the pharmacological manipulation of neural activity demonstrated that part of the calcium transients in OPCs are neuron-induced. Use of the EdU assay revealed that neural activity induced by pharmacological manipulation triggered OPC proliferation, mostly affecting neuron-rich area OPCs. Furthermore, intracellular calcium was necessary to trigger division induced by neural activity. My work gives new insights about OPC heterogeneity and function in the zebrafish spinal cord. Two subgroups of OPCs were identified, one primed for differentiation and the other one with possible differentiation potential only after a division event. Moreover, one subgroup, the neuron-rich area OPCs integrate more neural activity which induced proliferation, revealing the main effect on OPC fate of neural activity *in vivo*.

4.2 OPC properties and fates

General morphology and position

OPCs have been well characterised in rodents and have been found to constitute a heterogeneous population depending on age and brain regions (Bonetto et al., 2020). However, the function of different OPC subtypes, have been not yet described. Furthermore, it is still controversial whether the differences found represent a different subtype, or a different cell lineage state along the oligodendrocyte lineage. OPC heterogeneity had not yet been studied in zebrafish. As the main question was to study whether all OPCs communicate similarly with axons to regulate myelination, at first, I needed to characterise OPCs in zebrafish to identify possible diversity. I showed that all OPCs in the zebrafish spinal cord with their arborized processes form a dense network in the lateral zebrafish spinal cord. The lateral spinal cord, where OPC processes are extended, is constituted by myelinated and unmyelinated axons, as well as dendrites. I therefore gave a general description of the position of the cells involved in my study, showing that OPC processes have a stereotypical position in the zebrafish spinal cord projecting in the lateral spinal cord where also myelinated and unmyelinated axons run, and where synaptic contacts are formed. This suggests that all OPCs are in contact with the same axons running along the lateral tract of the spinal cord. The lateral side of the spinal cord, here referred to as axo-dendritic area, in developing zebrafish corresponds to the white matter (WM) described in the adult zebrafish. The central area of our system, which I called neuron-rich area, is instead densely filled with cell bodies and constitutes the grey matter (GM) in adulthood (Möllmert et al., 2020). Axo-dendritic areas and neuron-rich areas cannot be called WM and GM respectively, because they have obvious differences comparing these two areas with WM and GM in rodents. We have to take into account the difference in tissue size between the developing zebrafish and mice. Indeed, the zebrafish spinal cord has a relatively small volume with the spinal cord diameter of about 60 μ m allowing one single OPC to extend the processes in both lateral neuropil regions crossing the whole spinal cord. Whereas, the mouse spinal cord is about 3 mm wide and GM and WM are

two clearly separated regions (Ong and Wehrli, 2010). In both zebrafish and rodents, the myelinated axons are in a region called white matter. In addition, in zebrafish there is a strong segregation of cell bodies in the central spinal cord, and axons and dendrites in the lateral spinal cord, different than the composition of the grey matter in rodents which contain axons and dendrites as well. Therefore, taking into account our study in zebrafish, one hypothesis might be that within the grey matter in rodents there might be as well different OPC subtypes, depending on the surrounding environment enriched in either cell bodies, or in axons and dendrites.

Single cell OPC morphology and process dynamics

When we looked at single cell OPC morphology we identified differences in terms of morphology, process dynamics and soma position amongst OPC population. In particular, OPCs with their soma in the axo-dendritic areas showed a simpler morphology compared to the OPCs with their soma in the neuron-rich areas. This was in line with what has been previously described in the rat CNS, where OPC morphology was different amongst white matter and grey matter regions. OPCs in white matter regions showed a typical bipolar morphology with simpler process ramification. In grey matter regions, OPCs have a stellate morphology with processes extending from all around the cell body (Dawson et al., 2003). However, in our system both subtypes of OPCs projected their processes in the later side of the spinal cord, suggesting that they share the same environment and that the discriminating factor between the two OPCs in term of morphology, is their soma position. Another analogy of our study with the work by Dawson *et al.* takes into account the shape of the soma. Indeed, they reported an elongated cell body shape for the OPCs residing in the white matter (WM) regions as the soma shape of the axo-dendritic OPCs in our system. Instead, a rounded soma shape was described when they looked at OPCs in the grey matter (GM) regions as the cell body shape of neuron-dendritic areas in the zebrafish spinal cord.

Looking at process dynamics of the two subtypes of OPCs, work done by my colleague Tobias Hoche, we found that OPCs with their soma residing in the axo-dendritic areas displayed fast process remodelling compared to OPC with their soma residing in the neuron-rich areas. As already shown in developing zebrafish and mouse, OPC processes extend and retract their processes to explore the environment around them (Kirby et al., 2006, Hughes et al., 2013). Our finding suggests that OPCs with their soma in the axo-dendritic area explored the surrounding axons more actively compared to the neuron-rich area OPCs. This is in line with the differentiation potential of the axo-dendritic area OPCs which can directly differentiate to give rise to myelinating oligodendrocytes. The fast process remodelling behaviour might be an indication to explore surrounding environments and identify the axon that need to be myelinated.

Soma position and differentiation potential

After identifying differences in morphology and soma position comparing spinal cord OPCs, we then looked into the cell fate of these two subtypes of OPCs to understand whether both OPCs contributed equally to myelination. Long-term longitudinal analysis, done by my colleague Tobias Hoche, following both subtypes of OPCs for several days revealed that axo-dendritic area OPCs in the zebrafish spinal cord were primed to differentiation. These cells could directly differentiate into myelinating oligodendrocytes. Instead, neuron-rich area OPCs never directly differentiated but they always required a division event to give rise to a cell with a differentiation potential. Differences between the two subtypes of OPCs in the zebrafish spinal cord have been also confirmed by transcriptome analysis of single cells which I briefly mention in the previous section. Our group in collaboration with the Castelo-Branco's lab provided data on the molecular features of the two subgroups of OPCs identified in our system using single-cell RNA-seq. In particular, five clusters (#1-#5) have been characterised by the expression of oligodendrocyte lineage transcription factors (Marisca et al., 2020). Amongst them, four clusters (#1-#4) expressed OPC markers and one cluster (#5) markers for mature

oligodendrocytes. In-situ hybridization analysis correlated the differential gene expression amongst the clusters with the two OPC subgroups with different soma positions found in the live cell imaging. OPCs from cluster #1 were mostly found in the neuron-rich areas and OPCs from cluster #4 were instead found in the axo-dendritic areas. The other two clusters were found in both areas and expressed cell cycle markers. Interestingly, gene ontology analysis revealed that the genes upregulated in cluster #1, representing mostly neuron-rich area OPCs, were involved in neurotransmission and transmission across chemical synapses. Cluster #4 representing the axo-dendritic area OPCs was enriched in genes involved in early differentiation like *myrf* (Marisca et al., 2020).

Differences in differentiation potential were also found between WM and GM in mammals. The majority of the WM OPCs differentiated into mature oligodendrocytes suggesting a role for the surrounding environment in determining the differentiation capacity (Viganó et al., 2013). Most of the WM OPCs differentiated to give rise to myelinating oligodendrocytes, whereas GM OPCs were mostly proliferating (Dimou et al., 2008). To clarify whether the differentiation properties were linked to intrinsic cell diversity, rather than to environmental factors, homotopic and heterotopic transplantations in the mouse cerebral cortex were performed. WM-derived OPCs differentiate more frequently than GM-derived cells, even when transplanted in the GM environment (Viganó et al., 2013). This means that there is an intrinsic difference between these cells, but at the same time environmental cues could have influenced their nature before the transplantation. However, in my work I showed that in the zebrafish spinal cord all OPCs are in contact with the same axons running along the lateral side, suggesting that the differentiation potential does not depend on the presence of more myelination-competent axons. Instead, the cell body position is the feature that determines the fate and differentiation potential. One key role for the different behaviour regulated by the soma position, could be played by mechanical forces applied to the cell bodies in the two different areas. Indeed, OPCs are mechanosensitive, their capacity to proliferate, migrate and differentiate is dependent on the stiffness of the substrate *in vitro* (Jagielska et al., 2012). Mechanical stimuli promote OPC differentiation on soft substrates while growth of OPCs on stiff substrates prevents myelination

(Tsai and Casaccia 2019). In line with our findings, spinal cord tissue properties characterisation both in mammal and in zebrafish revealed that GM tissue is much stiffer compared to the WM one (Koser et al., 2015; Möllmert et al., 2020). This suggests that mechanical forces could prevent the neuron-rich area OPC to differentiate. Physical characteristics of the axonal microenvironments can also influence cell fate decision. Spatial constraints of densely packed axons and OPCs promote OPC differentiation. One hypothesis is that axons in the lateral spinal cord may compress OPC cell soma, which in the axo-dendritic areas present an elongated shape, causing structural rearrangements. Changes in size and shape of the nucleus may induce the transcription of genes involved in OPC differentiation (Rosenberg et al., 2008). Another factor that can regulate OPC fate could involve signalling molecules. The differences in differentiation between axo-dendritic area and neuron-rich area OPCs could be due also to cell surface molecules. Indeed, cell-adhesion molecules (CAMs) have been shown to play an important role in the signalling between axons and oligodendrocytes (Laursen and French-Constant, 2007). Axo-dendritic OPCs might participate in the signalling with axons through surface molecules, as their somata are in close proximity to the axons. In addition to cell-adhesion molecules, also the non-synaptic release of neurotransmitters along the axons has been shown to be involved in intercellular signalling and to induce myelination of active axons (Wake et al., 2015). The idea is that this signalling would mostly affect OPCs with their somata in the vicinity of axons, therefore the axon-dendritic area OPCs, triggering their differentiation. Further studies are required to investigate this hypothesis.

4.3 Hierarchy between OPC subgroups

Previous findings have also described OPCs as a heterogeneous population with different gene profiles and electrophysiological properties. However, an unsolved question was whether different OPCs resemble different states of cells along their lineage progression with the same function or whether they actually represent different subtypes executing different functions. Longitudinal analysis over time of single OPCs revealed that axo-dendritic area OPCs are the cells that usually differentiate compared to the neuron-rich area OPCs that contribute to myelination only after a division event.

This was also confirmed when we triggered myelination using splitomicin. Animals treated with splitomicin showed increase in oligodendrogenesis. New formed myelinating oligodendrocytes came from neuron-rich area OPCs after a division event. This suggests the importance of a recent proliferative event to form OPCs with a differentiation potential. Even in the presence of an external stimulus to induce myelination, neuron-rich area OPCs continue to require a division to create an OPC primed to differentiation.

Cell fate analysis highlighted the interrelation between the two OPC subgroups. Neuron-rich area OPCs need to proliferate to form a new daughter cell with axo-dendritic OPC features, primed to differentiate. Moreover, once OPCs get certain features as axo-dendritic or neuron-rich area OPCs, do not switch towards the other type. For this reason, in my thesis, I always referred to the two OPC subgroups as two subtypes and not two states along their lineage progression. The neuron-rich area OPCs cannot switch their function and directly differentiate, but they can divide and create new OPCs that have differentiation potential creating a connection between the two different subgroups (Fig. 4.1). Therefore, in our system, OPC subtypes are defined by both extrinsic and intrinsic factors. The extrinsic component is represented by the local environment around the soma which for the neuron-rich area OPCs is characterised by cell bodies, whereas for the axon-dendritic area OPCs by the neuropil. The intrinsic component that gives the differentiation potential to the OPCs is represented by the recent cell division which is necessary to make OPCs switch properties and fates.

In line with our findings, differentiation of newly divided OPCs has been identified also in the postnatal developing mouse brain (Hill et al., 2014). Another recent work showed that fear learning experience in young mice triggered OPC proliferation which was followed by an increase in OPC differentiation in the following weeks. The newly generated oligodendrocytes came from recently divided OPCs (Pan et al., 2020). However, other studies reported a direct increase in OPC differentiation in the adult mouse cortex after sensory enrichment and motor learning (Hughes et al. 2018; Xiao et al., 2016). A more recent study, reported increase in differentiation without increase in OPC proliferation in developmental and in remyelinating conditions, showing that motor learning could improve remyelination involving newly differentiated and pre-existing oligodendrocytes (Bacmeister et al., 2020). Therefore, it is still unclear whether differences in proliferation and differentiation is based on the developmental or adult myelination depending on the age of the animals or on the intrinsic age of the cells. This indicates that differentiating OPCs in adults are coming from newly divided cells, therefore intrinsically young cells. In remyelination, OPCs often fail to differentiate, this could be explained by thinking that OPCs need to be intrinsically young and surrounded by an appropriate local environment to be able to differentiate. Indeed, remyelination was shown to be more efficient in grey matter lesions than in white matter lesions (Albert et al. 2007). Further studies to impair specifically OPC proliferation without directly affecting differentiation are needed to confirm whether proliferation is necessary for activity-dependent differentiation of OPCs.

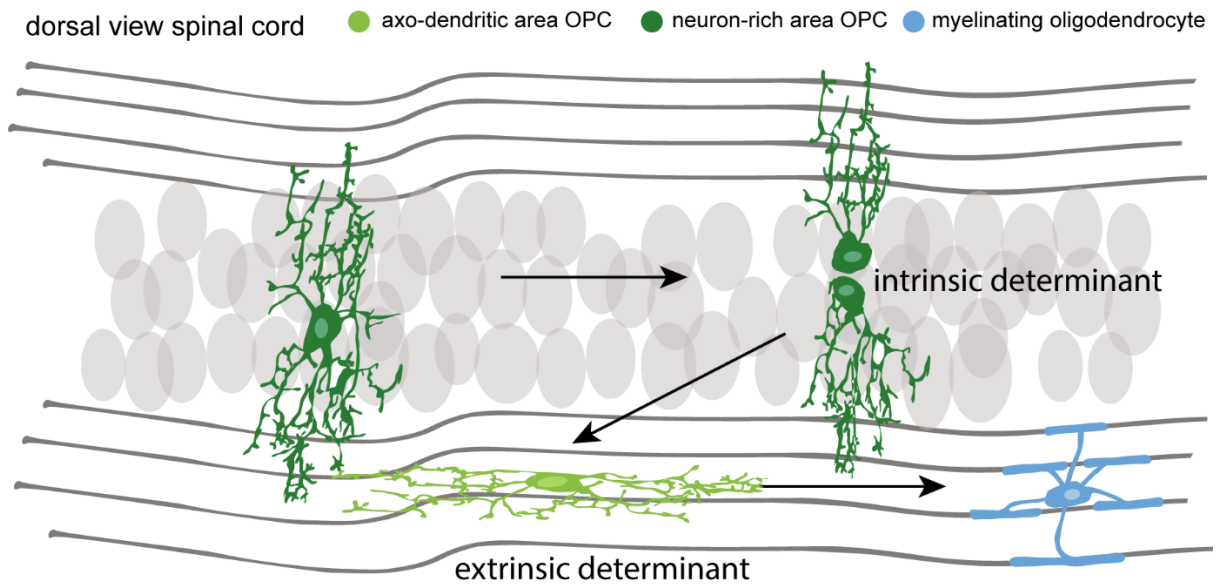


Fig. 4.1 OPC subtypes interconnection

Schematic representing the hierarchy between the two types of OPCs identified in the zebrafish spinal cord. OPC subtypes and their differentiation potential are controlled by two determinants. The extrinsic determinant is represented by the local environment surrounding OPC soma, axo-dendritic area OPCs can differentiate in myelinating oligodendrocytes. The intrinsic determinant is the recent cell division which neuron-rich area OPCs need to give rise to axo-dendritic area OPCs that are likely to differentiate. Neuron-rich area OPCs cannot switch their type and directly differentiate into oligodendrocytes, a division event is always necessary. (Marisca et al., 2020)

4.4 Integration of external stimuli by OPCs

Synaptic-like contacts in zebrafish OPCs

Axon-OPC synaptic contacts have been described for the first time 20 years ago (Bergles et al., 2000). However, it remained unclear if synapse-like contacts between axons and OPCs exist in zebrafish. From our RNA sequencing data, we know that OPCs express genes involved in the post-synaptic machinery, however evidences of expression in OPCs in zebrafish were missing. In my results sections, I illustrated some preliminary results about the expression and position of pre- and post-synaptic markers in the zebrafish spinal cord. At first, I tried to label synapses in the zebrafish spinal cord which, as expected, are mostly located in the lateral side where also dendrites and axons are. OPC processes project as well in the lateral spinal cord. At first, to endogenously label post-synaptic sites in OPCs I used antibodies to stain spinal cord sections. Immunostaining is reliable to detect the expression of endogenous post-synaptic proteins in OPCs. However, it was challenging to identify with precision the localisation of the post-synaptic puncta in OPCs since post-synaptic expression appeared quite dense in this area. Moreover, it was not possible to trace the cells and identify the soma position to categorise OPCs in one of the two subgroups. In addition, gene ontology analysis revealed that the cluster representing the neuron-rich area OPCs comprised terms related to protein-protein interaction at synapses. Therefore, I also used an *in vivo* approach to describe axon-OPC synaptic contacts in the zebrafish spinal cord. Using this approach, I could characterise OPC morphology and I sparsely expressed a post synaptic marker in OPCs, giving us a clearer idea of post-synaptic sites of OPCs. On the other hand, the live imaging transgenic approach can also induce the expression of post-synaptic proteins *in vivo* creating an artefact. When I combined pre- and post-synaptic markers in neurons and OPCs respectively, the co-localisation analysis showed that not all post-synaptic densities in OPCs have a pre-synaptic site in the proximity. This might be due to the transgenic line and markers used to individualise the synaptic contacts. The transgenic line used to label pre-synaptic sites in neurons might be not completely accurate in expressing pre-synaptic markers in all the neurons. Further

experiments are needed to validate the line. Furthermore, to label post-synaptic site in OPCs, I expressed the PSD95-EYFP fusion protein that may fail to properly localise and create false positive expressing cells. To confirm the post-synaptic marker expression in OPCs, further work is needed using an approach that would combine the antibody approach with the live-cell imaging. This is possible using recombinant antibody-like proteins, termed Fibronectin intrabodies generated with mRNA display (FingRs) that binds the endogenous PSD95 protein (Gross et al., 2013). This method allows the localisation of the endogenous post-synaptic proteins *in vivo*. FingR expression would be more accurate than exogenously expressing proteins that can cause morphological changes and not localise specifically as their endogenous equivalent. Moreover, FingR expression is transcriptionally controlled by a feedback system based on a zinc-finger DNA binding domain that accurately reports its endogenous expression level (Gross et al., 2013).

Post-synaptic density differences in OPC subtypes

PSD95 was differently expressed in the two OPC subgroups. The post-synaptic markers revealed a punctate enrichment mostly in OPC processes and were more densely expressed in the neuron-rich area OPC processes compared to the axo-dendritic area ones. It is plausible that the OPCs that show less process dynamics are able to form more stable synaptic contacts with axons, instead the ones that present fast processes remodelling are not capable to establish such contacts. In addition, neuron-rich area OPCs present a more complex morphology compared to the axo-dendritic OPCs. This morphological feature is consistent with the finding that blocking glutamatergic signalling through AMPARs results in a consistent reduction in the length of OPC processes and number of branch points (Fannon et al., 2015). This implies that synaptic signalling is important to maintain a complex process morphology typical of the neuron-rich area OPCs. Expression of PSD95 in OPCs is different than the one described in oligodendrocytes in zebrafish where PSD95 appeared either like puncta restricted to the ends of myelin sheaths or diffusing amongst the whole cell, or more rarely, puncta

localised along the length of sheaths (Hughes and Appel 2019). In addition, in mouse brain slices the transition from OPCs to pre-myelinating oligodendrocytes was accompanied by loss of synaptic input and a decrease in glutamate receptor expression (De Biase et al., 2010). Moreover, myelination of electrically active axons occurred through vesicular release via non-synaptic axo-glial junctions (Wake et al., 2015). These previous findings are related to my data showing that neuron-rich area OPCs form more synaptic contacts than the axo-dendritic area OPCs which are primed to differentiation. Axon-OPC synaptic contacts are therefore not regulating myelination, since in our system the cells that form synapses and integrate neural activity are the ones that are not differentiating into myelinating oligodendrocytes.

Finally, the result on the higher post-synaptic densities in neuron-rich area OPCs is in line with the ability of these OPCs in integrating neural activity and in having higher calcium amplitude (Fig. 4.2). Indeed, presynaptic neuron stimulations as well as GABAergic and glutamatergic synaptic inputs have been shown to trigger Ca^{2+} rises in OPCs (Haberlandt et al., 2011; Tong et al., 2009; Sun et al., 2016).

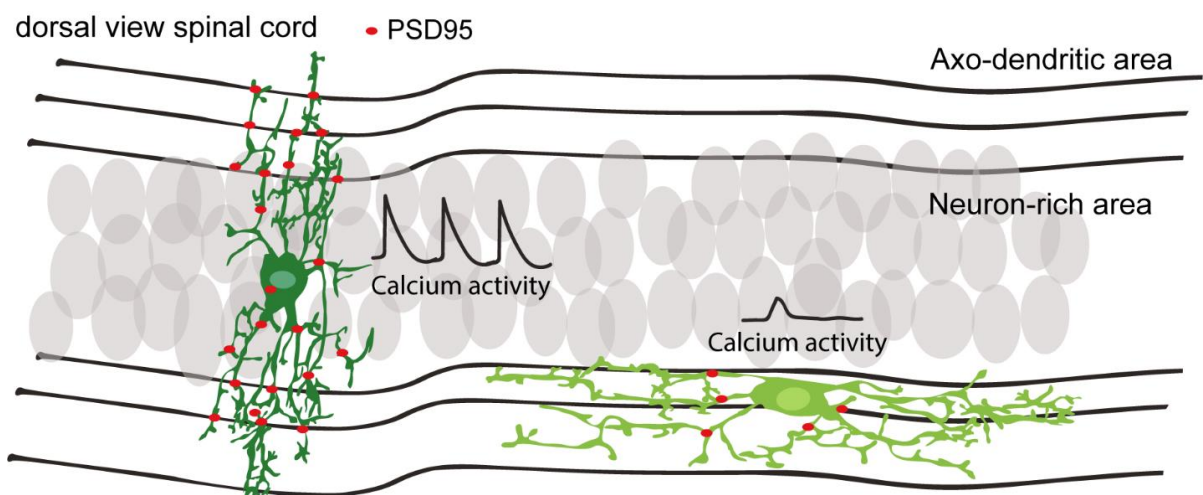


Fig. 4.2 Post-synaptic densities in OPC subtypes

Schematic representing the PSD95 post-synaptic densities in the two OPC subtypes. Neuron-rich area OPCs which show high amplitude and frequent GCaMP rises, present more post-synaptic expression along their ramified processes. Axo-dendritic area OPCs which present lower amplitude and less frequent GCaMP transients, present less dense post-synaptic marker expression and mostly localise in the processes closed to the soma.

4.5 OPC calcium dynamics

Single OPC GCaMP features

In my study, I described GCaMP dynamics in OPCs and I focused on differences between the two OPC subtypes that we have fully characterised in terms of morphology, fate behaviour and molecular signatures. My analysis identified two patterns of GCaMP events restricted to process subdomains or spreading through the whole cell. In line with this, a previous study, described GCaMP dynamics along oligodendrocyte differentiation, starting with pre-myelinating oligodendrocytes and both somatic and process terminal GCaMP events were described. Interestingly, process and somatic GCaMP events were less frequent and had lower amplitude while the maturation towards oligodendrocytes was progressing (Krasnow et al., 2018). This suggests that differentiating oligodendrocytes showed less GCaMP events compared to OPCs. Accordingly, my data on differences in GCaMP dynamics between the two OPC subtypes revealed that somatic GCaMP events occurred more frequently and exhibited higher amplitude in OPCs with their somata residing in the neuron-rich areas, compared to the ones in the axo-dendritic areas that will likely differentiate.

GCaMP transients in OPCs might be elicited by several inputs, including synaptic activity. Since the beginning of the 1990s, calcium (Ca^{2+}) channels have been detected in oligodendrocyte lineage cells and Ca^{2+} currents in OPCs through voltage gated calcium channels have been recorded in mice slices (Berger et al., 1992). Calcium entry in OPCs can be regulated by both glutamatergic and GABAergic synaptic activity. It has been shown that calcium rises in OPCs resulted from the activation of Ca^{2+} -permeable AMPA-receptors induced by electrical stimulation of pre-synaptic neurons (Bergles et al., 2000). The role of AMPAR in mediating intracellular calcium permeability was also proven by a recent work, in which a point modification of the AMPAR subunit GluA2 increased the calcium permeability in OPCs (Chen et al., 2018). GABAergic activity triggered, as well, Ca^{2+} rises in OPCs through the activation of Na^+ channels and $\text{Na}^+/\text{Ca}^{2+}$ exchangers in OPCs (Tong et al., 2009). In another study, Ca^{2+}

elevations in OPC processes, but not somata, were induced by the electrical stimulation of pre-synaptic neurons (Haberlandt et al., 2011).

In addition, OPC calcium currents appeared to reflect the level of glutamatergic synaptic activity in hippocampal slices (Sun et al., 2016). In this study, calcium signals localised to the somata and OPC arborisations were described. Both of these types of calcium signals had a slow decay time, on the order of seconds, comparable to my GCaMP data (Sun et al., 2016).

My single cell GCaMP data show that GCaMP transients restricted to process subdomains are more frequent than whole cell GCaMP transients. However, when I performed cell population GCaMP analysis, I often detected somatic GCaMP transients. The hypothesis is that GCaMP rises localised to the processes are synaptic-induced as neuron-OPC synapses were described along the processes (Bergles et al. 2000; Kukley et al., 2007). On the other hand, somatic GCaMP transients may be explained by taking into account that calcium responses in OPCs are neuronal stimulus-dependent. Therefore, to trigger whole cell GCaMP transients, a synchronised activity of the synapses localised to OPC processes might be necessary. The hypothesis would be that only when the summation of the synaptic activities reaches a certain threshold then the intracellular calcium rises in the whole cell. This idea is comparable to the action potential in neurons where the dendritic integration of different inputs has to reach a threshold to elicit an action potential.

Moreover, supporting the idea that GCaMP transients are triggered by synaptic activity, neuron-rich area OPCs are the cells that showed higher and more frequent somatic GCaMP transients. This OPC subgroup presents, as well, higher density of post-synaptic markers reflecting the sequencing data, which showed that these cells are enrich in genes involved in neurotransmitter signalling.

Slow GCaMP dynamics described in OPCs restricted to process subdomains or spreading through the whole cells are also found in astrocytes (Agarwal et al., 2017; Srinivasan et al., 2015). GCaMP events in astrocytes in mice have been fully characterised and can last for several seconds, similar to the ones I detected in OPCs (Stobart et al., 2016). Moreover, a

more recent study illustrated GCaMP dynamics in astrocyte-like cells in the zebrafish spinal cord and most of the GCaMP transients had a duration comparable to the ones detected in astrocytes in mice (Chen et al., 2020). As these two glia cells have relatively similar GCaMP dynamics, an attractive idea would be to study calcium signalling between astrocytes and OPCs to understand if there is any type of correlation.

OPC population GCaMP features

For the first time, my work provided data on GCaMP transients at the level of OPC population. This offers new insight to understand how OPCs are related to each other and to axons. My results indicate that somatic GCaMP transients spread in neighbouring OPCs with slow temporal resolution. GCaMP waves spreading in a group of OPCs or amongst all OPCs, in my field of view, suggest that there might be a sort of coupling amongst OPC population. This might be due to direct signalling between OPCs, to signalling induced by axonal activity or both combined. Indeed, as I described, all OPCs are in contact with the same cohort of axons in the lateral side of the zebrafish spinal cord. Calcium waves were identified for the first time 30 years ago also in astrocytes in culture, following studies showed that calcium waves in astrocytes were triggered by neural activity (Cornell-Bell et al.; 1990, Dani et al., 1992). One possible pathway by which Ca^{2+} signals can be transmitted between neighbouring cells is through intercellular gap junctions. Calcium waves in astrocytes are elicited by glutamatergic signalling and then the propagation amongst neighbouring cells is mediated by gap junctions (Finkbeiner, 1992). The idea is that OPC calcium waves and calcium subgroups are triggered by neural activity and then spread amongst OPCs in the vicinity via gap junctions (Fig. 4.3). To test this hypothesis further experiments are needed, using gap junction blockers combined with calcium imaging to visualise whether calcium waves amongst OPCs would be then blocked. Not much is known about the connexins forming gap junctions in oligodendrocyte lineage cells. Oligodendrocytes express connexin 29 (Cx29), Cx32, Cx45 and Cx47 and they are coupled to each other through homotypic gap junctions composed by Cx32 and Cx47

(Vejar et al., 2019). No published information is available on the connexins expressed in OPCs, but from our sequencing data Cx27.5 appeared highly expressed in the neuron-rich area OPCs. Other experiments are needed to confirm the expression and specificity of the Cx 27.5 in OPCs to understand its role in regulating gap junctions and calcium waves amongst OPC population (Fig 4.3).

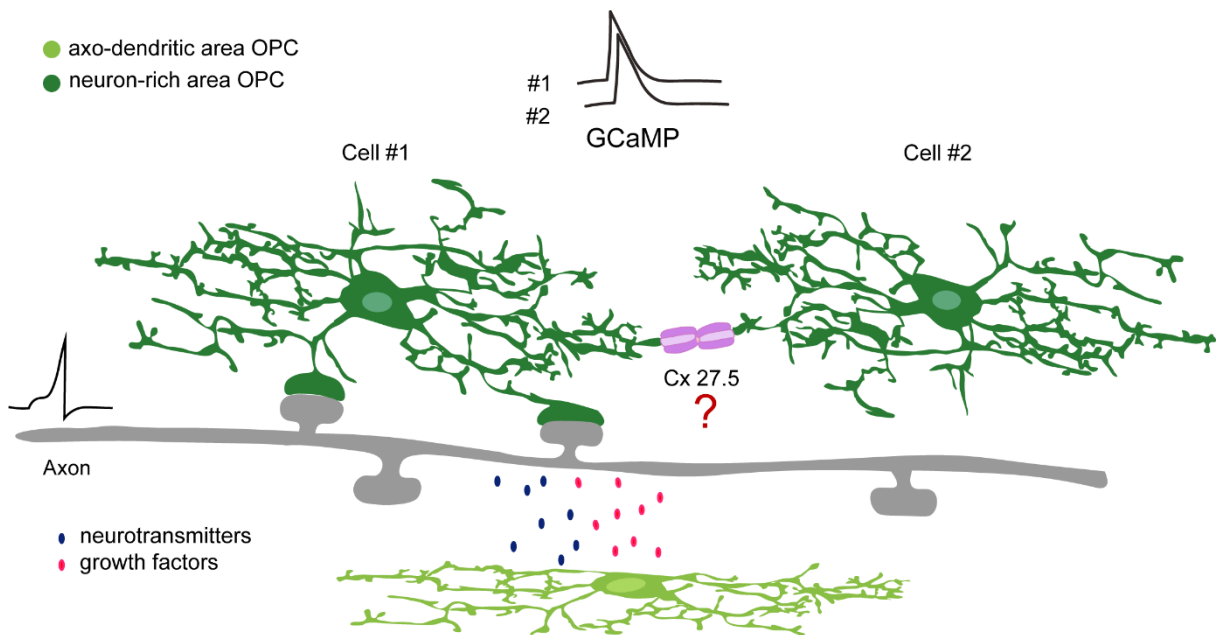


Fig. 4.3 OPC-OPC coupling hypothesis

Schematic suggesting a possible mechanism of interconnection between OPCs to explain the calcium spreading amongst neighbouring OPCs. The hypothesis is that OPCs sense neural activity through their synaptic contacts and then communicate through their gap junctions with OPCs in their proximity. One possible candidate to form OPC-OPC gap junction connection is the connexin 27.5 which appear to be highly expressed in neuron-rich area OPCs. On the other hand, axon-dendritic OPCs might sense neural activity via non-synaptic vesicle release of neurotransmitters and growth factors.

CaMPARI as a technique to study calcium dynamics

GCaMP analysis of OPCs at the population level highlighted GCaMP transients spreading through a group of OPCs or even through all OPCs in the field of view. However, these findings emphasised the limitations of this method to look at calcium at the population level, because it was clear that the GCaMP signalling might involve OPCs outside of the imaged area. Therefore, I used CaMPARI as an alternative method to further study coupling amongst OPCs. CaMPARI has been used since 2015 to track calcium activity of neurons in different species

(Fosque et al., 2015; Moeyaert et al., 2018; Trojanowski et al., 2021). This calcium integrator is based on the photoconversion from green to red, when high intracellular calcium is present in the cell while UV light treatment is applied. CaMPARI leaves a permanent trace of Ca^{2+} rises during the time of UV light exposure. My data suggest that this is a reliable technique showing variability in the red/green ratio amongst OPCs in the same animal, among different animals and conditions. Indeed, zebrafish treated with 4-AP displayed a significant increase in red/green ratio. CaMPARI has the great advantage to detect the calcium activity of the whole OPC population in a fixed time frame. In addition, more animals can be treated with the UV light and no compounds are needed to paralyse the fish. One limitation is the temporal resolution that cannot be as precise as the GCaMP imaging which is the method I used at first to describe calcium rises in OPCs. In my experiments, I performed the UV light treatment over a period of 5 minutes and in case of photoconversion, it is not possible to know when the calcium rise happened along the 5 minute time frame. However, this tool is useful to trace the overall calcium activity of all OPCs and to detect differences amongst animals and anatomical regions, which can tell us more about OPC coupling. Indeed, looking at the photoconversion rates, most animals showed an undulatory trend and neighbouring cells have comparable photoconversion rates, reflecting boundaries amongst OPCs. A subsequent experiment could be to perform GCaMP imaging across regions where these boundaries were identified to get a precise temporal resolution.

CaMPARI was recently created but already two more versions of this tool are available, CaMPARI2 has an improved sensor with brighter green and red fluorescence and decreased background photoconversion in low calcium conditions compared to the CaMPARI1 which I used for my experiments (Fosque et al., 2015; Moeyaert et al., 2018). However, the application of a lower UV-light treatment for my experiments, compared to the one used in the CaMPARI first publication, was already useful to reduce the background photoconversion. The newest version of this tool, rsCaMPARI, overcomes the irreversibility of the previous version, allowing multiple snapshots of neuronal activity of the same sample (Sha et al., 2020). For future studies, the OPC CaMPARI line can be combined with behavioural set-ups to study the overall

calcium activity in OPCs during diverse behavioural paradigms. This combination will help us to understand what is the additional function of OPCs in the neural circuit, considering that neuron-rich area OPCs do not contribute to myelination, but integrate neural activity.

4.6 Neuronal manipulation effects on OPC

Neuronal manipulation effects on OPC GCaMP transients

OPCs showed that GCaMP transients spread through group of cells, or even GCaMP waves spreading through the spinal cord. Moreover, OPCs showed GCaMP transients both somatic and localised to the processes. Therefore, since OPC processes are localised where axons run and they make synaptic contact with neurons, I studied whether these GCaMP events in OPCs are triggered by neural activity. At first, I have tried two chemogenetic approaches to manipulate neural activity. However, Designer Receptor Exclusively Activated by a Designer Drug (DREADD), widely used in mice, did not work in zebrafish probably because the CNO, its ligand, cannot be metabolise in zebrafish (Armbruster et al., 2007; Chen et al., 2016). The second approach, the rat TRPV1 (transient receptor potential cation channel subfamily V member 1), activated by the application of capsaicin, resulted to be toxic for the cells upon prolonged application (Chen et al., 2016).

Therefore, I decided to use a pharmacological approach to trigger or block neural activity, using 4-AP and TTX respectively.

Pharmacological neural manipulation, to study the effects on OPC calcium dynamics, revealed that enhancing neural activity using 4-AP increased the frequency of GCaMP transients in OPCs. GCaMP transients, induced by neural activity, were mostly affecting OPC processes. It is possible that 4-AP acts directly on OPCs considering that they express K⁺ channels. However, when the action potential blocker TTX was subsequently applied to the same sample previously treated with 4-AP, most of GCaMP transients 4-AP-induced were restored to basal levels. Moreover, the 4-AP pharmacological approach used in combination with the double transgenic line expressing two different calcium indicators in OPCs and neurons induced GCaMP transients in OPCs right after calcium transients in neurons depicted by RGECO. This suggests that the GCaMP transients in OPCs are neural-induced. These results are in accordance with previous electrophysiological studies that reported Ca²⁺ elevations in OPCs triggered by neuronal electrical stimulation through glutamatergic or GABAergic synapses

(Tong et al., 2009; Haberlandt et al., 2011; Sun et al., 2016). In addition, our neural manipulation results are consistent with the *in vivo* calcium imaging study from Krasnow *et al.* in which calcium transients of pre-myelinating oligodendrocytes correlated with neuronal electrical stimulation and were reduced after TTX injection (Krasnow et al., 2018).

More studies are necessary to show *in vivo* calcium correlation between the two subtypes of OPCs and axons. An optogenetic approach would be ideal to trigger only single neurons and detect calcium responses in surrounding OPCs. The expression of light-sensitive ion channels in neurons would allow us to specifically manipulate single neuron activity and to control their activation through light pulses. The combination of this approach with GCaMP imaging in OPCs would permit to identify GCaMP transients that are activated by the induced neural activity. This would give us a direct evidence that GCaMP transients, or at least a part of them, are induced by neural activity. Moreover, this method will be helpful to further investigate differences between the two subgroups of OPCs in sensing neural activity.

Induced neural activity trigger OPC proliferation

Neural activity is a key regulator of myelination and has been shown to modulate both OPC proliferation and differentiation. Raff and Barres carried out the first experiment in which electrical axon disruption caused a decrease in OPC proliferation (Barres and Raff, 1993). A more recent work reported OPC proliferation, oligodendrogenesis and myelination after optogenetic stimulation of neural activity (Gibson et al., 2014). Another study reported OPC proliferation and differentiation after pharmacological neural stimulation of axons in mice (Mitew et al., 2018). Data on the modulation of myelination are controversial, considering that enhanced neural activity triggers proliferation and differentiation of OPCs, and it is complicated to dissociate one effect from the other *in vivo*. However, our model is very useful to carry out timeline analysis following single cells over days, to delineate the cell fate and behaviour. Our data showed that neural activity induced by 4-AP treatment primarily enhances OPC proliferation and that this effect affected mostly neuron-rich area OPCs. This is in agreement

with our GCaMP analysis in which these cells appeared to be more sensitive to neural activity. A subsequent increase in myelinating oligodendrocytes was also detected after the 4-AP treatment, suggesting that the direct effect of neural activity on OPCs concerns OPC division, and differentiation is a later stage effect. When 4-AP was combined with TTX, there was no increment in OPC proliferation. Live imaging following neuron-rich area OPCs before and after 4-AP treatment highlighted the proliferation effect of neural activity on OPCs, even if a direct effect of 4-AP on OPCs cannot be excluded. Interestingly, the effects induced by 4-AP in OPCs relied on intracellular calcium in OPCs. Intracellular calcium is necessary to trigger proliferation 4-AP-induced. Further studies are needed to investigate the signalling pathway involved in regulating OPC behaviour through synaptic signalling. Indeed, glutamatergic synapses have been shown to trigger OPC differentiation (Gautier et al., 2015). In addition, proliferation and differentiation have been found to be regulated by different firing of neural activity (Nagy et al., 2017). One hypothesis is that the calcium-mediated proliferation induced by neural activity might involve the AMPA receptors. Increasing the calcium permeability of AMPA receptors triggered OPC proliferation and reduced the differentiation (Chen et al., 2018). However, interestingly loss of AMPA receptors resulted in no effects on OPC proliferation (Kougioumtzidou et al., 2017). The role of another type of receptor, NMDA receptors, needs to be further investigated as it might compensate the role of AMPAR. It is known that NMDAR ablation, caused increased Ca^{2+} mediated by AMPAR (De Biase et al. 2011). In addition to glutamatergic signalling, the role of GABAergic synapses should be considered as it was shown that loss of GABA_A receptor increased OPC proliferation and delayed OPC differentiation *in vivo* (Zonouzi et al., 2015). Therefore, GABAergic activity seems to have the opposite effects on OPC behaviour, compared to the glutamatergic one, reducing OPC proliferation and promoting their differentiation. To further investigate the roles of the different neurotransmitters in regulating OPC fate and behaviour, both pharmacological and optogenetic approaches could be used. Compounds like GABAzine or PTZ can be applied to inhibit GABAergic receptors and follow OPC responses in terms of proliferation and differentiation *in vivo*. However, this pharmacological manipulation will affect also other cell

types. Therefore, a more precise method to specifically manipulate neurotransmitter release from neurons, is offered by optogenetics.

Expressing opsins in neurons using drivers specific for different signalling by neurotransmitters like glutamate, GABA_A, aspartate and glycine would permit to specifically modulate one type of neuron signalling and explore the effects on OPCs. This approach would allow us to directly determine fates of the two OPC subgroups in response to a precise stimulus *in vivo*.

4.7 Future perspective

OPCs constitute a large population of the CNS and in the last years they have been characterised as a heterogeneous population with differences in gene profiles and electrophysiological properties amongst different brain regions and ages. In addition, OPCs can sense neuronal activity which affects both OPC proliferation and differentiation to myelinating oligodendrocytes. OPC heterogeneity and their ability to integrate neural activity lead to the question whether neural activity regulates differently the fates of heterogeneous OPCs.

My results show that in the zebrafish spinal cord there are two different OPC subgroups. One subgroup is primed to differentiation and the other does not directly contribute to myelination. Interestingly, this second subgroup is able to integrate more neural activity which triggers the proliferation of these OPCs.

This suggests that their main function is not myelination but being open to other functions. One idea is that they play additional important roles contributing to the neural circuit in a myelin-independent manner. Further work is needed to investigate this idea. One possible idea is to ablate OPCs and perform visual-motor behavioural assays to investigate their role in integrating different external stimuli.

Moreover, it would be interesting to understand how these two OPC subgroups respond to injury conditions. In demyelinating diseases, OPCs respond by differentiation but often fail to differentiate into oligodendrocyte inducing chronic demyelinated conditions (Duncan et al., 2009, Wolswijk et al. 1998). It is important to find the right target to restore myelination. In our system it seems that targeting OPCs sensitive to neural activity might be a good strategy considering that division events lead to subsequent differentiation. The intrinsic factor that gives OPCs the potential to differentiate in our system is represented by a recent cell division. This is in agreement with a new study in mice in which proliferation is defined as a requirement to induce OPC differentiation in remyelinating conditions (Foerster et al., 2020).

Another aspect that emerged from my analysis is that OPCs seem to create boundaries amongst themselves at cell population level, and it would be useful to understand what is the mechanism involved in their formation. In addition to that, it would be interesting to further explore the function of these boundaries to understand whether OPCs form networks in parallel to the neural ones. One idea is that specific calcium patterns might be correlated to different animal behaviours, which can be tested by combining GCaMP imaging with visual-motor behaviour experiments.

Our study points out the importance of characterising differences amongst the oligodendrocyte lineage population to get new insights on their normal role in brain physiology, and to identify the right approach to restore myelination in demyelinating diseases.

5 REFERENCES

- Agarwal A, Wu P-H, Hughes EG, Fukaya M, Tischfield MA, Langseth AJ, Wirtz D, Bergles DE (2017) Transient Opening of the Mitochondrial Permeability Transition Pore Induces Microdomain Calcium Transients in Astrocyte Processes. *Neuron* 93:587-605.e7.
- Albert M, Antel J, Brück W, Stadelmann C (2007) Extensive Cortical Remyelination in Patients with Chronic Multiple Sclerosis. *Brain Pathol* 17:129–138.
- Almeida RG, Czopka T, French-Constant C, Lyons DA (2011) Individual axons regulate the myelinating potential of single oligodendrocytes in vivo. *Development* 138:4443–4450.
- Almeida RG, Lyons DA (2015) Intersectional Gene Expression in Zebrafish Using the Split KalTA4 System. *Zebrafish* 12:377–386.
- Armbruster BN, Li X, Pausch MH, Herlitz S, Roth BL (2007) Evolving the lock to fit the key to create a family of G protein-coupled receptors potently activated by an inert ligand. *Proc National Acad Sci* 104:5163–5168.
- Arnett HA, Fancy SPJ, Alberta JA, Zhao C, Plant SR, Kaing S, Raine CS, Rowitch DH, Franklin RJM, Stiles CD (2004) bHLH Transcription Factor Olig1 Is Required to Repair Demyelinated Lesions in the CNS. *Science* 306:2111–2115.
- Auer F, Vagionitis S, Czopka T (2018) Evidence for Myelin Sheath Remodeling in the CNS Revealed by In Vivo Imaging. *Curr Biol* 28:549-559.e3.
- Bacmeister CM, Barr HJ, McClain CR, Thornton MA, Nettles D, Welle CG, Hughes EG (2020) Motor learning promotes remyelination via new and surviving oligodendrocytes. *Nat Neurosci* 23:819–831.
- Baraban M, Koudelka S, Lyons DA (2018) Ca²⁺ activity signatures of myelin sheath formation and growth in vivo. *Nat Neurosci* 21:19–23.
- Barbarese E, Barry C, Chou CJ, Goldstein DJ, Nakos GA, Hyde-DeRuyscher R, Scheld K, Carson JH (1988) Expression and Localization of Myelin Basic Protein in Oligodendrocytes and Transfected Fibroblasts. *J Neurochem* 51:1737–1745.
- Barres BA, Raff MC (1993) Proliferation of oligodendrocyte precursor cells depends on electrical activity in axons. *Nature* 361:258–260.
- Battefeld A, Popovic MA, Vries SI de, Kole MHP (2019) High-Frequency Microdomain Ca²⁺ Transients and Waves during Early Myelin Internode Remodeling. *Cell Reports* 26:182-191.e5.
- Berger T, Schnitzer J, Orkand PM, Kettenmann H (1992) Sodium and Calcium Currents in Glial Cells of the Mouse Corpus Callosum Slice. *Eur J Neurosci* 4:1271–1284.
- Bergles DE, Roberts JDB, Somogyi P, Jahr CE (2000) Glutamatergic synapses on oligodendrocyte precursor cells in the hippocampus. *Nature* 405:187–191.
- Bonetto G, Kamen Y, Evans KA, Káradóttir RT (2020) Unraveling Myelin Plasticity. *Front Cell Neurosci* 14:156.
- Caterina MJ, Schumacher MA, Tominaga M, Rosen TA, Levine JD, Julius D (1997) The capsaicin receptor: a heat-activated ion channel in the pain pathway. *Nature* 389:816–824.

- Chen Y, Wu H, Wang S, Koito H, Li J, Ye F, Hoang J, Escobar SS, Gow A, Arnett HA, Trapp BD, Karandikar NJ, Hsieh J, Lu QR (2009) The oligodendrocyte-specific G protein-coupled receptor GPR17 is a cell-intrinsic timer of myelination. *Nat Neurosci* 12:1398–1406.
- Chen T-W, Wardill TJ, Sun Y, Pulver SR, Renninger SL, Baohan A, Schreiter ER, Kerr RA, Orger MB, Jayaraman V, Looger LL, Svoboda K, Kim DS (2013) Ultrasensitive fluorescent proteins for imaging neuronal activity. *Nature* 499:295–300.
- Chen S, Chiu CN, McArthur KL, Fetcho JR, Prober DA (2016) TRP channel mediated neuronal activation and ablation in freely behaving zebrafish. *Nat Methods* 13:147–150.
- Chen T-J, Kula B, Nagy B, Barzan R, Gall A, Ehrlich I, Kukley M (2018) In Vivo Regulation of Oligodendrocyte Precursor Cell Proliferation and Differentiation by the AMPA-Receptor Subunit GluA2. *Cell Reports* 25:852-861.e7.
- Chen J, Poskanzer KE, Freeman MR, Monk KR (2020) Live-imaging of astrocyte morphogenesis and function in zebrafish neural circuits. *Nat Neurosci* 23:1297–1306.
- Chittajallu R, Aguirre A, Gallo V (2004) NG2-positive cells in the mouse white and grey matter display distinct physiological properties. *J Physiology* 561:109–122.
- Clarke LE, Young KM, Hamilton NB, Li H, Richardson WD, Attwell D (2012) Properties and Fate of Oligodendrocyte Progenitor Cells in the Corpus Callosum, Motor Cortex, and Piriform Cortex of the Mouse. *J Neurosci* 32:8173–8185.
- Coolen M, Thieffry D, Drivenes Ø, Becker TS, Bally-Cuif L (2012) miR-9 Controls the Timing of Neurogenesis through the Direct Inhibition of Antagonistic Factors. *Dev Cell* 22:1052–1064.
- Cornell-Bell A, Finkbeiner S, Cooper M, Smith S (1990) Glutamate induces calcium waves in cultured astrocytes: long-range glial signaling. *Science* 247:470–473.
- Crawford AH, Tripathi RB, Richardson WD, Franklin RJM (2016) Developmental Origin of Oligodendrocyte Lineage Cells Determines Response to Demyelination and Susceptibility to Age-Associated Functional Decline. *Cell Reports* 15:761–773.
- Czopka T, French-Constant C, Lyons DA (2013) Individual Oligodendrocytes Have Only a Few Hours in which to Generate New Myelin Sheaths In Vivo. *Dev Cell* 25:599–609.
- Dana H, Mohar B, Sun Y, Narayan S, Gordus A, Hasseman JP, Tsegaye G, Holt GT, Hu A, Walpita D, Patel R, Macklin JJ, Bargmann CI, Ahrens MB, Schreiter ER, Jayaraman V, Looger LL, Svoboda K, Kim DS (2016) Sensitive red protein calcium indicators for imaging neural activity. *Elife* 5:e12727.
- Dani JW, Chernjavsky A, Smith SJ (1992) Neuronal activity triggers calcium waves in hippocampal astrocyte networks. *Neuron* 8:429–440.
- Dawson MRL, Polito A, Levine JM, Reynolds R (2003) NG2-expressing glial progenitor cells: an abundant and widespread population of cycling cells in the adult rat CNS. *Mol Cell Neurosci* 24:476–488.
- De Biase LM, Nishiyama A, Bergles DE (2010) Excitability and Synaptic Communication within the Oligodendrocyte Lineage. *J Neurosci* 30:3600–3611.
- De Biase LM, Kang SH, Baxi EG, Fukaya M, Pucak ML, Mishina M, Calabresi PA, Bergles DE (2011) NMDA Receptor Signaling in Oligodendrocyte Progenitors Is Not Required for Oligodendrogenesis and Myelination. *J Neurosci* 31:12650–12662.

- Demerens C, Stankoff B, Logak M, Anglade P, Allinquant B, Couraud F, Zalc B, Lubetzki C (1996) Induction of myelination in the central nervous system by electrical activity. *Proc National Acad Sci* 93:9887–9892.
- Dimou L, Simon C, Kirchhoff F, Takebayashi H, Götz M (2008) Progeny of Olig2-Expressing Progenitors in the Gray and White Matter of the Adult Mouse Cerebral Cortex. *J Neurosci* 28:10434–10442.
- Duncan ID, Brower A, Kondo Y, Curlee JF, Schultz RD (2009) Extensive remyelination of the CNS leads to functional recovery. *Proc National Acad Sci* 106:6832–6836.
- Early JJ, Cole KL, Williamson JM, Swire M, Kamadurai H, Muskavitch M, Lyons DA (2018) An automated high-resolution in vivo screen in zebrafish to identify chemical regulators of myelination. *Elife* 7:e35136.
- Ellis LD, Seibert J, Soanes KH (2012) Distinct models of induced hyperactivity in zebrafish larvae. *Brain Res* 1449:46–59.
- Emery B, Agalliu D, Cahoy JD, Watkins TA, Dugas JC, Mulinyawe SB, Ibrahim A, Ligon KL, Rowitch DH, Barres BA (2009) Myelin Gene Regulatory Factor Is a Critical Transcriptional Regulator Required for CNS Myelination. *Cell* 138:172–185.
- Fannon J, Tarmier W, Fulton D (2015) Neuronal activity and AMPA-type glutamate receptor activation regulates the morphological development of oligodendrocyte precursor cells. *Glia* 63:1021–1035.
- Faria O, Gonsalvez DG, Nicholson M, Xiao J (2019) Activity-dependent central nervous system myelination throughout life. *J Neurochem* 148:447–461.
- Fields RD (2015) A new mechanism of nervous system plasticity: activity-dependent myelination. *Nat Rev Neurosci* 16:756–767.
- Finkbeiner S (1992) Calcium waves in astrocytes-filling in the gaps. *Neuron* 8:1101–1108.
- Foerster S, Hill MFE, Franklin RJM (2019) Diversity in the oligodendrocyte lineage: Plasticity or heterogeneity? *Glia* 67:1797–1805.
- Foerster S, Neumann B, McClain C, Canio LD, Chen CZ, Reich DS, Simons BD, Franklin RJ (2020) Proliferation is a requirement for differentiation of oligodendrocyte progenitor cells during CNS remyelination. *Biorxiv*:2020.05.21.108373.
- Fosque BF, Sun Y, Dana H, Yang C-T, Ohyama T, Tadross MR, Patel R, Zlatic M, Kim DS, Ahrens MB, Jayaraman V, Looger LL, Schreier ER (2015) Labeling of active neural circuits in vivo with designed calcium integrators. *Science* 347:755–760.
- Freeman J, Vladimirov N, Kawashima T, Mu Y, Sofroniew NJ, Bennett DV, Rosen J, Yang C-T, Looger LL, Ahrens MB (2014) Mapping brain activity at scale with cluster computing. *Nat Methods* 11:941–950.
- Fu H, Qi Y, Tan M, Cai J, Takebayashi H, Nakafuku M, Richardson W, Qiu M (2002) Dual origin of spinal oligodendrocyte progenitors and evidence for the cooperative role of Olig2 and Nkx2.2 in the control of oligodendrocyte differentiation. *Dev Camb Engl* 129:681–693.
- Fulton D, Paez PM, Fisher R, Handley V, Colwell CS, Campagnoni AT (2010) Regulation of L-type Ca⁺⁺ currents and process morphology in white matter oligodendrocyte precursor cells by golli-myelin proteins. *Glia* 58:1292–1303.

Fünfschilling U, Supplie LM, Mahad D, Boretius S, Saab AS, Edgar J, Brinkmann BG, Kassmann CM, Tzvetanova ID, Möbius W, Diaz F, Meijer D, Suter U, Hamprecht B, Sereda MW, Moraes CT, Frahm J, Goebbels S, Nave K-A (2012) Glycolytic oligodendrocytes maintain myelin and long-term axonal integrity. *Nature* 485:517–521.

Gau P, Poon J, Ufret-Vincenty C, Snelson CD, Gordon SE, Raible DW, Dhaka A (2013) The Zebrafish Ortholog of TRPV1 Is Required for Heat-Induced Locomotion. *J Neurosci* 33:5249–5260.

Gautier HOB, Evans KA, Volbracht K, James R, Sitnikov S, Lundgaard I, James F, Lao-Peregrin C, Reynolds R, Franklin RJM, Káradóttir RT (2015) Neuronal activity regulates remyelination via glutamate signalling to oligodendrocyte progenitors. *Nat Commun* 6:8518.

Gibson EM, Purger D, Mount CW, Goldstein AK, Lin GL, Wood LS, Inema I, Miller SE, Bieri G, Zuchero JB, Barres BA, Woo PJ, Vogel H, Monje M (2014) Neuronal activity promotes oligodendrogenesis and adaptive myelination in the mammalian brain. *Sci New York N Y* 344:1252304.

Gnuegge L, Schmid S, Neuhauss SCF (2001) Analysis of the Activity-Deprived Zebrafish Mutant *macho* Reveals an Essential Requirement of Neuronal Activity for the Development of a Fine-Grained Visuotopic Map. *J Neurosci* 21:3542–3548.

Gomez JL, Bonaventura J, Lesniak W, Mathews WB, Sysa-Shah P, Rodriguez LA, Ellis RJ, Richie CT, Harvey BK, Dannals RF, Pomper MG, Bonci A, Michaelides M (2017) Chemogenetics revealed: DREADD occupancy and activation via converted clozapine. *Science* 357:503–507.

Goodman AD, Stone RT (2013) Enhancing Neural Transmission in Multiple Sclerosis (4-Aminopyridine Therapy). *Neurotherapeutics* 10:106–110.

Gross GG, Junge JA, Mora RJ, Kwon H-B, Olson CA, Takahashi TT, Liman ER, Ellis-Davies GCR, McGee AW, Sabatini BL, Roberts RW, Arnold DB (2013) Recombinant Probes for Visualizing Endogenous Synaptic Proteins in Living Neurons. *Neuron* 78:971–985.

Guo F, Maeda Y, Ko EM, Delgado M, Horiuchi M, Soulika A, Miers L, Burns T, Itoh T, Shen H, Lee E, Sohn J, Pleasure D (2012) Disruption of NMDA Receptors in Oligodendroglial Lineage Cells Does Not Alter Their Susceptibility to Experimental Autoimmune Encephalomyelitis or Their Normal Development. *J Neurosci* 32:639–645.

Haberlandt C, Derouiche A, Wyczynski A, Haseleu J, Pohle J, Karram K, Trotter J, Seifert G, Frotscher M, Steinhäuser C, Jabs R (2011) Gray Matter NG2 Cells Display Multiple Ca²⁺-Signaling Pathways and Highly Motile Processes. *Plos One* 6:e17575.

Harlow DE, Saul KE, Culp CM, Vesely EM, Macklin WB (2014) Expression of Proteolipid Protein Gene in Spinal Cord Stem Cells and Early Oligodendrocyte Progenitor Cells Is Dispensable for Normal Cell Migration and Myelination. *J Neurosci* 34:1333–1343.

Hildebrand C, Remahl S, Persson H, Bjartmar C (1993) Myelinated nerve fibres in the CNS. *Prog Neurobiol* 40:319–384.

Hill RA, Patel KD, Goncalves CM, Grutzendler J, Nishiyama A (2014) Modulation of oligodendrocyte generation during a critical temporal window after NG2 cell division. *Nat Neurosci* 17:1518–1527.

- Hill RA, Patel KD, Medved J, Reiss AM, Nishiyama A (2013) NG2 Cells in White Matter But Not Gray Matter Proliferate in Response to PDGF. *J Neurosci* 33:14558–14566.
- Hines JH, Ravanelli AM, Schwindt R, Scott EK, Appel B (2015) Neuronal activity biases axon selection for myelination in vivo. *Nat Neurosci* 18:683–689.
- Hughes EG, Kang SH, Fukaya M, Bergles DE (2013) Oligodendrocyte progenitors balance growth with self-repulsion to achieve homeostasis in the adult brain. *Nat Neurosci* 16:668–676.
- Hughes EG, Orthmann-Murphy JL, Langseth AJ, Bergles DE (2018) Myelin remodeling through experience-dependent oligodendrogenesis in the adult somatosensory cortex. *Nat Neurosci* 21:696–706.
- Hughes AN, Appel B (2019) Oligodendrocytes express synaptic proteins that modulate myelin sheath formation. *Nat Commun* 10:4125.
- Jagielska A, Norman AL, Whyte G, Vliet KJV, Guck J, Franklin RJM (2012) Mechanical Environment Modulates Biological Properties of Oligodendrocyte Progenitor Cells. *Stem Cells Dev* 21:2905–2914.
- Káradóttir R, Cavelier P, Bergersen LH, Attwell D (2005) NMDA receptors are expressed in oligodendrocytes and activated in ischaemia. *Nature* 438:1162–1166.
- Káradóttir R, Hamilton NB, Bakiri Y, Attwell D (2008) Spiking and nonspiking classes of oligodendrocyte precursor glia in CNS white matter. *Nat Neurosci* 11:450–456.
- Karttunen MJ, Czopka T, Goedhart M, Early JJ, Lyons DA (2017) Regeneration of myelin sheaths of normal length and thickness in the zebrafish CNS correlates with growth of axons in caliber. *Plos One* 12:e0178058.
- Kessarlis N, Fogarty M, Iannarelli P, Grist M, Wegner M, Richardson WD (2006) Competing waves of oligodendrocytes in the forebrain and postnatal elimination of an embryonic lineage. *Nat Neurosci* 9:173–179.
- Khakh BS, Deneen B (2019) The Emerging Nature of Astrocyte Diversity. *Annu Rev Neurosci* 42:187–207.
- Kirby BB, Takada N, Latimer AJ, Shin J, Carney TJ, Kelsh RN, Appel B (2006) In vivo time-lapse imaging shows dynamic oligodendrocyte progenitor behavior during zebrafish development. *Nat Neurosci* 9:1506–1511.
- Koser DE, Moeendarbary E, Hanne J, Kuerten S, Franze K (2015) CNS Cell Distribution and Axon Orientation Determine Local Spinal Cord Mechanical Properties. *Biophys J* 108:2137–2147.
- Kougioumtzidou E, Shimizu T, Hamilton NB, Tohyama K, Sprengel R, Monyer H, Attwell D, Richardson WD (2017) Signalling through AMPA receptors on oligodendrocyte precursors promotes myelination by enhancing oligodendrocyte survival. *Elife* 6:e28080.
- Krasnow AM, Ford MC, Valdivia LE, Wilson SW, Attwell D (2018) Regulation of developing myelin sheath elongation by oligodendrocyte calcium transients in vivo. *Nat Neurosci* 21:24–28.
- Kuhlbrodt K, Herbarth B, Sock E, Hermans-Borgmeyer I, Wegner M (1998) Sox10, a Novel Transcriptional Modulator in Glial Cells. *J Neurosci* 18:237–250.

- Kuhn S, Gritti L, Crooks D, Dombrowski Y (2019) Oligodendrocytes in Development, Myelin Generation and Beyond. *Cells* 8:1424.
- Kukley M, Capetillo-Zarate E, Dietrich D (2007) Vesicular glutamate release from axons in white matter. *Nat Neurosci* 10:311–320.
- Kukley M, Kiladze M, Tognatta R, Hans M, Swandulla D, Schramm J, Dietrich D (2008) Glial cells are born with synapses. *Faseb J* 22:2957–2969.
- Kukley M, Nishiyama A, Dietrich D (2010) The Fate of Synaptic Input to NG2 Glial Cells: Neurons Specifically Downregulate Transmitter Release onto Differentiating Oligodendroglial Cells. *J Neurosci* 30:8320–8331.
- Kwan KM, Fujimoto E, Grabher C, Mangum BD, Hardy ME, Campbell DS, Parant JM, Yost HJ, Kanki JP, Chien C (2007) The Tol2kit: A multisite gateway-based construction kit for Tol2 transposon transgenesis constructs. *Dev Dynam* 236:3088–3099.
- Laursen LS, Ffrench-Constant C (2007) Adhesion molecules in the regulation of CNS myelination. *Neuron Glia Biol* 3:367–375.
- Lee S, Leach MK, Redmond SA, Chong SYC, Mellon SH, Tuck SJ, Feng Z-Q, Corey JM, Chan JR (2012) A culture system to study oligodendrocyte myelination processes using engineered nanofibers. *Nat Methods* 9:917–922.
- Lee Y, Morrison BM, Li Y, Lengacher S, Farah MH, Hoffman PN, Liu Y, Tsingalia A, Jin L, Zhang P-W, Pellerin L, Magistretti PJ, Rothstein JD (2012) Oligodendroglia metabolically support axons and contribute to neurodegeneration. *Nature* 487:443–448.
- Levison SW, Young GM, Goldman JE (1999) Cycling cells in the adult rat neocortex preferentially generate oligodendroglia. *J Neurosci Res* 57:435–446.
- Lin S, Bergles DE (2004) Synaptic signaling between GABAergic interneurons and oligodendrocyte precursor cells in the hippocampus. *Nat Neurosci* 7:24–32.
- Linnington C, Webb M, Woodhams PL (1984) A novel myelin-associated glycoprotein defined by a mouse monoclonal antibody. *J Neuroimmunol* 6:387–396.
- Liu J, Dietz K, DeLoyht JM, Pedre X, Kelkar D, Kaur J, Vialou V, Lobo MK, Dietz DM, Nestler EJ, Dupree J, Casaccia P (2012) Impaired adult myelination in the prefrontal cortex of socially isolated mice. *Nat Neurosci* 15:1621–1623.
- Lu QR, Yuk D, Alberta JA, Zhu Z, Pawlitzky I, Chan J, McMahon AP, Stiles CD, Rowitch DH (2000) Sonic Hedgehog–Regulated Oligodendrocyte Lineage Genes Encoding bHLH Proteins in the Mammalian Central Nervous System. *Neuron* 25:317–329.
- Makinodan M, Rosen KM, Ito S, Corfas G (2012) A Critical Period for Social Experience–Dependent Oligodendrocyte Maturation and Myelination. *Science* 337:1357–1360.
- Mangin J-M, Li P, Scafidi J, Gallo V (2012) Experience-dependent regulation of NG2 progenitors in the developing barrel cortex. *Nat Neurosci* 15:1192–1194.
- Marisca R, Hoche T, Agirre E, Hoodless LJ, Barkey W, Auer F, Castelo-Branco G, Czopka T (2020) Functionally distinct subgroups of oligodendrocyte precursor cells integrate neural activity and execute myelin formation. *Nat Neurosci* 23:363–374.

Marques S et al. (2016) Oligodendrocyte heterogeneity in the mouse juvenile and adult central nervous system. *Science* 352:1326–1329.

Marques S, Bruggen D van, Vanichkina DP, Floriddia EM, Munguba H, Våremo L, Giacomello S, Falcão AM, Meijer M, Björklund ÅK, Hjerling-Leffler J, Taft RJ, Castelo-Branco G (2018) Transcriptional Convergence of Oligodendrocyte Lineage Progenitors during Development. *Dev Cell* 46:504-517.e7.

Masuda T, Sankowski R, Staszewski O, Prinz M (2020) Microglia Heterogeneity in the Single-Cell Era. *Cell Reports* 30:1271–1281.

McKenzie IA, Ohayon D, Li H, Faria JP de, Emery B, Tohyama K, Richardson WD (2014) Motor skill learning requires active central myelination. *Science* 346:318–322.

Mensch S, Baraban M, Almeida R, Czopka T, Ausborn J, Manira AE, Lyons DA (2015) Synaptic vesicle release regulates myelin sheath number of individual oligodendrocytes in vivo. *Nat Neurosci* 18:628–630.

Meyer MP, Smith SJ (2006) Evidence from In Vivo Imaging That Synaptogenesis Guides the Growth and Branching of Axonal Arbors by Two Distinct Mechanisms. *J Neurosci* 26:3604–3614.

Mitew S, Gobius I, Fenlon LR, McDougall SJ, Hawkes D, Xing YL, Bujalka H, Gundlach AL, Richards LJ, Kilpatrick TJ, Merson TD, Emery B (2018) Pharmacogenetic stimulation of neuronal activity increases myelination in an axon-specific manner. *Nat Commun* 9:306.

Miyazawa H, Okumura K, Hiyoshi K, Maruyama K, Kakinuma H, Amo R, Okamoto H, Yamasu K, Tsuda S (2018) Optical interrogation of neuronal circuitry in zebrafish using genetically encoded voltage indicators. *Sci Rep-uk* 8:6048.

Moeyaert B et al. (2018) Improved methods for marking active neuron populations. *Nat Commun* 9:4440.

Möllmert S, Kharlamova MA, Hoche T, Taubenberger AV, Abuhattum S, Kuscha V, Kurth T, Brand M, Guck J (2020) Zebrafish Spinal Cord Repair Is Accompanied by Transient Tissue Stiffening. *Biophys J* 118:448–463.

Mount CW, Monje M (2017) Wrapped to Adapt: Experience-Dependent Myelination. *Neuron* 95:743–756.vv

Nagy B, Hovhannisyan A, Barzan R, Chen T-J, Kukley M (2017) Different patterns of neuronal activity trigger distinct responses of oligodendrocyte precursor cells in the corpus callosum. *Plos Biol* 15:e2001993.

Niell CM, Meyer MP, Smith SJ (2004) In vivo imaging of synapse formation on a growing dendritic arbor. *Nat Neurosci* 7:254–260.

Nishiyama A, Lin X -H., Giese N, Heldin C -H., Stallcup WB (1996) Co-localization of NG2 proteoglycan and PDGF α -receptor on O2A progenitor cells in the developing rat brain. *J Neurosci Res* 43:299–314.

Ong HH, Wehrli FW (2010) Quantifying axon diameter and intra-cellular volume fraction in excised mouse spinal cord with q-space imaging. *Neuroimage* 51:1360–1366.

- Orduz D, Maldonado PP, Balia M, Vélez-Fort M, Sars V de, Yanagawa Y, Emiliani V, Angulo MC (2015) Interneurons and oligodendrocyte progenitors form a structured synaptic network in the developing neocortex. *Elife* 4:e06953.
- Ortiz FC, Habermacher C, Graciarena M, Houry P-Y, Nishiyama A, Nait-Oumesmar B, Angulo MC (2019) Neuronal activity in vivo enhances functional myelin repair. *Jci Insight* 4.
- Ozerdem U, Grako KA, Dahlin-Huppe K, Monosov E, Stallcup WB (2001) NG2 proteoglycan is expressed exclusively by mural cells during vascular morphogenesis. *Dev Dynam* 222:218–227.
- Paez PM, Lyons DA (2020) Calcium Signaling in the Oligodendrocyte Lineage: Regulators and Consequences. *Annu Rev Neurosci* 43:1–24.
- Paez PM, Fulton DJ, Spreuer V, Handley V, Campagnoni CW, Macklin WB, Colwell C, Campagnoni AT (2009) Golli Myelin Basic Proteins Regulate Oligodendroglial Progenitor Cell Migration through Voltage-Gated Ca²⁺ Influx. *J Neurosci* 29:6663–6676.
- Pan S, Mayoral SR, Choi HS, Chan JR, Kheirbek MA (2020) Preservation of a remote fear memory requires new myelin formation. *Nat Neurosci* 23:487–499.
- Peña F, Tapia R (1999) Relationships Among Seizures, Extracellular Amino Acid Changes, and Neurodegeneration Induced by 4-Aminopyridine in Rat Hippocampus: A Microdialysis and Electroencephalographic Study. *J Neurochem* 72:2006–2014.
- Pringle NP, Mudhar HS, Collarini EJ, Richardson WD (1992) PDGF receptors in the rat CNS: during late neurogenesis, PDGF alpha-receptor expression appears to be restricted to glial cells of the oligodendrocyte lineage. *Dev Camb Engl* 115:535–551.
- Raff MC, Miller RH, Noble M (1983) A glial progenitor cell that develops in vitro into an astrocyte or an oligodendrocyte depending on culture medium. *Nature* 303:390–396.
- Richardson WD, Pringle N, Mosley MJ, Westermarck B, Dubois-Dalcq M (1988) A role for platelet-derived growth factor in normal gliogenesis in the central nervous system. *Cell* 53:309–319.
- Richardson WD, Kessaris N, Pringle N (2006) Oligodendrocyte wars. *Nat Rev Neurosci* 7:11–18.
- Rosenberg SS, Kelland EE, Tokar E, Torre ARDL, Chan JR (2008) The geometric and spatial constraints of the microenvironment induce oligodendrocyte differentiation. *Proc National Acad Sci* 105:14662–14667.
- Rungta RL, Chaigneau E, Osmanski B-F, Charpak S (2018) Vascular Compartmentalization of Functional Hyperemia from the Synapse to the Pia. *Neuron* 99:362-375.e4.
- Sampaio-Baptista C, Khrapitchev AA, Foxley S, Schlagheck T, Scholz J, Jbabdi S, DeLuca GC, Miller KL, Taylor A, Thomas N, Kleim J, Sibson NR, Bannerman D, Johansen-Berg H (2013) Motor Skill Learning Induces Changes in White Matter Microstructure and Myelination. *J Neurosci* 33:19499–19503.
- Schebesta M, Serluca FC (2009) olig1 expression identifies developing oligodendrocytes in zebrafish and requires hedgehog and notch signaling. *Dev Dynam* 238:887–898.
- Schlegel AA, Rudelson JJ, Tse PU (2012) White Matter Structure Changes as Adults Learn a Second Language. *J Cognitive Neurosci* 24:1664–1670.

- Scholz J, Klein MC, Behrens TEJ, Johansen-Berg H (2009) Training induces changes in white-matter architecture. *Nat Neurosci* 12:1370–1371.
- Sha F, Abdelfattah AS, Patel R, Schreiter ER (2020) Erasable labeling of neuronal activity using a reversible calcium marker. *Elife* 9:e57249.
- Sierra A, Paolicelli RC, Kettenmann H (2019) Cien Años de Microglía: Milestones in a Century of Microglial Research. *Trends Neurosci* 42:778–792.
- Skoff RP, Price DL, Stocks A (1976) Electron microscopic autoradiographic studies of gliogenesis in rat optic nerve. II. Time of origin. *J Comp Neurol* 169:313–333.
- Snaidero N, Möbius W, Czopka T, Hekking LHP, Mathisen C, Verkleij D, Goebbels S, Edgar J, Merkler D, Lyons DA, Nave K-A, Simons M (2014) Myelin Membrane Wrapping of CNS Axons by PI(3,4,5)P3-Dependent Polarized Growth at the Inner Tongue. *Cell* 156:277–290.
- Spitzer SO, Sitnikov S, Kamen Y, Evans KA, Kronenberg-Versteeg D, Dietmann S, Faria O de, Agathou S, Káradóttir RT (2019) Oligodendrocyte Progenitor Cells Become Regionally Diverse and Heterogeneous with Age. *Neuron* 101:459–471.e5.
- Srinivasan R, Huang BS, Venugopal S, Johnston AD, Chai H, Zeng H, Golshani P, Khakh BS (2015) Ca²⁺ signaling in astrocytes from *Ip3r2*^{-/-} mice in brain slices and during startle responses in vivo. *Nat Neurosci* 18:708–717.
- Stallcup WB (1981) The NG2 antigen, a putative lineage marker: Immunofluorescent localization in primary cultures of rat brain. *Dev Biol* 83:154–165.
- Steele CJ, Bailey JA, Zatorre RJ, Penhune VB (2013) Early Musical Training and White-Matter Plasticity in the Corpus Callosum: Evidence for a Sensitive Period. *J Neurosci* 33:1282–1290.
- Stobart JL, Ferrari KD, Barrett MJP, Stobart MJ, Looser ZJ, Saab AS, Weber B (2016) Long-term In Vivo Calcium Imaging of Astrocytes Reveals Distinct Cellular Compartment Responses to Sensory Stimulation. *Cereb Cortex* 28:184–198.
- Sun W, Matthews EA, Nicolas V, Schoch S, Dietrich D (2016) NG2 glial cells integrate synaptic input in global and dendritic calcium signals. *Elife* 5:e16262.
- Takebayashi H, Yoshida S, Sugimori M, Kosako H, Kominami R, Nakafuku M, Nabeshima Y (2000) Dynamic expression of basic helix-loop-helix Olig family members: implication of Olig2 in neuron and oligodendrocyte differentiation and identification of a new member, Olig3. *Mech Develop* 99:143–148.
- Thiele TR, Donovan JC, Baier H (2014) Descending Control of Swim Posture by a Midbrain Nucleus in Zebrafish. *Neuron* 83:679–691.
- Tomassy GS, Berger DR, Chen H-H, Kasthuri N, Hayworth KJ, Vercelli A, Seung HS, Lichtman JW, Arlotta P (2014) Distinct Profiles of Myelin Distribution Along Single Axons of Pyramidal Neurons in the Neocortex. *Science* 344:319–324.
- Tong X, Li X, Zhou B, Shen W, Zhang Z, Xu T, Duan S (2009) Ca²⁺ signaling evoked by activation of Na⁺ channels and Na⁺/Ca²⁺ exchangers is required for GABA-induced NG2 cell migration. *J Cell Biology* 186:113–128.
- Trapp BD, Nishiyama A, Cheng D, Macklin W (1997) Differentiation and Death of Premyelinating Oligodendrocytes in Developing Rodent Brain. *J Cell Biology* 137:459–468.

- Tripathi RB, Clarke LE, Burzomato V, Kessar N, Anderson PN, Attwell D, Richardson WD (2011) Dorsally and Ventrally Derived Oligodendrocytes Have Similar Electrical Properties but Myelinate Preferred Tracts. *J Neurosci* 31:6809–6819.
- Trojanowski NF, Bottorff J, Turrigiano GG (2021) Activity labeling in vivo using CaMPARI2 reveals intrinsic and synaptic differences between neurons with high and low firing rate set points. *Neuron* 109:663-676.e5.
- Tsai E, Casaccia P (2019) Mechano-modulation of nuclear events regulating oligodendrocyte progenitor gene expression. *Glia* 67:1229–1239.
- Vejar S, Oyarzún JE, Retamal MA, Ortiz FC, Orellana JA (2019) Connexin and Pannexin-Based Channels in Oligodendrocytes: Implications in Brain Health and Disease. *Front Cell Neurosci* 13:3.
- Vélez-Fort M, Maldonado PP, Butt AM, Audinat E, Angulo MC (2010) Postnatal Switch from Synaptic to Extrasynaptic Transmission between Interneurons and NG2 Cells. *J Neurosci* 30:6921–6929.
- Viganò F, Dimou L (2016) The heterogeneous nature of NG2-glia. *Brain Res* 1638:129–137.
- Viganò F, Möbius W, Götz M, Dimou L (2013) Transplantation reveals regional differences in oligodendrocyte differentiation in the adult brain. *Nat Neurosci* 16:1370–1372.
- Virchow, R. (1856) *Gesammelte Abhandlungen zur Wissenschaftlichen Medizin*, Meidinger, (in German).
- Wake H, Lee PR, Fields RD (2011) Control of Local Protein Synthesis and Initial Events in Myelination by Action Potentials. *Science* 333:1647–1651.
- Wake H, Ortiz FC, Woo DH, Lee PR, Angulo MC, Fields RD (2015) Nonsynaptic junctions on myelinating glia promote preferential myelination of electrically active axons. *Nat Commun* 6:7844.
- Walton EM, Cronan MR, Beerman RW, Tobin DM (2015) The Macrophage-Specific Promoter *mfap4* Allows Live, Long-Term Analysis of Macrophage Behavior during Mycobacterial Infection in Zebrafish. *Plos One* 10:e0138949.
- Watanabe M, Toyama Y, Nishiyama A (2002) Differentiation of proliferated NG2-positive glial progenitor cells in a remyelinating lesion. *J Neurosci Res* 69:826–836.
- Watkins TA, Emery B, Mulinyawe S, Barres BA (2008) Distinct Stages of Myelination Regulated by γ -Secretase and Astrocytes in a Rapidly Myelinating CNS Coculture System. *Neuron* 60:555–569.
- Winter MJ, Windell D, Metz J, Matthews P, Pinion J, Brown JT, Hetheridge MJ, Ball JS, Owen SF, Redfern WS, Moger J, Randall AD, Tyler CR (2017) 4-dimensional functional profiling in the convulsant-treated larval zebrafish brain. *Sci Rep-uk* 7:6581.
- Wolswijk G (1998) Chronic Stage Multiple Sclerosis Lesions Contain a Relatively Quiescent Population of Oligodendrocyte Precursor Cells. *J Neurosci* 18:601–609.
- Xiao L, Ohayon D, McKenzie IA, Sinclair-Wilson A, Wright JL, Fudge AD, Emery B, Li H, Richardson WD (2016) Rapid production of new oligodendrocytes is required in the earliest stages of motor-skill learning. *Nat Neurosci* 19:1210–1217.

- Yamaguchi S, Rogawski MA (1992) Effects of anticonvulsant drugs on 4-aminopyridine-induced seizures in mice. *Epilepsy Res* 11:9–16.
- Young KM, Psachoulia K, Tripathi RB, Dunn S-J, Cossell L, Attwell D, Tohyama K, Richardson WD (2013) Oligodendrocyte Dynamics in the Healthy Adult CNS: Evidence for Myelin Remodeling. *Neuron* 77:873–885.
- Yu X, Taylor AMW, Nagai J, Golshani P, Evans CJ, Coppola G, Khakh BS (2018) Reducing Astrocyte Calcium Signaling In Vivo Alters Striatal Microcircuits and Causes Repetitive Behavior. *Neuron* 99:1170-1187.e9.
- Zhao Y, Araki S, Wu J, Teramoto T, Chang Y-F, Nakano M, Abdelfattah AS, Fujiwara M, Ishihara T, Nagai T, Campbell RE (2011) An Expanded Palette of Genetically Encoded Ca²⁺ Indicators. *Science* 333:1888–1891.
- Zhou Q, Wang S, Anderson DJ (2000) Identification of a Novel Family of Oligodendrocyte Lineage-Specific Basic Helix–Loop–Helix Transcription Factors. *Neuron* 25:331–343.
- Zhu X, Hill RA, Dietrich D, Komitova M, Suzuki R, Nishiyama A (2011) Age-dependent fate and lineage restriction of single NG2 cells. *Development* 138:745–753.
- Zhu X, Bergles DE, Nishiyama A (2008) NG2 cells generate both oligodendrocytes and gray matter astrocytes. *Development* 135:145–157.
- Ziskin JL, Nishiyama A, Rubio M, Fukaya M, Bergles DE (2007) Vesicular release of glutamate from unmyelinated axons in white matter. *Nat Neurosci* 10:321–330.
- Zonouzi M, Scafidi J, Li P, McEllin B, Edwards J, Dupree JL, Harvey L, Sun D, Hübner CA, Cull-Candy SG, Farrant M, Gallo V (2015) GABAergic regulation of cerebellar NG2 cell development is altered in perinatal white matter injury. *Nat Neurosci* 18:674–682.

6 PUBLICATIONS

Marisca R, Hoche T, Agirre E, Hoodless LJ, Barkey W, Auer F, Castelo-Branco G, Czopka T (2020) Functionally distinct subgroups of oligodendrocyte precursor cells integrate neural activity and execute myelin formation. *Nat Neurosci* 23:363–374. **[Shared co-first authorship with Tobias Hoche]**

7 EIDESTÄTTLICHE VERSICHERUNG

Hiermit versichere ich an Eides statt, dass ich die vorliegende Dissertation "*Investigating Mechanisms of Axon-Oligodendrocyte Precursor Cell Communication in vivo*" selbstständig angefertigt habe, mich außer der angegebenen keiner weiteren Hilfsmittel bedient und alle Erkenntnisse, die aus dem Schrifttum ganz oder annähernd übernommen sind, als solche kenntlich gemacht und nach ihrer Herkunft unter Bezeichnung der Fundstelle einzeln nachgewiesen habe.

I hereby confirm that the dissertation "*Investigating Mechanisms of Axon-Oligodendrocyte Precursor Cell Communication in vivo*" is the result of my own work and that I have only used sources or materials listed and specified in the dissertation.

München, den 18.03.2021

Unterschrift

Roberta Marisca

8 DECLARATION OF AUTHOR CONTRIBUTION

Experimental design: RM, TC

Setup design/assembly: RM, TC

Conducting experiments: RM, LH, TH

Analysis of experiments: RM, LH

Visualizing the results of experiments: RM

Supervision, project administration: TC

Thesis writing: RM

17th March 2021, Munich

Date, place

Signature Roberta Marisca

Signature Laura Hoodless

Signature Tobias Hoche

Signature Dr. Tim Czopka